CCD OBSERVATIONS OF CLUSTERS

OF GALAXIES

Thesis by

Donald P. Schneider

In Partial Fulfillment for the Requirements

for the Degree of

Doctor of Philosophy

California Institute of Technology

Pasadena, California

1982

(Submitted April 13, 1982)

To Mom and Dad

ACKNOWLEDGMENTS

It is a pleasure to thank my advisor, Jim Gunn. His enthusiasm, guidance, and patience made this project possible. The only ill treatment I received was subjection to several nights of classical tunes.

Two fellow students, Peter Young and John Hoessel, contributed substantially to this work. Both aided in the data acquisition, gave useful advice, and taught me everything I know about observational technique.

This project would not have been feasible without the generous hardware and software aid given by Jerry Kristian, James Westphal, Rich Lucinio, Bob Deverill, and Barbara Zimmerman (who was constantly rescuing me from the clutches of FORTH).

Thanks do not go to Jesse Greenstein and Richard Wade, whose contagious enthusiasm for cataclysmic variables resulted in my spending a great deal of time on intractable problems.

Kam-Ching Leung, my undergraduate advisor, guided my first efforts at astronomical research and must bear some responsibility for this work.

I also wish to thank:

- Steve Shectman, Gary Yanik, and Ken Clardy for their efforts with the Reticon systems that were used for several projects.

ABSTRACT

A sample of 84 Abell clusters has been investigated to
determine photometric and metric properties of brightest
cluster galaxies as a function of cluster richness. The
clusters are distributed fairly uniformly in Abell richness
class. Seventy-five new measurements of cluster redshifts
are presented (previously published redshifts were used for
the nine other clusters). The selection criteria resulted
in a strong redshift-richness correlation in the sample.
Poor clusters (richness classes 0 and 1) have redshifts
~0.09, while the richest clusters have redshifts roughly as
twice as large.

Direct imaging of the core of each cluster was affected
using a CCD area photometer. The wavelength response of the
CCD is so different from that of previous photometric de-
vices that a new photometric system is required. The re-
ductions employ photon based k-corrections (instead of energy
based ones) and galactic absorption determined by the neutral
hydrogen column density.

The luminosity of the brightest cluster galaxy (G1)
within an aperture of 16 kpc radius is shown to be a good
standard candle. Previous aperture measurements of 135
first-ranked cluster galaxies are placed on the CCD photo-
metric system. Nearly 200 G1's with redshifts less than
0.3 have been measured, and they effectively determine the

luminosity of giant ellipticals at the present epoch. Their
aperture luminosity dispersion is 0.34 mag, which can be re-
duced/slightly under 0.3 mag by removing richness and mor-
phological trends. The richness correction is reasonably
well established at 0.10 magnitudes per Abell richness class,
with the rich clusters having brighter galaxies. The trend
of luminosity with Bautz-Morgan type matches those of pre-
vious investigations, ~0.12 mag per subclass, with BM I
clusters having brightest cluster galaxies which are 0.3 mag
brighter than the average G1.

Aperture magnitudes were also determined for the second
and third ranked cluster galaxies (G2 and G3), which are
defined as the next two brightest galaxies within 250 kpc
of G1. The limiting radius was adopted because of the
relatively small area covered by the detector. The dispersion
in the aperture luminosity for G2 is 0.55 mag; for G3 the
dispersion is 0.65 mag. On average G2 is 0.8 mag and G3
1.3 mag fainter than G1. The luminosity dependence of G2
and G3 on Abell richness class is roughly the same as that
for G1, except for the richest clusters where G2 and G3 are
much brighter than expected. There is no significant
BM-luminosity correlation for either G2 or G3
in this sample. The observed colors for the
brightest three cluster galaxies indicate that no color
evolution has taken place since redshifts of 0.25 (~four

billion years).

The radius surface brightness profiles inside 16 kpc
for G1, G2, and G3 are fit fairly well by either a
de Vaucouleurs model or a modified Hubble law. At 16 kpc
the surface brightness for G1 falls   off like a power
law with an index of -1.6 to -1.8. For first-ranked gal-
axies the mean effective radius is 28 kpc and the mean core
radius is 2.1 kpc. These scale lengths are three and five
times the values for G2 and G3, respectively. The strong
correlation of G1's structure with its absolute magnitude
and with cluster morphology are confirmed. The average
aperture correction factor (α) for first-ranked cluster gal-
axies is 0.7; this reduces the sensitivity of the Hubble
diagram to q_o by 35%.

Nearly half of the brightest cluster galaxies have
multiple nuclei, roughly five times the number expected
from projection effects. The multiple systems are, on
average, ~ 0.13 magnitudes brighter than the single systems.
An evolutionary correction to q_o of $\sim +1.5$ is required if the
multiple systems are interpreted as mergers induced by
dynamical friction. The merger process, however, can be
calibrated from the α-luminosity relations; this allows
corrections to be applied to each galaxy individually.

There is a strong effective radius-surface brightness
relation for brightest cluster galaxies. The surface bright-
ness at the effective radius $I(R_e)$, determines the effective

radius (R_e) to ~25%. The observed effective radii (deter-
mined from fits to the inner 16 kpc) range from ~4 kpc to
over 100 kpc. The outer regions (> 30 kpc) of galaxies with
extended envelopes do not match the de Vaucouleurs profile
found by fitting the inner regions. An angular diameter
test based on the effective radii is impractical due to the
large intrinsic scatter; a test using the surface brightness
corrected effective radii conveys the same information as
the standard redshift-magnitude test. The effective radius-
surface brightness relation explains the small dispersion
in the aperture magnitudes of G1, and predicts that the total
luminosities of brightest cluster galaxies grow as the 0.7
power of the scale length. If the mass-to-light ratio in
ellipticals is constant, the luminosity-scale length
correlation is incompatible with the Faber-Jackson relation.
Application of the R_e-$I(R_e)$ relation to the brightest gal-
axies in Virgo (NGC 4472 and NGC 4486) yields a null result
(no infall) for the distortion of the local Hubble flow.
Infall velocities of 250 km s^{-1} are excluded at the 2σ
level. The second and third ranked galaxies follow a
similar R_e-$I(R_e)$ relation. The exponent in the luminosity
scale length relation for G2 is about 10% smaller than that
for G1. For G3 the luminosity increases as the square root
of the scale length.

Data of sufficient quality to allow construction of

luminosity functions were obtained for 60 of the 84 clusters. The limited size of the field required that the luminosity functions be determined inside a given metric radius (250 kpc). The observed luminosity functions were fit to Schechter functions using maximum likelihood techniques. The brightest cluster galaxy cannot be drawn from a universal luminosity function. It is impossible to reconcile the small total luminosity-richness correlation with the relatively large (0.6 mag) dispersion in their total luminosities. The first-ranked galaxies are also about one magnitude too bright to be drawn from a Schechter function. Excluding G1 from the luminosity function results in satisfactory Schechter function fits to the rest of the cluster members. The power-law slope at low luminosities is ~-1, but is not well determined. The observations find a mean M_* in close agreement with other investigations. The observed dispersion of M_* about the mean as a function of cluster richness is similar to that predicted from numerical simulations.

Cluster richness is defined as the total luminosity found by integrating over all luminosities the best fitting Schechter function determined from galaxies within 250 kpc of the brightest cluster galaxy. This definition correlates well but not perfectly with Abell richness class. Richness (actually central density) varies by nearly a factor of 40 from the poorest to the richest clusters in this sample,

and in several poor clusters the brightest galaxy out-
shines the rest of the core. The total luminosity of G1 is
weakly correlated with richness (at the same level as with
Abell richness class). The luminosities of G2 and G3, how-
ever, exhibit a strong positive relationship with cluster
richness.

Surface photometry of ~2000 cluster members indicates
that they may form the basis for a very powerful angular
diameter (or luminosity) test for the deceleration parameter,
but uncertainties in the seeing corrections and object
selection effects must first be resolved.

The evidence for dynamical evolution, while admittedly
circumstantial, is nevertheless persuasive. The strong
structure-luminosity relation and the frequency of multiple
systems are strong arguments in favor of galactic cannibalism.
A detailed spectroscopic and photometric study of a brightest
cluster galaxy composed of nine nuclei, V Zw 311, indicates
that dynamical friction can radically alter a galaxy in a
time scale of only a billion years. The lack of strong
luminosity-richness correlation is the most often advanced
objection to the merger picture, but dynamical studies of
rich systems are required before their capture rates can be
calculated.

TABLE OF CONTENTS

PRELIMINARY REMARKS

This thesis presents an investigation of moderate red-
shift clusters of galaxies using a CCD area photometer.
The work is divided into four chapters, each a self-con-
tained article to be submitted to The Astrophysical Journal.
The first three chapters describe a comprehensive study of
a sample of 84 Abell clusters; the data consist of redshifts
of the first ranked cluster galaxies and direct imaging of
the central 150 to 500 kpc (radius) of the cluster. Chapter
I presents the redshifts and magnitudes of the brightest
cluster galaxies, defines the CCD photometric system, and
discusses the implications for the Hubble diagram. Chapter
II investigates the structures and magnitudes of the bright-
est three galaxies in the cores of these clusters, and
Chapter III discusses the luminosity functions and general
properties of a subset of 60 clusters. Chapter IV covers a
very unusual multiple nucleus system - V Zw 311. Nine dis-
tinct nuclei are embedded in an extended envelope and seem
to be forming a cD galaxy in a very sparse cluster. Much of
this research was done in collaboration with Jim Gunn and
John Hoessel.

CHAPTER I

MAGNITUDES AND REDSHIFTS FOR

84 BRIGHTEST CLUSTER GALAXIES

Authors: Donald P. Schneider, James E. Gunn, and

John G. Hoessel

(Paper I)

I. INTRODUCTION

The classic test of the global properties of the universe is the redshift-magnitude relation, or Hubble diagram. Several recent systematic studies (Gunn and Oke 1975; Sandage, Kristian, and Westphal 1976; Kristian, Sandage, and Westphal 1978; Hoessel, Gunn, and Thuan 1980; hereinafter GO, SKW, KSW, and HGT respectively) have used the brightest cluster galaxy as a standard candle. The intrinsic dispersion in the luminosity of these sources is ~0.35 mag, which is reduced to ~0.25 mag by applying corrections for morphological type, cluster richness, and galaxy structure (see KSW and HGT).

These investigations yielded values of q_o from -0.55 to 1.7; the reason for this discrepancy is not yet understood, but may arise in the selection procedures. The other major impediment to finding a believable value for the deceleration parameter is the unfortunate fact that galaxies evolve. The luminosity of all galaxies will change due to evolution of their stellar populations (Tinsley and Gunn 1976). The brightest cluster of galaxies may also experience significant changes due to their cannibalism of other cluster members induced by dynamical friction (Ostriker and Tremaine 1975; Gunn and Tinsley 1976; Hausman and Ostriker 1978; Hoessel 1980).

The measurements in HGT (116 galaxies) determine the luminosity of first ranked ellipticals at the present epoch quite well; it would require a massive effort to improve on this data base substantially. A study of a well-defined sample of clusters at high redshift (0.25 to 1.0) is described in Gunn, Hoessel, and Oke (1982). The present paper presents work on clusters of intermediate redshift (0.15) with a wide range of properties including the very rich clusters which are missing in the nearby HGT sample.

The sample in this paper consists of 84 clusters chosen from Leir and van den Bergh's (1977, hereafter LVDB) catalog of Abell (1958) clusters. All clusters with richness class three or greater and $|b| > 30°$ were selected (excluding those in HGT). Abell 545, a richness 4 cluster at somewhat lower latitude, was included as well. For richness classes 0 to 2, the LVDB magnitudes were chosen to lie in the range 14.2 to 15.5. Twenty clusters in each of these richness classes were randomly selected subject to these restrictions. These procedures result in a selection of poor (richness 0, 1, and 2) clusters considerably brighter and nearer than the rarer very rich ones. The penalty for this is that photometric and metric trends with richness are inevitably contaminated by seeing effects (which we feel we deal with quite accurately) and by cosmological model dependences which cannot in principle be dealt with.

The cosmological effects for this sample, however, are very small. Choosing a sample homogeneous in distance would have been preferable but would have resulted in an unacceptable increase in observing time. Hereafter this group of clusters will be designated as the "richness sample."

The clusters were identified from enlargements of POSS-E prints and the positions given in LVDB. In the majority of the cases the cluster was obvious and an improved position of the brightest galaxy was measured. In a few instances (primarily the richness 0 clusters) no cluster was evident, so the galaxy nearest to the position was chosen (see § II). The initial galaxy selected for clusters 1081, 1934, 2246, and 2686 were actually foreground spirals. The correct objects were found from inspection of direct image data obtained on the field. Table 1 gives a summary of the richness sample. The positions are for the chosen brightest galaxy in each cluster, and are accurate to 15". In all but four cases, these coordinates are for the galaxies that have their magnitudes and redshifts in Table 1. For 1190, 1689, 1825, and 2377 it was discovered that a nearby galaxy (within 90") was brighter than the original choice by~0.07 mag. The coordinates for these clusters give the position of the brightest galaxy. Galactic coordinates, Abell richness and distance classes, and Bautz-Morgan (1970) types are listed in successive columns. Throughout this paper all

dimensions are calculated assuming $H_o = 60$ km s^{-1} Mpc^{-1} and $q_o = 0.5$.

The redshifts and photometry of the brightest cluster galaxies are described in §§ II and III. Section IV describes a photometric system suited for cosmological investigations with ground-based CCD's. The properties of these galaxies and the implications for the Hubble diagram are discussed in § V. The structure of the brightest three galaxies in these clusters is discussed by Schneider, Gunn, and Hoessel (1982, hereinafter Paper II); the luminosity function of the cores of 60 of the clusters and a new definition of richness is presented in Schneider (1982).

II. REDSHIFTS

Spectra of the first ranked cluster galaxy candidates were acquired using a multitude of detection systems during 1979-81. Table 2 is a journal of spectroscopic observations giving the relevant instrumentation parameters. Detailed descriptions of the detectors can be found in Schechter and Gunn (1979) [SIT]; Gunn and Westphal (1982) [CCD]; and Young, Schneider, and Shectman (1981) [Reticon]. The exposures were generally 400 seconds in length, except for the 1.5-m data where integrations of 2000-4000 seconds were required. The observations were made through a two arcsecond slit. Observing conditions ranged from nearly overcast to photometric; the seeing from one to eight arcseconds.

Figure 1 displays examples of spectra taken with the various systems.

Wavelength calibration was performed using He or He/Ar lamps. The reduction process for the SIT spectra is very similar to that given in Schneider and Gunn (1982). After processing to one-dimensional data, the spectra were re-binned on a logarithmic wavelength scale (bin sizes of 350 km s^{-1} and 200 km s^{-1} for the low- and high-resolution data) and correlated with two radial velocity templates (K giants) using the Fourier quotient technique of Sargent, Schechter, Boksenberg, and Shortridge (1977). Redshifts for the CCD and Reticon data were measured directly from plots of the spectra. The adopted redshifts of all 84 clusters are given in Table 1. The velocities have a solar motion term of 300 sin l cos b removed.

Several checks on the accuracy of the SIT numbers are possible. Redshifts determined using the two templates agreed to ~90 km s^{-1} for the high resolution, ~100 km s^{-1} for the low-resolution data. Five galaxies were observed at both high- and low-resolution. The scatter in the velocities was of the order of 100 km s^{-1}. Comparison of nine of our measurements with those of other workers shows agreements on the scale of ~300 km s^{-1}. Systematic errors of this order are to be expected considering beam bending (Schechter and Gunn 1979) and the lack of comparison lines

in the relevant part of the spectrum. The only measurement
which was in serious disagreement with previous ones was the
redshift for 1689. Our value is over 1000 km s^{-1} larger
than that of Humason, Mayall, and Sandage (1956). Both
measurements refer to the mean of two close components which
our data show differ in velocity by more than 2000 km s^{-1}.
Measurement of several features in the CCD and Reticon have
an internal consistency of ~250 km s^{-1}.

Table 3 lists clusters that had more than one member's
redshift measured. Usually this was the result of a com-
panion accidentally falling on the slit. In a few cases an
effort was made to observe galaxies which had luminosity
comparable to the designated brightest one. For clusters
that had two close (< 10") equal components, the cluster
redshift was taken as the mean of the two. Usually these
components differed by only several hundred km s^{-1}, but the
pair in 1689 has a velocity difference of 2000 km s^{-1}. For
nine clusters redshifts were taken from the literature and
can be identified in Table 1 by a reference number in
parenthesis following the redshift. Clusters whose redshift
is the mean of two components have their value followed by
an asterisk. A "P" after the entry indicates the obser-
vation was performed with the CCD system, an "R" denotes
the Reticon observation.

Figure 2 displays a histogram of the redshifts broken

down by richness class (the HGT clusters are also plotted).
It is clear that Abell richness class and distance are
rather correlated in this sample. There were two surprises -
1018 and 1224. These seemingly innocuous richness one
clusters turned out to be at redshifts of nearly 0.3,
larger than any previously measured Abell cluster.

Some interesting insights can be drawn by relating
these numbers with the postulated redshifts of LVDB. They
estimated cluster distances based on the appearance of the
brightest galaxy and various cluster properties. Comparison
with ~100 published cluster redshifts indicated an accuracy
of ~20%. Figure 3 is a plot of their velocities vs. those
of HGT and Table 1. Two lines are plotted, a line of unit
slope passing through the origin and the best fitting
straight line. The flattening of the relation may be due to
selection effects - as one proceeds to higher redshift (more
volume) one encounters more diverse cluster types (including
rare, rich ones which stand out). Placing the distant
clusters on the same relation as nearby ones may skew the
relation, causing a distance underestimate of the distance
clusters and an overestimate of the nearby ones. It is more
likely, however, that we are simply overinterpreting this
effect; Figure 3 shows that the line with unit slope fits
almost as well.

Some of the scatter is due to problems of identification

and/or catalog error, since in some instances there is no obvious cluster at the catalog position. For example, no cluster is found at the position of 2516, which was in the richness sample originally. In this obvious case, another cluster, 279, was drawn from the pool to replace it. Rather more serious is the case of Abell 34, which is at one-quarter of its LVDB distance. There were only two other "cluster" members on the CCD frame; there is no doubt that the object is not a cluster at all, and it was excluded in the analysis. Notice that there is no danger of bias from this arbitrary procedure. The "brightest galaxy" in the cluster stands four standard deviations from the Hubble line, and the cluster would in any case never have been selected in the distant samples to be used for cosmological tests.

One of the clusters, 2597 (see Fig. 1), has a remarkable emission-line spectrum. It is the only one of over 100 galaxies that shows any emission. The galaxy was identified with the radio source PKS 2322-12 (Schmidt 1965), and has a radio luminosity of 6×10^{42} erg s^{-1}. A search of a radio source list (Dixon 1970) found 13 other radio sources within 2.5' of a position in Table 1. The resulting radio luminosities range from $2-40 \times 10^{41}$ erg s^{-1}. This is roughly 30% of the clusters in the richness sample in the relevant redshift range (< 0.14). Richness classes 0, 1, 2, and 3 were represented. No richness 4 clusters have radio counterparts,

but then the nearest (545) is more distant than any of the radio clusters.

III. PHOTOMETRY

Direct imaging of the central few arcminutes of each cluster was obtained with the PFUEI/CCD system. Observations were made in the g and r filters of Thuan and Gunn (1976), and the instrumental magnitudes transformed to this system from observations of six to twelve photometric standards each night. Typical residuals in the r magnitude were 2-2.5%; they never exceeded 4%. Difficulty was experienced on some nights with the g photometry, a phenomenon almost certainly connected with chemical effects in the "dead layer" in the unpassivated silicon surface of the CCD. The residuals on these nights often change systematically in the sense that the detector becomes less sensitive with time. This behavior can be compensated given enough standards, and this has been done.

CCD's are truly marvelous detectors, but they do have one troublesome property - their wavelength response is so different from photoemissive devices that it is difficult to tie broadband photometry to existing systems based on photomultipliers. This presents a serious problem to us, as we wish to compare the observations in this paper with the values in HGT. We have decided to handle this problem in an inelegant but practical way. The Thuan-Gunn g and r

magnitudes for the standards were adopted; the transformations of the CCD data to these numbers work well for stars with $-0.8 < (g-r)_{TG} < +0.9$, while standards with $(g-r)_{TG} > 1.0$ had transformation $(g-r)$'s which were over 0.1 mag redder than the TG values (several photomultiplier measurements were kindly communicated to us by S. Kent). This result is not unexpected, as M stars have complex spectra which play havoc with attempts to move between broadband photometric systems. The galaxy observations were reduced with the above transformations. See the end of § IV for a further discussion.

The measurements of the brightest cluster galaxies are given in Table 1. These are the observed magnitudes, no reddening corrections have been applied. They refer to the light inside a 16 kpc radius in the $q_o = 0.5$ $H_o = 60$ model. For the more distant clusters this radius is less than four arcseconds, and atmospheric seeing (usually 1.1-1.7 arcsec) cannot be ignored. The adopted correction procedure is described in Paper II. Briefly, the seeing profile was determined from a star on the frame (a suitable candidate could always be found); then the radial profile of the galaxy was fitted to both a de Vaucouleurs law and a modified Hubble model

$$I(x) = \frac{I_o}{[1+(x/a)^2]^{0.9}} \tag{1}$$

convolved with a double gaussian fit to the seeing (the 0.9 in the Hubble profile comes from the mean slope in the region around 16 kpc in brightest cluster galaxies, see Paper II). A 16 kpc seeing correction factor was calculated and then applied to the actual aperture measurement. This correction was usually negligible, only rising to 0.025 mag for the most distant clusters.

Photometric data on all the clusters were obtained with the 1.5-m system (see Schneider and Gunn [1982] for a description) from August 1979 to August 1980. The exposure times were 300 s for both g and r filters. Half of the photometric measurements were in very poor seeing; these clusters were redone on nights with good seeing (< 1.5"). The non-photometric good seeing pictures (r filter, 500 to 1500 s exposures) were tied to the photometric ones by comparing multi-aperture magnitudes for the brightest galaxy. This was tested out with clusters which had photometric data with good and bad seeing. These galaxies had magnitudes consistent to 0.04 mag. The only problems arose with a few of the most distant clusters which had uncertainties of 0.07 mag.

Hoessel (1980) found that ~30% of first ranked cluster galaxies were multiple-nucleus systems; i.e., more than one "galaxy" occurred within the 16 kpc aperture (for an extreme example of this, see Schneider and Gunn [1982]). We shall

adopt as a working definition of the brightest cluster galaxy the region of maximum light enclosed in an aperture with a radius of 16 kpc. The second, third, etc. are de-fined in an analogous way. This procedure has several practical advantages - including objectivity and algorithmic simplicity with linear image data. It also can be applied to clusters at vastly different redshifts. The drawback, as is readily seen in Schneider and Gunn (1982), is that the resulting profile can be very bizarre (see Paper II for a discussion). The profiles for the most extreme of these systems are, of course, fitted very poorly by either modi-fied Hubble or de Vaucouleurs laws, but this procedure has the enormous advantage of not introducing distance-dependent biases. One has the option of rejecting extreme cases through the α-parameter, which is determined in a roughly seeing-independent way.

The (g-r) colors were measured by comparing the inte-grated colors in several apertures with radii of ~16 kpc. Errors in the sky subtraction manifest themselves by rapid changes of color with radius; in nearly all our data on brightest galaxies, the internal consistency was ~2% in the 12-16 kpc range. Approximately 20 clusters had two measure-ments taken on different nights. These two measurements were obtained with different CCD's and slightly different g filters. Despite the dissimilarity of the photometric

transformation equations, 80% agreed to 0.03 mag. The galaxies with large residuals were reobserved.

IV. A STANDARD COSMOLOGICAL PHOTOMETRIC SYSTEM

In this paper we present observations in only the g and r passbands, but wish to include two other filters in the following discussion of photometric data processing; i (Wade et al. 1979), and z (this paper). These last two filters are required for observations of high redshift clusters, so that one can observe near a given wavelength in the rest frame of the galaxy. This system has several advantages for ground-based CCD's. The filters span the response range of this detector (4500-11,000 $\overset{o}{A}$), and several strong sky lines are avoided (Hg 4358 and 5460, and [O II] 5577). The z filter consists of a RG 850 filter (50% of peak transmission at 8400 $\overset{o}{A}$, peak transmission of 93% reached at 10,200 $\overset{o}{A}$), one reflection off aluminum, and the PFUEI plus a Texas Instruments 800 x 800 CCD. The response curve for the PFUEI can be found in Gunn and Westphal (1982). The relative response curves of the griz system are shown in Figure 4; all factors except atmospheric extinction have been included.

The clusters (except for A545) have been restricted to galactic latitudes greater than 30° to minimize galactic obscuration. From van de Hulst's curve #15 (Johnson 1968) we find

$$A(g) = 3.29 \ E(B-V)$$

$$A(r) = 2.23 \ E(B-V)$$

$$A(i) = 1.63 \ E(B-V) \quad \quad (2)$$

$$A(z) = 1.22 \ E(B-V) \ .$$

Burstein and Heiles (1978) present a comprehensive study of galactic reddening as a function of the column density of neutral hydrogen. We took their points with $|b| > 30°$ and $N_H < 400$ (N_H is the column density of neutral hydrogen/2.23 x 10^{18}, which is the unit used in the contour maps of Heiles [1975]). A linear fit to 46 points gave

$$E(B-V) = 1.90 \times 10^{-4} \ (N_H - 68.9)$$

$$\text{RMS scatter in } E(B-V) = 0.026 \ .$$

The absorption becomes zero at a non-zero value of the column density. This phenomenon is in part due to the presence of emission from the galactic plane in the dish sidelobes, but perhaps not entirely (see Stark and Heiles 1981). Its origin is not of primary interest to us, since we wish to use the Heiles contour maps only as an inter-polation device for the reddening. Defining

$$N' = N_H - 68.9 \quad ,$$

for a galaxy at rest

$$A(g) = 6.24 \times 10^{-4} \ N'$$

$$A(r) = 4.23 \times 10^{-4} \ N'$$

$$A(i) = 3.09 \times 10^{-4} N'$$

$$A(z) = 2.31 \times 10^{-4} N' \; . \tag{3}$$

For galaxies at non-zero redshifts, the absorption was calculated by interpolating in the above formulae using the effective wavelength of the galaxy (see Fig. 4). If the column density becomes greater than 400 (for 545, for example), the color excess is read from the $E(B-V)$ vs. N_H graph of Burstein and Heiles (1978), and the absorption calculated from (2). The polar reddening is known to be small (Sandage 1973); these formulae result in essentially no absorption at the poles. The galactic absorption in the red band for each cluster is listed in Table 1. The same absorption correction procedure was applied to the HGT sample. Two of the HGT clusters have small negative galactic absorption with this scheme, $A(r) = -0.002$ mag ($N_H = 65$); none of the richness clusters had negative absorption. This procedure is open to a good deal of improvement, as the errors in the r magnitude induced by uncertainty in the reddening is 0.06 mag.

We now turn to the problem of correcting the observations for redshift related effects, i.e., the fact that one observes a different portion of the spectrum as the redshift increases. We propose a slightly new way of handling this problem. We note that the detectors employed are photon-counting systems, not energy sensitive devices. (The same

is true, of course, of photomultipliers; our new definition of the k-correction is the correct one for all such detectors.) For each filter (j) define $S_j(\nu)$ to be the probability that a photon of frequency ν will be detected by the system. This folds in filter and atmospheric (airmass 1.2) transmission, reflectivity of aluminum, and response of the detector. (Note that the response curves in Fig. 4 do not include the atmospheric transmission factor.) The apparent magnitude m_j is defined as:

$$m_j = C_j - 2.5 \log \int_0^\infty n_\nu \, S_j(\nu) d\nu$$

$$n_\nu = \frac{\text{number of photons incident on atmosphere}}{\text{sec} \quad \text{cm}^2 \quad \text{Hz}}.$$

$$C_j = \text{constant found from photometric standards.}$$

The absolute magnitude of an object is:

$$M_j = C_j - 2.5 \log \frac{\int_0^\infty N_\nu S_j(\nu) d\nu}{4\pi \, D_o^2} . \qquad D_o = 10 \text{ pc}$$

The photon flux from an object at redshift z is

$$n_\nu = \frac{N_\nu(1+z) H_o^2}{4\pi c^2 Z_q^2(z)} = \frac{N_\nu(1+z)(1+z)^2}{4\pi \, D_L^2} , \text{ where}$$

$$Z_q(z) = \frac{1}{q_o^2(1+z)} \{q_o z + (q_o-1)(\sqrt{1+2q_o z} - 1)\}$$

and

$$D_L = \text{luminosity distance} = \frac{cZ_q(z)(1+z)}{H_o}. \qquad \text{(Weinberg 1972)}$$

Thus

$$m_j = C_j - 2.5 \log \int_0^\infty \frac{N_{\nu(1+z)}(1+z)^2 S_j(\nu) d\nu}{4\pi D_L^2}$$

or

$$m_j = M_j - 5 \log \frac{D_O}{D_L} + 2.5 \log \frac{1}{(1+z)^2} \frac{\int_0^\infty N_\nu S_j(\nu) d\nu}{\int_0^\infty N_{\nu(1+z)} S_j(\nu) d\nu} \quad .$$

Define the k-correction $k_j(z)$ as

$$k_j(z) = 2.5 \log \frac{1}{(1+z)^2} \frac{\int_0^\infty N_\nu S_j(\nu) d\nu}{\int_0^\infty N_{\nu(1+z)} S_j(\nu) d\nu}$$

$$= 2.5 \log \frac{1}{1+z} \frac{\int_0^\infty \frac{f_\nu}{\nu} S_j(\nu) d\nu}{\int_0^\infty \frac{f_{\nu(1+z)}}{\nu} S_j(\nu) d\nu} \quad .$$

The absolute magnitude is then

$$M_j = m_j - 5 \log D_L - 25 - k_j(z) \quad . \qquad (D_L \text{ in Mpc})$$

Following GO, we shall define the reduced absolute magnitude (RAM or μ) as

$$\mu_j = M_j + 5 \log[c/H_O] - 5$$

or

$$\mu_j = m_j - 5 \log[Z_q(z)(1+z)] - k_j(z) \quad .$$

This quantity removes the effects of H_O on the absolute (i.e., standard) magnitudes. The meaning of the reduced absolute magnitude is easily visualized, it is the k-corrected apparent magnitude of an object placed at a

luminosity distance of one Hubble radius. In our model, R_h = c/H_o = 5000 Mpc, z_{R_h} = 0.866, and the distance modulus 5 log R_h - 5 = 43.49 mag. The formalism thus far is very similar to those of past investigators (Sandage 1961; GO, SKW, KSW, and HGT) except for the definition of the k-correction. Basing the k-correction on photons instead of energy does result in differences of up to 0.015 mag when sharp features (i.e., the 4000 $\overset{o}{A}$ break) enter the filter bandpass. In these instances the photon k-corrections are smoother than the energy ones; this being the result of the detector seeing a big drop in the high-energy photons.

In order to construct a Hubble diagram, a passband in the rest frame of the galaxy must be selected. One wants to chose one at the blue end so that it is accessible at high redshift, but not so blue that line blanketing will render the magnitude sensitive to metallicity. The g filter is an excellent compromise for our system, as the detector is insensitive at shorter wavelengths and redshifts greater than 0.74 are required to push g out of our observational range. Hereafter g_I will represent this standard magnitude.

For historical reasons (GO) we will define

$$g_I = C_g - 2.5 \log \left[\int_o^\infty \frac{f_\nu}{\nu} S_g [\nu(1+z)] d\nu \right]$$

$$g_I = m_g - k_g(z) - 2.5 \log(1+z) \quad .$$

The (1+z) term makes g_I behave like a monochromatic magnitude;

it is roughly the monochromatic magnitude at the redshifted wavelength which corresponds to the center of the g band in the galaxy rest frame. Note the g_I = g at z = 0.

If all galaxies had the same spectral shape, an observation in a single filter would suffice to obtain the magnitude in a preselected bandpass. HGT presented a method in which observations were obtained in two filters which bracketed the position of the desired wavelength region. We will adopt their procedure with a few minor modifications.

One needs to know the effective wavelengths for the various filters; this, however, is an ill-defined problem for any filter of finite width. We define the effective frequency for a given filter as

$$\nu_{j,eff} = \hat{\nu}_j = \exp\left[\frac{\int_0^\infty n_\nu \, S_j(\nu) \, \ln\nu \, d\nu}{\int_0^\infty n_\nu \, S_j(\nu) \, d\nu}\right]$$

where n_ν is a fiducial source, in our case NGC 4889. Notice that this definition is in a sense halfway between an effective frequency and an effective wavelength, and is chosen over those purely for aesthetic reasons. As the object moves to higher redshift

$$\bar{\nu}_j(z) = \exp\left[\frac{\int_0^\infty n_{\nu(1+z)} S_j(\nu) \, \ln\nu \, d\nu}{\int_0^\infty n_{\nu(1+z)} S_j(\nu) \, d\nu}\right]$$

and

$$\bar{\lambda}_j(a) = \frac{c}{\bar{\nu}_j(z)} \quad .$$

Figure 5 displays the z-dependence of the effective wavelength in the griz system. One diagonal line is the position of the effective wavelength of our selected passband (g_I), the other is the "break" at 4000 $\overset{o}{A}$. As the break enters a given bandpass, the effective wavelength moves to the red.

Let $\hat{v}_{g_I}$ = effective frequency of the desired region
(= $\bar{v}_g(o)$),/ and filters j and k be the lower and upper (frequency) bounds (selected from Fig. 5). One can calculate a g_I from both the k and j filters applying the appropriate $k(z)$ correction.

$$g_I(j) = m_j - k_j(z) + (g-j)_o - 2.5 \log(1+z)$$

where $(g-j)_o$ is the color of the standard galaxy at rest. Then

$$g = \frac{\ln\left[\dfrac{\hat{v}_{g_I}(1+z)}{\bar{v}_k}\right] g_I(j) + \ln\left[\dfrac{\bar{v}_j}{\hat{v}_{g_I}(1+z)}\right] g_I(k)}{\ln\left[\dfrac{\bar{v}_j}{\bar{v}_k}\right]} . \qquad (4)$$

For a galaxy at rest, adding 0.06 mag to g will yield the AB magnitude (flux scale of Oke and Schild [1971]) at 5000 $\overset{o}{A}$.

A small modification in the interpolation equation (4) was adopted in the handling of the richness sample (CCD) data. Double weight was given to the r measurement because of the temporal response variations and associated reduction difficulties in the g band. The HGT data had equal weight

given to $g_I(g)$ and $g_I(r)$. For the two richness clusters that have g_I shifted above the r band, g_I was set equal to $g_I(r)$.

We must now address the problem with the CCD photometric system mentioned in the previous section. The filters used with the PFUEI were convolved with the PFUEI plus CCD response curve, one reflection off aluminum, and the atmospheric transmissivity at 1.2 airmasses. From our CCD photometry and photometric multichannel scans lent us by J. B. Oke, we find

$$r = r_c + 0.044 \ (g-r)_c$$
$$g-r = 1.99 \ (g-r)_c$$
$$r-i = 1.127 \ (r-i)_c$$
$$i-z = 0.925 \ (i-z)_c \quad .$$

The subscript "c" indicates the natural CCD magnitudes, and the left-hand side represents the adopted griz system magnitudes. These magnitudes are equal to the original Thuan-Gunn magnitudes for objects whose spectra are smooth. To understand how galaxies behave with the CCD system, scans of NGC 4889 and the large-aperture composite galaxy of Whitford (1971) were numerically convolved with the photoelectric and CCD response functions. The resulting "natural" CCD colors were then transformed with the linear transformations appropriate to placing the standards on the

photoelectric system. The transformed CCD r agreed with the photoelectric r to better than 1% for galaxies with z < 0.30. The (g-r) values, however, were discrepant; the photoelectric color was over 0.15 mag redder than the transformed CCD value at z = 0.2. This is due to the changed character of the g filter. In the photoelectric system the filter has $\hat{\lambda}_g$ = 4947 Å and reaches down to 4200 Å. The CCD g response is basically dead by 4500 Å, and $\hat{\lambda}_g$ = 5242 Å. As the galaxy redshift increases, the photoelectric g sees the "break" much earlier than the CCD g does, thus the photoelectric colors turn redder. Our system is this linearly transformed "natural" system. It has standard photometry negligibly different from the photoelectric system for the subdwarf standards by which that system is defined. To calculate colors on it from scans, however, one produces natural magnitudes with the CCD response functions and then applies the above transformations. Predicted k-corrections were produced in this fashion and are given in Table 4. Photometric transformations for brightest cluster galaxies (at rest) are

$$g = r + 0.47 \qquad B = g + 0.68$$
$$r = i + 0.31 \qquad B = V + 0.97$$
$$i = z + 0.22 \qquad J = V + 0.34$$
$$r = R + 0.3 \qquad J = F + 1.1$$

(The J and F relations are from Oemler [1974].)

The galaxies of HGT were placed on the CCD system by taking the r magnitude (with no change) and setting (g-r) = (g-r)HGT + $\Delta(z)$, where $\Delta(z)$ was found from the previously mentioned scans. The reduced absolute magnitudes for these galaxies are given in Table 5. Nineteen galaxies from GO were also put on the CCD system (adopting g_I = VI + 0.27 from the scan of NGC 4889), their magnitudes can be found in Table 6. Figure 6 shows the observed (g-r) colors vs. the predictions of Table 4. It is clear that the points are consistent with the existence of a standard galaxy for z < 0.25.

V. DISCUSSION

Figure 6, along with a similar plot in KSW, presents reassuring evidence that one can use the k-correction procedure with a good deal of confidence. For the HGT and the richness clusters the average difference between the observed (g-r) and the calculated one is +0.008 magnitudes with a standard deviation of 0.055 (this is reflected in a discrepancy of similar size between $g_I(g)$ and $g_I(r)$). There appears to be no color evolution in giant ellipticals out to a redshift of 0.25 (~4 billion years).

Table 7 lists the mean absolute magnitudes for the three 16-kpc samples. All three indicate that the luminosity of the brightest cluster galaxy has a dispersion of about

0.35 mag, which is similar to the value of SKW and KSW.
Tables 8 and 9 and Figure 6 and 7 present the results of
binning the HGT and richness samples into richness and
Bautz-Morgan classes (BM types from LVDB).

Our data support the tentative conclusions of HGT of
an approximately 0.1 magnitude per richness class brightening
of the brightest galaxy from richness class 0 to richness
class 3. The richness 4 clusters (plus the one richness 5
one, Abell 665) do not continue this trend, however; their
average falls 0.2 magnitudes below that of richness class 3.
This result is significant at the 99% level. SKW found, on
the basis of a sample some two and a half times smaller, a
change of only 0.05 magnitudes per class. It is unlikely
to be the result of the difference of aperture sizes used,
since the larger aperture of SKW (36 kpc radius) should be
more subject to contamination in the rich clusters which
would accentuate the brightening with richness class.

It is important to note that the conclusion regarding
the richness effect is not cosmology-independent, since the
mean redshift in our sample increases so markedly with rich-
ness. The observed change of 0.3 magnitudes from richness
0 to richness 3 over a range in mean redshift from 0.079 to
0.146, however, requires a q_o in excess of 7 if the effect
is entirely cosmological in origin. Alternatively, an un-
certainty of 0.5 in q_o corresponds to an uncertainty of only

7% in the richness correction.

Adopting 21.11 for the mean reduced absolute magnitude for brightest cluster galaxies, we arrive at BM corrections of -0.28, -0.13, -0.06, +0.02, and +0.19 mag for BM classes I through III (vs. -0.37, -0.13, -0.04, +0.07, and +0.19 for KSW). The larger KSW correction for BM I is likely due to their use of a larger aperture. BM I clusters tend to harbor cD galaxies, and their large envelopes would explain their brightening relative to normal ellipticals as one moved to larger apertures. The Bautz-Morgan classes are distributed fairly homogeneously with distance, as indicated in Table 9, so the conclusions about the BM correction are essentially independent of the cosmological model.

Although both cluster richness and Bautz-Morgan class have definite relations with the luminosity of brightest cluster galaxies, removing their effects does not greatly reduce the cosmic scatter. The clusters of HGT and this paper have an uncorrected dispersion of 0.34. mag Application of the deduced richness and Bautz-Morgan corrections reduce this value to 0.32 and 0.30 mag respectively, while the dispersion becomes 0.29 mag if both effects are corrected for. Hoessel (1980) found that both these corrections are subsumed in a structural correction which can be calculated from surface photometry of the galaxy itself, and which arises in a natural way from dynamical evolution.

We will investigate this "α-correction" further in the second paper in this series.

The classic Hubble diagram (apparent magnitude vs. redshift), while quite illustrative of some relativistic effects, leaves something to be desired when one wishes to emphasize the geometric effects of various world models. We chose to plot the reduced absolute magnitude against a redshift related quantity. The motivation for this choice is easy to understand. The calculated absolute magnitudes assume a given world model; if we have selected the correct one and brightest cluster galaxies are standard candles, the points will lie on a horizontal line. The reduced absolute magnitudes described in this paper will be the ordinate. The abcissa is

$$x = \log\left[\frac{2(1+z - \sqrt{1+z})}{z}\right] = \log\left[\frac{Z_{1/2}(z)}{Z_1(z)}\right] .$$

The advantages of this selection are apparent in Figure 9, which displays the behavior of reduced absolute magnitudes as a function of z and q_0. The "edge" of the universe is the right-hand side ($z = \infty$ and $x = \log 2$). Note the remarkable linearity of the models. Both the $q_0 = 0.5$ and $q_0 = 1.0$ models are precisely linear. The intercepts at $z = \infty$ are $5 \log(1/2\, q_0)$ (relative to the $q_0 = 0.5$ line, because $Z_q(\infty) = 1/q_0$). The models with q_0 greater than 0.5 (closed universes) lie above our standard $q_0 = 0.5$ line

because we have used too large a luminosity distance in calculating the absolute magnitude; the reverse applies to the open models.

Another feature is the clear presentation of the aperture correction (see GO and Hoessel 1980). If q_o does not equal 0.5, we are no longer measuring the same metric diameter at different redshifts. Defining

$$\alpha = \frac{\ln L}{\ln r}\Big|_{r=r_o}$$

GO showed that the sensitivity to q_o is reduced by the factor $(1-\alpha/2)$.

This appears naturally in our Hubble diagram, for the deviation from the horizontal ($q_o = 0.5$) line is

$$\mu_{q_o} - \mu_{1/2} = \Delta\mu = (5-2.5\alpha) \log\left[\frac{z_{1/2}}{z_{q_o}}\right]$$

or

$$(5-2.5\alpha)(1-2q_o)x \quad \text{for small } x \quad .$$

The rapidity with which the various curves deviate from the $q_o = 0.5$ line is linear in α, as the above expression shows. If galaxies were point sources ($\alpha = 0$) there is no aperture correction. The sensitivity of the test vanishes for $\alpha = 2$ (constant surface brightness) since there is no cosmological information in surface brightness. We shall show in the following paper in the series that the mean α for our sample is about 0.7, a bit larger than that found by Hoessel (1980)

but the same as that used by GO; the aperture correction thus reduces the sensitivity to q_0 by roughly a factor of 1/3.

In Figure 10 we have plotted the galaxies of GO, HGT, and the richness sample on this modified Hubble diagram. Also shown are some world models with $\alpha = 0.7$ and $\langle \mu \rangle$ of 21.14 from the nearby complete sample of HGT. The $q_0 = -0.5$ model is unphysical, and was obtained simply by evaluating the analytic expression for $Z_{q_0}(z)$ for that value of q_0. The first-order cosmological effects are dependent on q_0 alone, and the curve shown should be accurate for small redshifts.

It is clear that one can say little of cosmological interest on the basis of data shown; nor was that the object of acquiring data on this sample. The low-redshift end of the Hubble diagram is now, however, determined about as well as is possible without the expenditure of enormous effort. The present sample could be enlarged about a factor of three without exhausting the Abell catalog within our selection criteria. To go further would inevitably lead to increasing the mean redshift of the sample, thus contaminating the low-redshift sample with cosmological effects.

TABLE 1

DATA ON THE RICHNESS SAMPLE

Abell	R.A. 1950.0	Dec	l	b	R	D	BM	z		r	g-r	Gal Abs	G I	RAM
22	00 18 12	-25 59 20	42.9	-83.0	3	6	I	0.1432	*	16.44	+0.67	0.02	16.58	20.88
34	00 24 47	-09 04 57	104.5	-70.8	2	6	I-II	0.0410		15.47	+0.51	0.05	15.77	22.73
42	00 26 07	-23 55 04	65.8	-83.8	3	5	I	0.1087		15.87	+0.64	0.02	16.09	20.97
43	00 26 17	+17 18 29	115.3	-45.0	0	4	III:	0.1114		16.64	+0.73	0.04	16.87	21.69
77	00 37 48	+29 16 52	120.1	-33.3	1	5	I:	0.0719		15.00	+0.63	0.09	15.24	20.99
98	00 43 52	+20 11 45	121.4	-42.4	3	5	II-III:	0.1033	(1,2)	15.84	+0.69	0.04	16.08	21.06
136	01 01 33	+24 48 57	126.6	-37.7	2	6	I	0.1569		16.57	+0.79	0.09	16.64	20.74
140	01 02 09	-24 14 35	166.9	-85.7	3	6	II:	0.1591		16.44	+0.72	0.02	16.55	20.63
160	01 10 21	+15 13 39	130.6	-47.1	0	4	III	0.0442		14.30	+0.64	0.06	14.67	21.47
186	01 20 19	-10 39 39	148.3	-71.7	1	5	II	0.1066		15.47	+0.64	0.05	15.67	20.59
279	01 53 43	+00 48 07	154.5	-57.8	1	5	I-II	0.0797		15.12	+0.61	0.02	15.41	20.94
326	02 11 12	-07 22 49	171.0	-62.1	0	5	III:	0.0558	*	14.63	+0.54	0.02	14.94	21.24
410	03 01 28	+03 32 13	174.1	-45.6	1	5	II	0.0897		16.59	+0.71	0.13	16.76	22.04
423	03 08 55	-12 19 12	195.3	-54.0	2	5	III	0.0797	*	15.54	+0.65	0.09	15.77	21.30
458	03 43 52	-24 27 15	218.9	-50.8	2	5	I-II:	0.1050		15.73	+0.67	0.02	15.98	20.93
545	05 30 05	-11 34 40	214.6	-22.7	4	5	III	0.154	(2)	17.81	+0.88	0.49	17.46	21.60
655	08 21 57	+47 17 47	172.7	+35.2	3	5	I-II	0.1245	(3)	15.64	+0.77	0.07	15.82	20.41
665	08 26 18	+66 00 41	149.8	+34.7	5	6	III:	0.1832	(1)	17.34	+0.88	0.06	17.37	21.15
733	08 57 48	+55 51 13	161.5	+40.3	1	6	I:	0.1159		15.72	+0.75	0.02	15.97	20.71
777	09 23 32	+78 30 19	133.8	+34.2	4	5	III	0.224	(3)	17.91	+0.90	0.00	17.87	21.23
819	09 29 37	+09 54 14	223.5	+40.0	0	5	III	0.0759		15.11	+0.67	0.04	15.42	21.05
858	09 40 41	+06 08 33	229.6	+40.6	0	5	II	0.0881		15.54	+0.75	0.04	15.84	21.17
882	09 48 43	+08 33 14	228.1	+43.5	0	5	I	0.1408		16.43	+0.69	0.03	16.58	20.91
910	09 59 12	+67 24 53	143.6	+42.6	4	6	II-III	0.2055		17.54	+0.95	0.06	17.51	21.05
1018	10 25 19	+17 49 23	221.5	+55.6	1	6	III	0.297	P	18.49	+1.09	0.04	18.24	21.02
1081	10 42 04	+35 47 29	187.7	+61.0	2	5	II-III	0.1588		16.34	+0.74	0.02	16.46	20.54
1123	10 52 59	+75 46 27	131.9	+39.6	2	5	III	0.1235		16.27	+0.79	0.07	16.46	21.06
1149	11 00 23	+07 52 18	245.1	+57.7	0	4	III	0.0710		15.13	+0.63	0.04	15.43	21.21
1155	11 01 55	+35 29 52	186.7	+65.9	0	5	II-III:	0.0738		15.56	+0.60	0.02	15.86	21.56
1169	11 05 01	+44 10 55	167.3	+63.3	1	5	III:	0.0582		15.26	+0.58	0.00	15.62	21.02
1170	11 04 56	+08 15 56	246.0	+58.0	2	6	III	0.1620		16.99	+0.82	0.04	17.10	21.13
1190	11 08 58	+41 07 06	172.0	+65.4	2	5	II:	0.0794		15.36	+0.63	0.00	15.69	21.23
1224	11 18 02	+36 44 41	181.3	+68.7	1	6	II	0.2897		18.32	+1.37	0.02	18.11	20.92
1227	11 18 52	+48 19 14	156.8	+62.8	2	5	II-III	0.1117		16.08	+0.67	0.00	16.33	21.15
1235	11 20 39	+19 52 40	228.7	+68.5	2	5	II:	0.1036		15.90	+0.77	0.00	16.22	21.19
1264	11 24 25	+17 24 14	235.7	+68.1	2	5	III:	0.1267		16.57	+0.68	0.02	16.76	21.31
1346	11 38 38	+06 00 44	261.8	+62.9	1	5	II-III:	0.0970		15.82	+0.63	0.02	16.07	21.19
1373	11 42 58	-02 10 26	272.1	+56.4	2	5	III	0.1314		17.12	+0.66	0.04	17.27	21.75
1401	11 49 13	+37 32 20	170.4	+73.9	3	5	III	0.1670		17.58	+0.75	0.00	17.70	21.67
1413	11 52 45	+23 40 49	226.2	+76.8	3	5	I	0.1431		16.16	+0.83	0.02	16.35	20.65
1461	12 01 53	+42 50 24	151.7	+71.8	0	5	II-III:	0.0538		14.85	+0.56	0.00	15.21	21.58
1514	12 15 26	+20 57 01	251.3	+80.0	3	6	III	0.1995		17.51	+0.87	0.04	17.51	21.11
1548	12 26 24	+19 42 29	267.9	+80.7	3	6	I-II	0.1608		16.54	+0.83	0.05	16.65	20.70
1559	12 31 06	+67 24 19	125.7	+49.9	1	5	II	0.1042		15.43	+0.67	0.01	15.69	20.66
1589	12 38 49	+18 50 59	287.2	+81.1	0	5	II-III:	0.0699		14.78	+0.63	0.02	15.10	20.92
1630	12 49 21	+04 50 57	303.2	+67.5	1	5	II-III	0.0649		14.88	+0.65	0.02	15.24	21.21

TABLE 1 (Continued)

DATA ON THE RICHNESS SAMPLE

Abell	R.A.	1950.0			Dec		l	b	R	D	BM	z		r	g-r	Gal Abs	G I	RAM
1674	13	00	52	+67	44	53	121.3	+49.6	3	5	II-III	0.1055		16.08	+0.66	0.01	16.33	21.27
1689	13	08	57	-01	04	30	313.4	+61.1	4	6	II-III	0.1784	*	17.07	+0.84	0.02	17.15	20.98
1738	13	23	16	+57	51	36	114.2	+59.0	2	5	I:	0.1146		15.55	+0.68	0.00	15.80	20.56
1785	13	42	42	+38	22	53	80.8	+74.3	2	5	I-II	0.0792		15.41	+0.62	0.01	15.73	21.27
1825	13	55	40	+20	52	36	13.4	+73.5	0	5	III	0.0632		15.00	+0.55	0.03	15.29	21.32
1827	13	55	47	+21	54	59	16.8	+73.9	1	5	III:	0.0668		14.87	+0.66	0.02	15.22	21.14
1800	14	10	36	+22	33	10	22.8	+70.9	1	5	III	0.1413		16.40	+0.70	0.02	16.56	20.88
1918	14	24	08	+63	25	06	106.4	+50.8	3	6	I-II	0.1415		16.34	+0.75	0.00	16.53	20.85
1921	14	27	05	+23	19	57	28.1	+67.5	1	5	II	0.1352		16.56	+0.75	0.03	16.75	21.16
1934	14	31	12	+29	40	20	44.9	+67.5	3	6	II	0.2195	P	16.87	+0.86	0.00	16.84	20.24
1940	14	33	55	+55	20	53	96.1	+56.2	3	5	III	0.1393		16.37	+0.76	0.00	16.57	20.92
1984	14	50	24	+28	10	06	41.8	+63.2	2	5	II	0.1231	*	16.00	+0.77	0.04	16.21	20.82
2036	15	08	52	+18	13	14	24.6	+56.6	0	4	II-III	0.1163		16.24	+0.65	0.04	16.43	21.16
2110	15	37	51	+30	52	29	48.8	+53.2	1	5	I-II	0.0978		15.70	+0.67	0.04	15.94	21.04
2125	15	40	48	+66	25	23	101.1	+43.0	4	6	II-III	0.2465	(3)	17.46	+1.04	0.04	17.33	20.50
2104	16	19	46	+50	20	25	77.9	+44.3	0	4	III:	0.0550		15.20	+0.59	0.00	15.57	21.90
2218	16	35	40	+66	19	00	97.8	+38.1	4	6	II:	0.1710	(3)	17.21	+0.79	0.04	17.28	21.21
2244	17	00	53	+34	08	06	56.8	+36.3	2	5	I-II:	0.0970		15.50	+0.69	0.04	15.75	20.07
2246	17	00	26	+64	17	28	94.4	+36.2	3	6	II-III	0.225	P	17.55	+0.92	0.02	17.49	20.84
2263	17	21	12	+26	55	59	49.7	+30.3	0	5	I	0.1051		16.29	+0.84	0.08	16.54	21.49
2283	17	44	54	+69	42	43	100.1	+31.1	1	6	I	0.1830		16.94	+0.86	0.08	16.94	20.72
2377	21	43	22	-10	19	30	45.1	-43.2	2	5	II	0.0808		15.53	+0.62	0.06	15.77	21.28
2388	21	51	11	+08	00	49	65.9	-34.3	0	5	II-III	0.0615		15.26	+0.62	0.09	15.52	21.61
2400	21	55	02	-11	38	57	45.4	-46.4	1	5	II:	0.0881		15.50	+0.69	0.06	15.75	21.08
2420	22	07	39	-12	25	04	46.5	-49.5	2	5	I	0.0838		15.26	+0.60	0.06	15.40	20.91
2440	22	21	23	-01	50	12	62.5	-46.4	0	4	II	0.0904		15.61	+0.68	0.07	15.85	21.11
2459	22	34	06	-15	59	50	46.0	-56.8	0	4	III	0.0736		15.34	+0.65	0.07	15.61	21.31
2462	22	36	30	-17	35	52	43.8	-58.0	0	5	I-II:	0.0755	P	15.05	+0.67	0.05	15.35	21.00
2469	22	38	07	+12	03	07	79.9	-39.4	1	5	II:	0.0656		15.40	+0.64	0.09	15.66	21.61
2496	22	48	17	-16	40	20	47.7	-60.1	2	5	I-II	0.1233		15.82	+0.67	0.04	15.99	20.60
2521	22	59	32	-22	17	35	38.6	-64.7	2	5	I	0.1359	*	16.06	+0.72	0.03	16.24	20.64
2554	23	09	41	-21	46	36	41.5	-66.8	3	5	II:	0.1060	(3)	15.89	+0.63	0.03	16.11	21.04
2559	23	10	27	-13	53	29	58.5	-63.4	1	5	I-II	0.0796		15.28	+0.60	0.03	15.55	21.09
2597	23	22	45	-12	23	57	65.4	-64.9	0	5	III	0.0826		15.55	+0.58	0.03	15.81	21.26
2622	23	32	32	+27	05	42	102.8	-32.5	0	4	II-III:	0.0621		14.69	+0.63	0.08	14.96	21.03
2645	23	38	43	-09	17	44	77.2	-65.5	4	6	II-III:	0.246	(3)	17.76	+1.10	0.04	17.64	20.81
2686	23	56	45	-21	03	34	58.2	-76.5	1	5	II	0.1124	R	16.04	+0.70	0.02	16.28	21.08
2694	23	59	50	+08	07	13	102.7	-52.5	3	5	I:	0.0958		15.14	+0.55	0.08	15.28	20.43

*) Redshift is mean of two close, roughly equal components

P) Redshift obtained with PFUEI/CCD
R) Redshift obtained with Reticon

References

1) Sargent 1973
2) Sandage, Kristian, and Westphal 1976
3) Kristian, Sandage, and Westphal 1978

TABLE 2

SPECTROSCOPIC DATA SYSTEMS

Telescope	Detector	Dispersion	Pixel size	Resolution	Clusters
200"	SIT	295 Å mm^{-1}	23 μ	9 Å	63
200"	SIT	140 Å mm^{-1}	23 μ	5 Å	7
200"	CCD	435 Å mm^{-1}	15 μ	25 Å	1
60"	CCD	435 Å mm^{-1}	15 μ	35 Å	3
200"	Reticon	17 Å mm^{-1}	30 μ	2 Å	1
Literature					9

TABLE 3

CLUSTERS WITH MORE THAN ONE GALAXY REDSHIFT

Cluster	Galaxy	cz	Cluster	Galaxy	cz
22	N	43140	1373	G1	39390
	S	42690		8' PA 43	36150
160	G1	13260	1689	E	52490
	4' PA 70	13150		W	54470
326	NW	16380	1880	G1	42340
	SE	17080		10' PA 25	46620
423	E	23760	1921	G1	40520
	W	23980		30" E	41740
545	G1	46170	1934	G1	65800
	35" PA 160	48360		5" W	66310
				38" W	65220
882	G1	42210	1984	N	36080
	10" W	42290		S	37740
910	G1	61610	2244	G1	29330
	20" W	62290		40" E	28280
1123	G1	37040	2521	E	41300
	8" E	36500		W	40130

TABLE 4

FILTER REDSHIFT CORRECTIONS k(z)

Redshift	g	r	i	z
0.00	0.00	0.00	0.00	0.00
0.02	0.05	0.02	0.02	0.02
0.04	0.10	0.04	0.04	0.04
0.06	0.16	0.05	0.06	0.06
0.08	0.21	0.07	0.08	0.08
0.10	0.26	0.09	0.09	0.10
0.12	0.32	0.12	0.11	0.11
0.14	0.38	0.14	0.13	0.12
0.16	0.45	0.16	0.15	0.14
0.18	0.52	0.20	0.16	0.15
0.20	0.61	0.24	0.18	0.17
0.22	0.72	0.27	0.19	0.18
0.24	0.83	0.31	0.21	0.20
0.26	0.95	0.34	0.22	0.21
0.28	1.07	0.37	0.24	0.23
0.30	1.18	0.40	0.26	0.25
0.32	1.28	0.43	0.28	0.26
0.34	1.40	0.45	0.30	0.28
0.36	1.51	0.48	0.32	0.30
0.38	1.65	0.51	0.35	0.32
0.40	1.74	0.55	0.37	0.33
0.42	1.87	0.59	0.41	0.35
0.44	1.93	0.65	0.43	0.36
0.46	2.03	0.71	0.46	0.37
0.48	2.09	0.76	0.47	0.38
0.50	2.16	0.82	0.49	0.39
0.52	2.23	0.88	0.50	0.40
0.54	2.28	0.95	0.52	0.41
0.56	2.34	1.03	0.53	0.42
0.58	2.39	1.10	0.54	0.43
0.60	2.43	1.19	0.56	0.44
0.62		1.27	0.57	0.46
0.64		1.34	0.60	0.48
0.66		1.42	0.63	0.50
0.68		1.49	0.65	0.52
0.70		1.57	0.69	0.53
0.72		1.65	0.72	0.54
0.74		1.72	0.75	0.55
0.76		1.80	0.79	0.56
0.78		1.86	0.82	0.57
0.80		1.92	0.86	0.58
0.82		1.98	0.91	0.60
0.84		2.00	0.97	0.62
0.86		2.06	1.03	0.65
0.88		2.11	1.10	0.68
0.90		2.16	1.17	0.71
0.92		2.22	1.24	0.74
0.94		2.26	1.30	0.78
0.96		2.30	1.37	0.83
0.98		2.36	1.44	0.87
1.00		2.39	1.50	0.91

TABLE 5

GALAXIES FROM HOESSEL, GUNN, AND THUAN (1980)

Cluster	z	RAM	Cluster	z	RAM	Cluster	z	RAM
21	0.0948	20.63	1216	0.0524	21.53	2022	0.0565	21.16
76	0.0377	21.14	1228	0.0344	21.59	2028	0.0772	20.90
85	0.0556	20.78	1238	0.0716	21.28	2029	0.0777	20.36
88	0.1086	21.10	1254	0.0628	21.39	2040	0.0456	21.71
104	0.0822	21.12	1291	0.0586	21.89	2048	0.0945	20.88
119	0.0446	21.06	1318	0.0189	21.85	2052	0.0351	21.26
147	0.0441	21.54	1364	0.1070	21.13	2061	0.0782	20.73
151	0.0526	20.62	1365	0.0763	21.25	2063	0.0337	21.31
154	0.0612	20.75	1367	0.0205	21.31	2065	0.0722	21.17
166	0.1156	21.57	1377	0.0509	21.31	2067	0.0726	21.56
168	0.0457	21.23	1382	0.1046	21.05	2079	0.0657	20.82
189	0.0349	21.68	1383	0.0598	21.68	2089	0.0743	20.94
193	0.0478	20.90	1399	0.0913	21.41	2092	0.0669	21.45
194	0.0178	20.89	1412	0.0839	21.48	2107	0.0421	20.87
225	0.0692	21.14	1436	0.0646	21.10	2124	0.0671	20.92
246	0.0753	21.59	1468	0.0853	21.35	2142	0.0911	21.30
274	0.1289	20.85	1474	0.0778	21.68	2147	0.0377	21.21
277	0.0947	20.95	1496	0.0961	21.45	2151	0.0360	21.25
389	0.1160	20.90	1541	0.0892	21.05	2152	0.0444	21.32
399	0.0725	21.05	1644	0.0456	21.26	2162	0.0318	21.25
400	0.0231	21.53	1651	0.0842	20.96	2175	0.0978	21.18
401	0.0752	21.05	1656	0.0230	20.67	2197	0.0303	20.75
496	0.0326	21.21	1691	0.0722	20.88	2199	0.0312	20.59
500	0.0666	21.16	1749	0.0562	20.98	2255	0.0747	20.99
514	0.0697	21.34	1767	0.0712	21.00	2256	0.0550	20.58
634	0.0266	21.42	1773	0.0776	20.93	2328	0.1470	20.43
671	0.0497	20.81	1775	0.0718	20.98	2347	0.1196	21.13
779	0.0201	20.92	1793	0.0849	21.34	2382	0.0648	21.44
787	0.1355	20.87	1795	0.0631	21.02	2384	0.0943	21.27
957	0.0437	20.97	1809	0.0788	20.73	2399	0.0587	21.47
978	0.0527	21.05	1831	0.0749	20.80	2410	0.0806	20.97
993	0.0530	20.92	1837	0.0376	21.75	2457	0.0597	20.94
1020	0.0650	21.60	1904	0.0719	20.69	2634	0.0315	20.91
1035	0.0799	20.99	1913	0.0533	21.49	2657	0.0414	22.06
1126	0.0828	20.72	1927	0.0740	21.50	2666	0.0273	20.69
1139	0.0376	21.61	1983	0.0458	21.78	2670	0.0774	20.79
1185	0.0349	20.99	1991	0.0589	21.14	2675	0.0726	21.17
1187	0.0791	20.94	1999	0.1032	21.00	2700	0.0978	20.94
1213	0.0484	21.11	2005	0.1251	20.89			

TABLE 6

GALAXIES FROM GUNN AND OKE (1975)

Cluster	z	RAM
UMa II G1	0.136	21.63
1534 +37 G1	0.153	21.45
Hydra G8+G9	0.202	20.67
1604 +39	0.235	21.56
0308 +16	0.260	21.88
PHL 1093 G2	0.270	21.97
1318 +31	0.270	21.40
3C 323 G1	0.270	21.05
1612 +42	0.275	21.97
1607 +39	0.280	21.23
1021 +04	0.286	21.04
1610 +41	0.300	21.42
0948 +45	0.305	21.41
1049 -09 G1	0.330	21.62
0948 +44	0.361	21.19
1446 +26 G4	0.373	21.41
0024 +16 G1	0.380	20.98
0949 +44	0.385	21.79
3C 295	0.465	20.43

TABLE 7

MEAN REDUCED ABSOLUTE MAGNITUDES

Sample	N	$\langle Z \rangle$	$\langle RAM \rangle$	SIG RAM
HGT 1980	116	0.066	21.14	0.33
THIS PAPER	83	0.121	21.07	0.35
GUNN OKE 1975	19	0.291	21.37	0.42

TABLE 8

RICHNESS   CORRECTIONS

CLASS	OBJECTS	N	\<Z\>	SIG Z	\<RAM\>	SIG RAM
0	HGT 1980	11	0.035	0.011	21.13	0.31
1		82	0.066	0.022	21.19	0.33
2		21	0.076	0.035	20.96	0.32
3		2	0.103	0.036	20.82	0.04
0	THIS PAPER	20	0.079	0.024	21.30	0.27
1		20	0.117	0.067	21.09	0.37
2		19	0.115	0.027	21.02	0.32
3		16	0.146	0.041	20.85	0.35
4		8	0.201	0.035	21.07	0.33
0	TOTAL SAMPLE	31	0.063	0.030	21.24	0.29
1		102	0.076	0.041	21.17	0.33
2		40	0.094	0.037	20.99	0.32
3		18	0.142	0.042	20.85	0.33
4		8	0.201	0.035	21.07	0.33

TABLE 9

BAUTZ-MORGAN CORRECTIONS

CLASS	OBJECTS	N	\<Z\>	SIG Z	\<RAM\>	SIG RAM
I	HGT 1980	13	0.060	0.022	20.89	0.28
I-II		11	0.061	0.024	21.08	0.31
II		23	0.065	0.032	21.00	0.26
II-III		22	0.062	0.021	21.16	0.30
III		44	0.070	0.026	21.29	0.32
I	THIS PAPER	12	0.124	0.032	20.76	0.18
I-II		11	0.106	0.028	20.88	0.24
II		21	0.116	0.055	21.09	0.38
II-III		18	0.138	0.077	21.08	0.31
III		21	0.117	0.052	21.34	0.29
I	TOTAL SAMPLE	25	0.091	0.089	20.83	0.24
I-II		22	0.084	0.194	20.98	0.29
II		44	0.089	0.110	21.05	0.32
II-III		40	0.096	0.119	21.13	0.30
III		65	0.086	0.083	21.30	0.31

REFERENCES

Abell, G. O. 1958, Ap. J. Suppl., 3, 211.

Bautz, L. P., and Morgan, W. W. 1970, Ap. J. (Letters),

162, L149.

Burstein, D., and Heiles, C. 1978, Ap. J., 225, 40.

Dixon, R. S. 1970, Ap. J. Suppl., 20, 1.

Gunn, J. E., Hoessel, J. G., and Oke, J. B. 1982, in

preparation.

Gunn, J. E., and Oke. J. B. 1975, Ap. J., 195, 255 (GO).
Gunn, J. E., and Tinsley, B. M. 1976, Ap. J., 210, 1.
Gunn, J. E., and Westphal, J. A. 1982, preprint.

Hausman , M. A., and Ostriker, J. P. 1978, Ap. J., 224, 320.

Heiles, C. 1975, Astr. Ap. Suppl., 20, 37.

Hoessel, J. G. 1980, Ap. J., 241, 493.

Hoessel, J. G., Gunn, J. E., and Thuan, T. X. 1980, Ap. J.,

241, 486 (HGT).

Humason, M. L., Mayall, N. U., and Sandage, A. R. 1956,

A. J., 61, 97.

Johnson, H. L. 1968, Nebulae and Interstellar Matter, ed.

B. Middlehurst and L. Aller (Chicago and London:

University of Chicago Press), p. 167.

Kristian, J. A., Sandage, A., and Westphal, J. A. 1978,

Ap. J., 221, 383 (KSW).

Leir, A. A., and van den Bergh, S. 1977, Ap. J. Suppl.,

34, 381 (LVDB).

Oemler, A. 1974, Ap. J., 194, 1.

Oke, J. B., and Schild, R. E. 1971, Ap. J., 161, 1015.

Ostriker, J. P., and Tremaine, S. D. 1975, Ap. J. (Letters), 202, L113.

Sandage, A. 1961, Ap. J., 133, 335.

_____. 1973, Ap. J., 183, 711.

Sandage, A., Kristian, J. A., and Westphal, J. A. 1976, Ap. J., 205, 688 (SKW).

Sargent, W. L. W. 1973, Pub. A.S.P., 85, 281.

Sargent, W. L. W., Schechter, P. L., Boksenberg, A., and Shortridge, K. 1977, Ap. J., 212, 326.

Schechter, P. L., and Gunn, J. E. 1979, Ap. J., 229, 472.

Schmidt, M. 1965, Ap. J., 141, 1.

Schneider, D. P. 1982, preprint.

Schneider, D. P., and Gunn, J. E. 1982, preprint.

Schneider, D. P., Gunn, J. E., and Hoessel, J. G. 1982, preprint (Paper II).

Stark, A., and Heiles, C. 1981, Ap. J., in press.

Thuan, T. X., and Gunn, J. E. 1976, Pub. A.S.P., 88, 543.

Tinsley, B. M., and Gunn, J. E. 1976, Ap. J., 206, 525.

Wade, R. A., Hoessel, J. G., Elias, J. H., and Huchra, J. P. 1979, Pub. A.S.P., 91, 35.

Weinberg, S. 1972, Gravitation and Cosmology, (New York: Wiley and Sons).

Whitford, A. E. 1971, Ap. J., 169, 215.

Young, P., Schneider, D. P., and Shectman, S. A. 1981,

   Ap. J., 244, 259.

FIGURE CAPTIONS

Fig. 1. - Six spectra which cover the range of observational conditions. All are on a linear flux scale, with 1 DN = mag 25.0. The data have been rebinned so that there are roughly two points per resolution element. The top four galaxies were observed with the 200" SIT spectrograph. The lower two were acquired with the PFUEI/CCD system; A1018 at the Palomar 60" (4000 seconds), A1934 with the Hale telescope (1000 seconds). See Table 2 for a summary of the different data systems.

Fig. 2. - A histogram of the redshift distribution of the richness sample. The dotted line represents the galaxies in HGT. The correlation of richness with redshift in the richness sample is clear.

Fig. 3. - Comparison of the redshifts from Leir and van den Bergh (1977) [z_L] with those of HGT (+) and the richness sample (x). One solid line is log z = log z_L, the other is the best linear fit: log z = 1.18 log z_L +0.18. The regression line indicates an accuracy in z_L of ~25%. See text for discussion.

Fig. 4. - The transmission function S(ν) for the filters, PFUEI, and one reflection from aluminum of the griz system.

Fig. 5. - Effective wavelengths of the griz filters convolved with the spectrum of NGC 4889. Diagonal lines

represent the positions of the effective wavelength of

g_I (= g at z = 0.0, $\hat{\lambda}_{g_I}$ = 5242 $\overset{\circ}{A}$) and the "break" at 4000 $\overset{\circ}{A}$. This system allows interpolation for g_I up to a redshift of 0.74.

Fig. 6. - Predicted (g-r) colors of first rank cluster galaxies as a function of redshift (from a scan of NGS 4889). Observations of HGT (+) and this paper (x) are plotted. The only correction applied to the data is removal of galactic absorption. The observations fit the prediction quite well; the dispersion is only 0.055 mag.

Fig. 7. - Relation between the reduced absolute magnitude and Abell richness class for HGT (+) and this paper (x). A correction of ~0.1 mag per class represents the data reasonably well.

Fig. 8. - Same as Figure 7 but using Bautz-Morgan class as the abcissa. As the brightest galaxy becomes more dominant, it becomes brighter.

Fig. 9. - The Reduced Absolute Magnitude-Redshift relation for various world models. The right-hand edge corresponds to z = ∞. The lines represent the behavior of standard candles which have q_o = 0.5 RAM's of 21.0. See text for explanation.

Fig. 10. - Hubble diagram for the galaxies of HGT (+), the richness sample (x), and GO ($\Diamond$). Some world models with

appropriate aperture corrections have been drawn in.

Figure   1

Figure 2

Figure 3

Figure 4

$$\lambda_{gal} = \lambda_{g_I}$$

z = 0.742

z = 0.520

z = 0.275

$$\lambda_{gal} = 4000 \text{ Å}$$

z

i

r

g

$\bar{\lambda}(\text{Å})$

Z
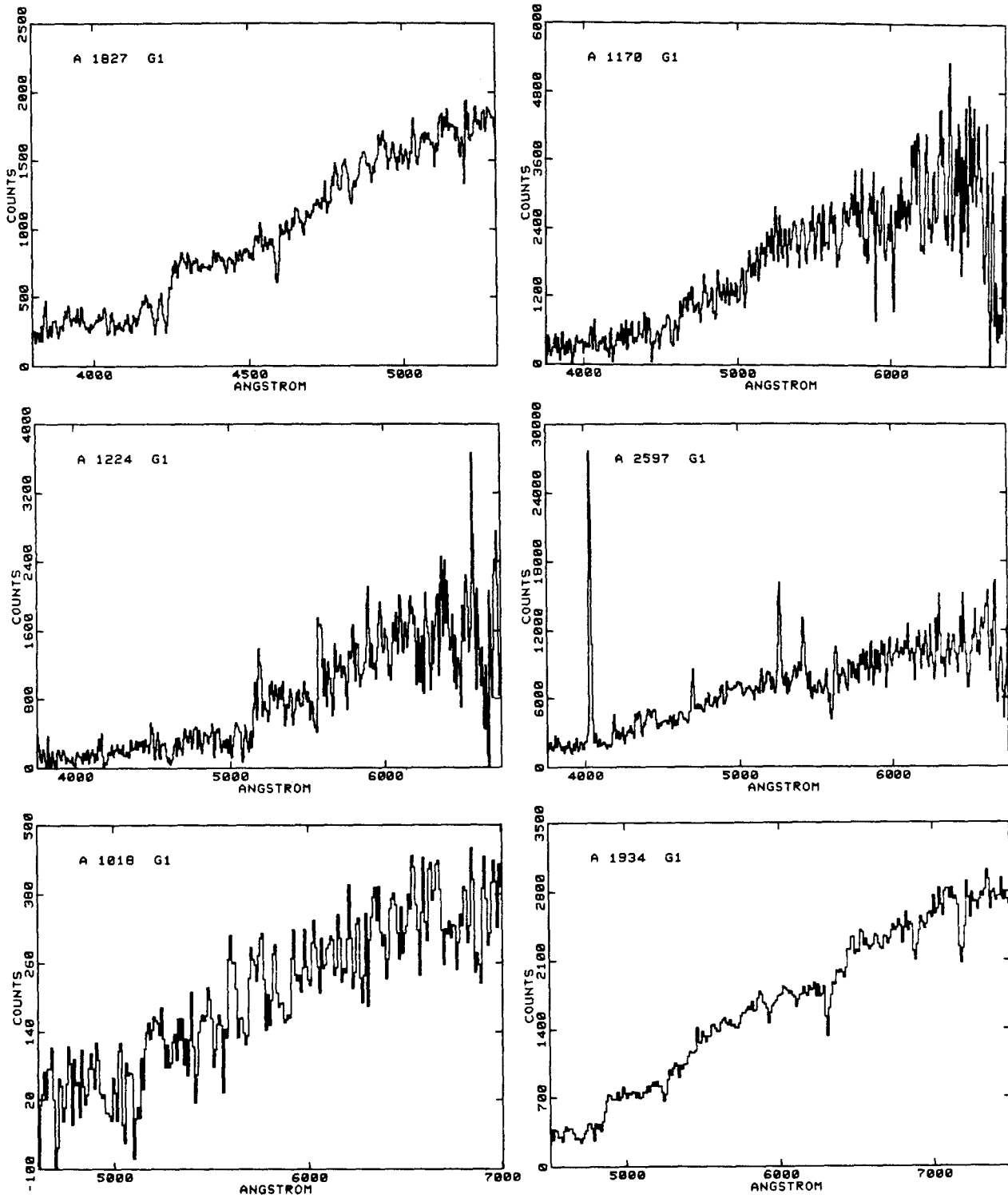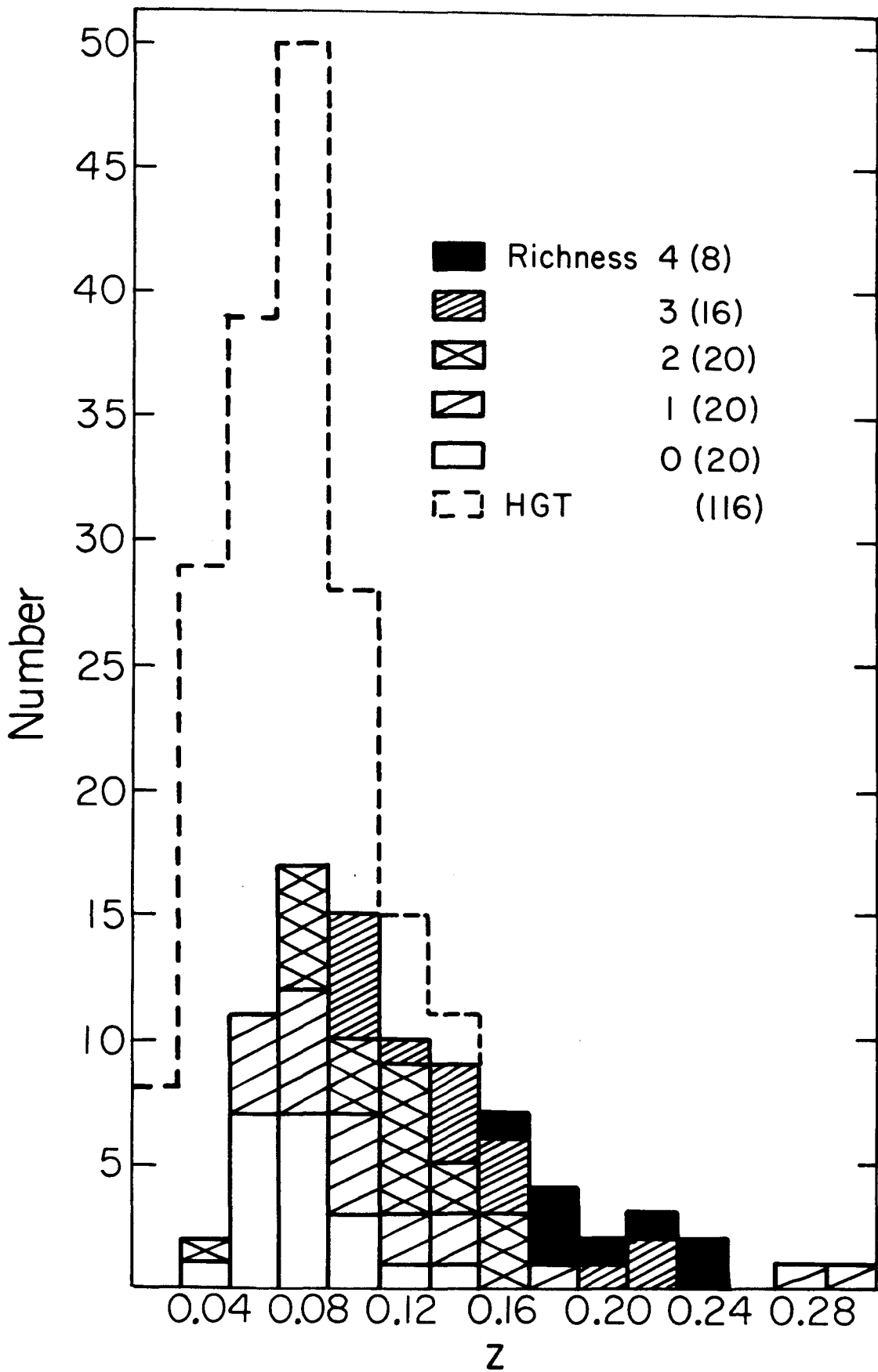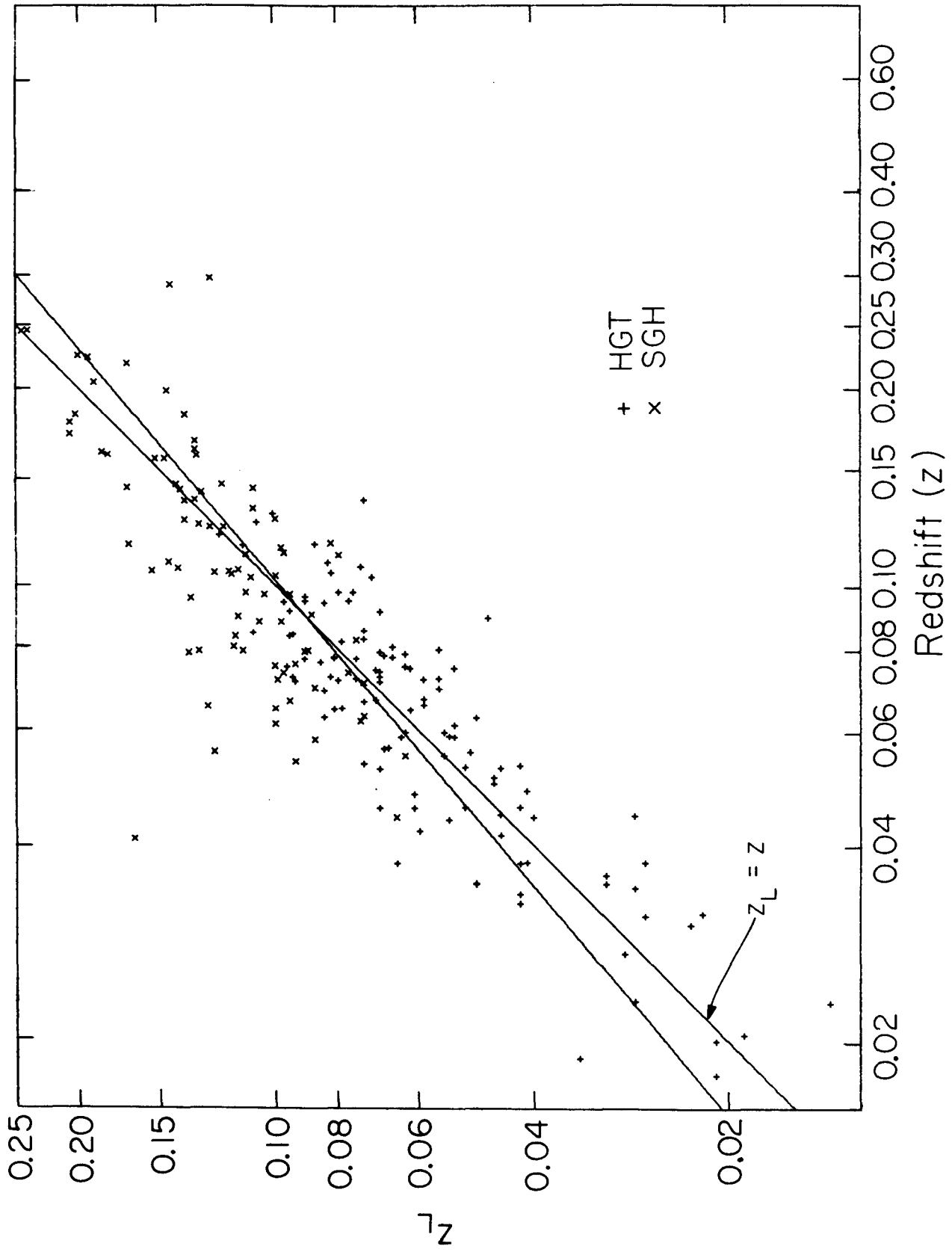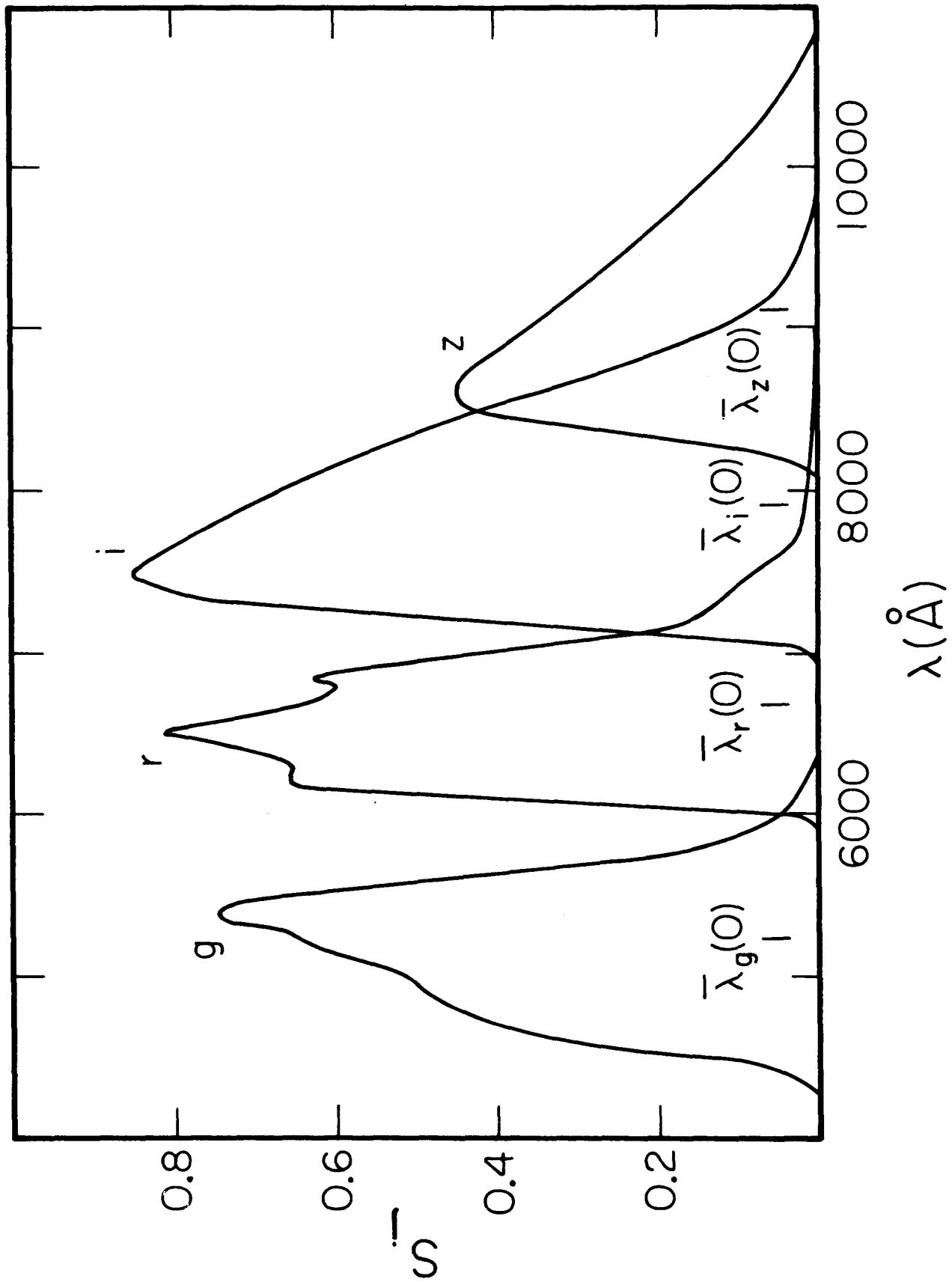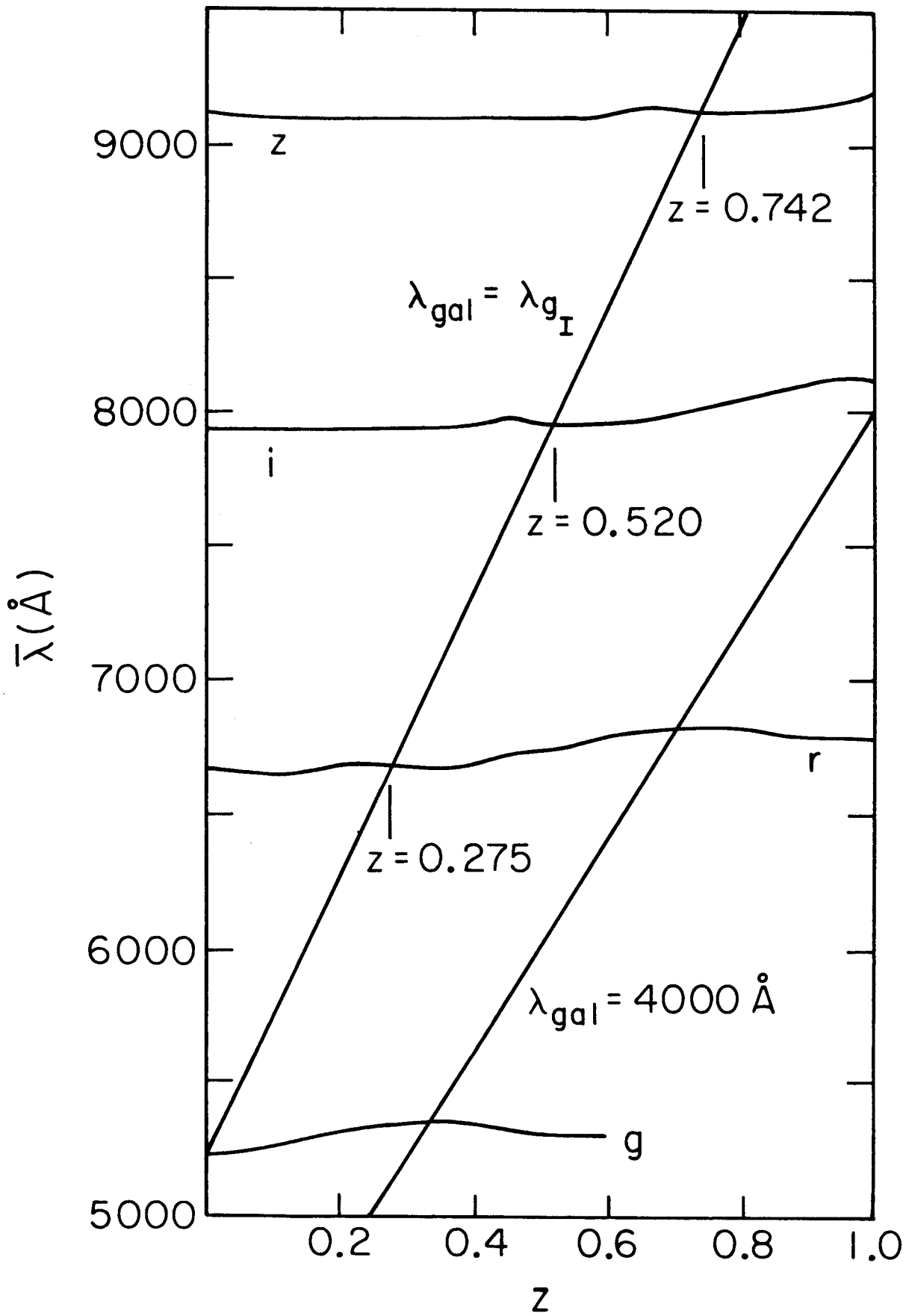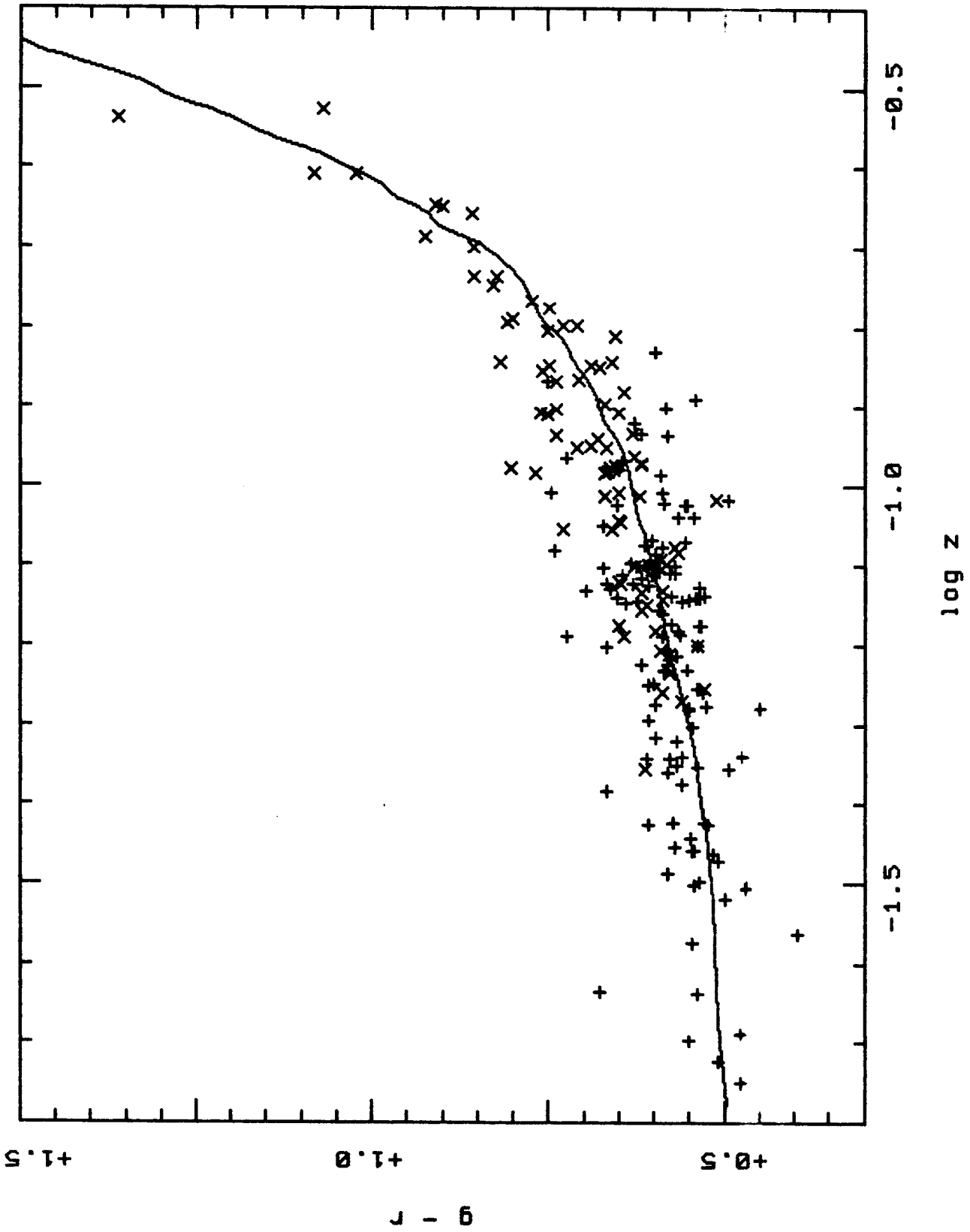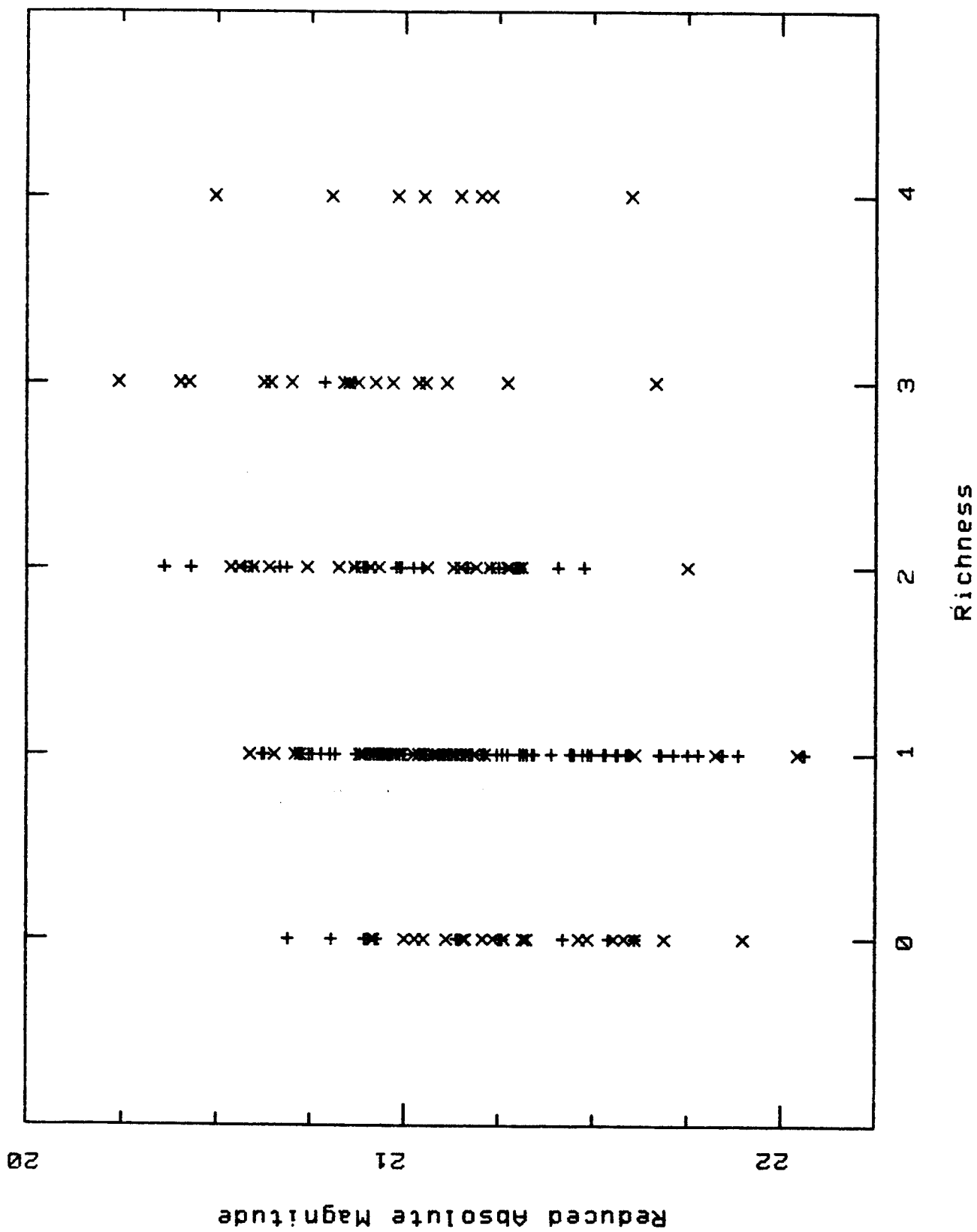
Figure 5
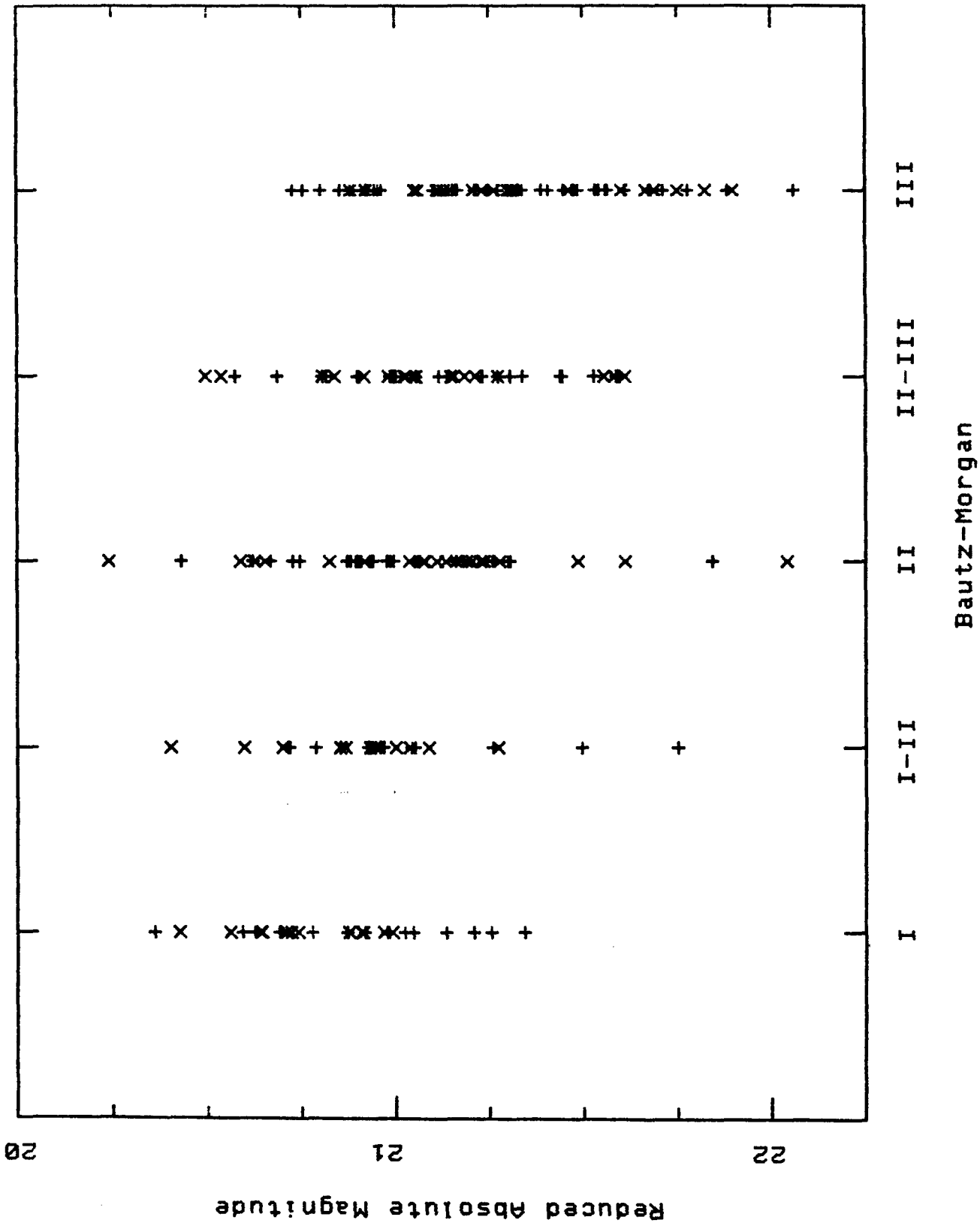
Figure 6
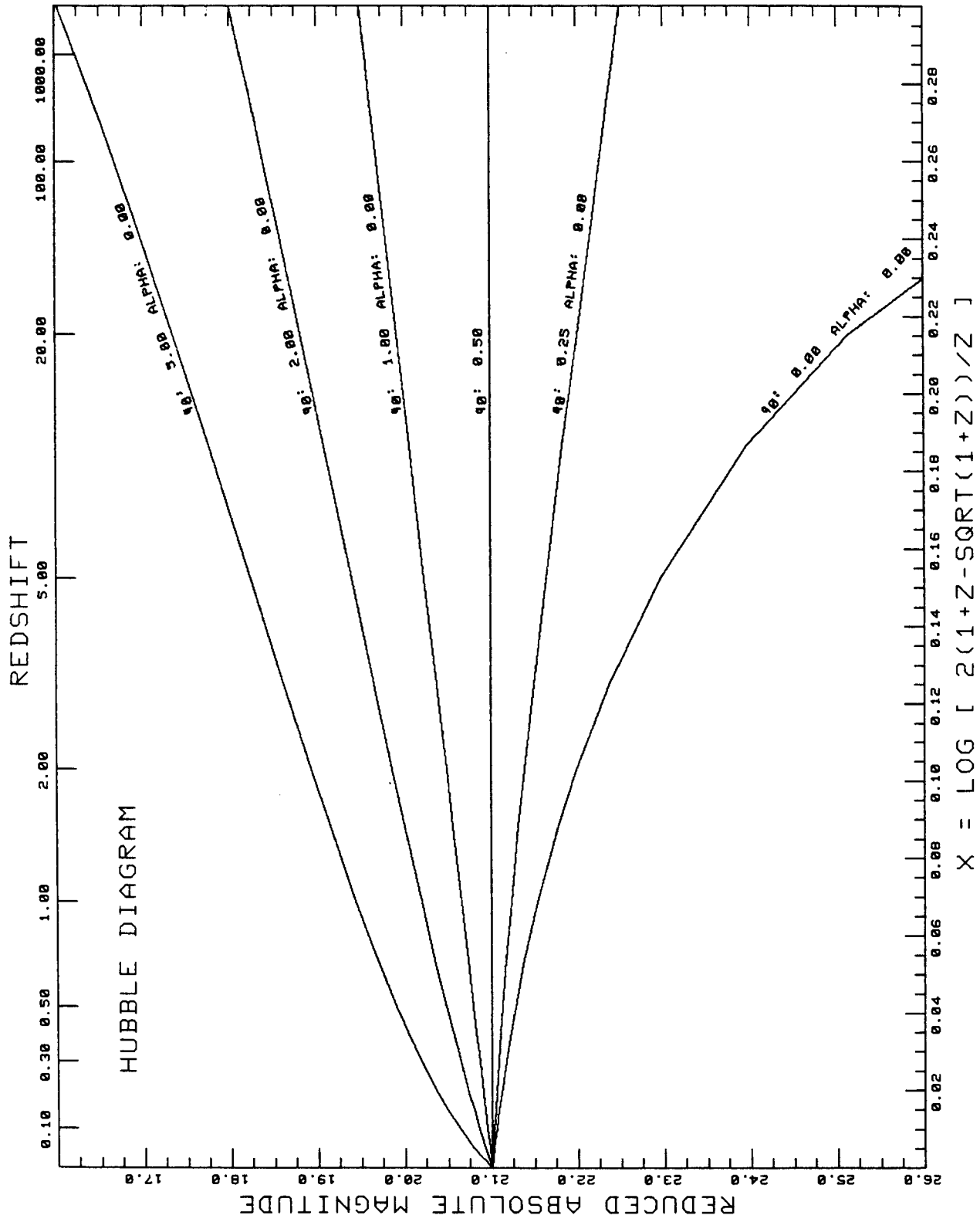
Figure 7
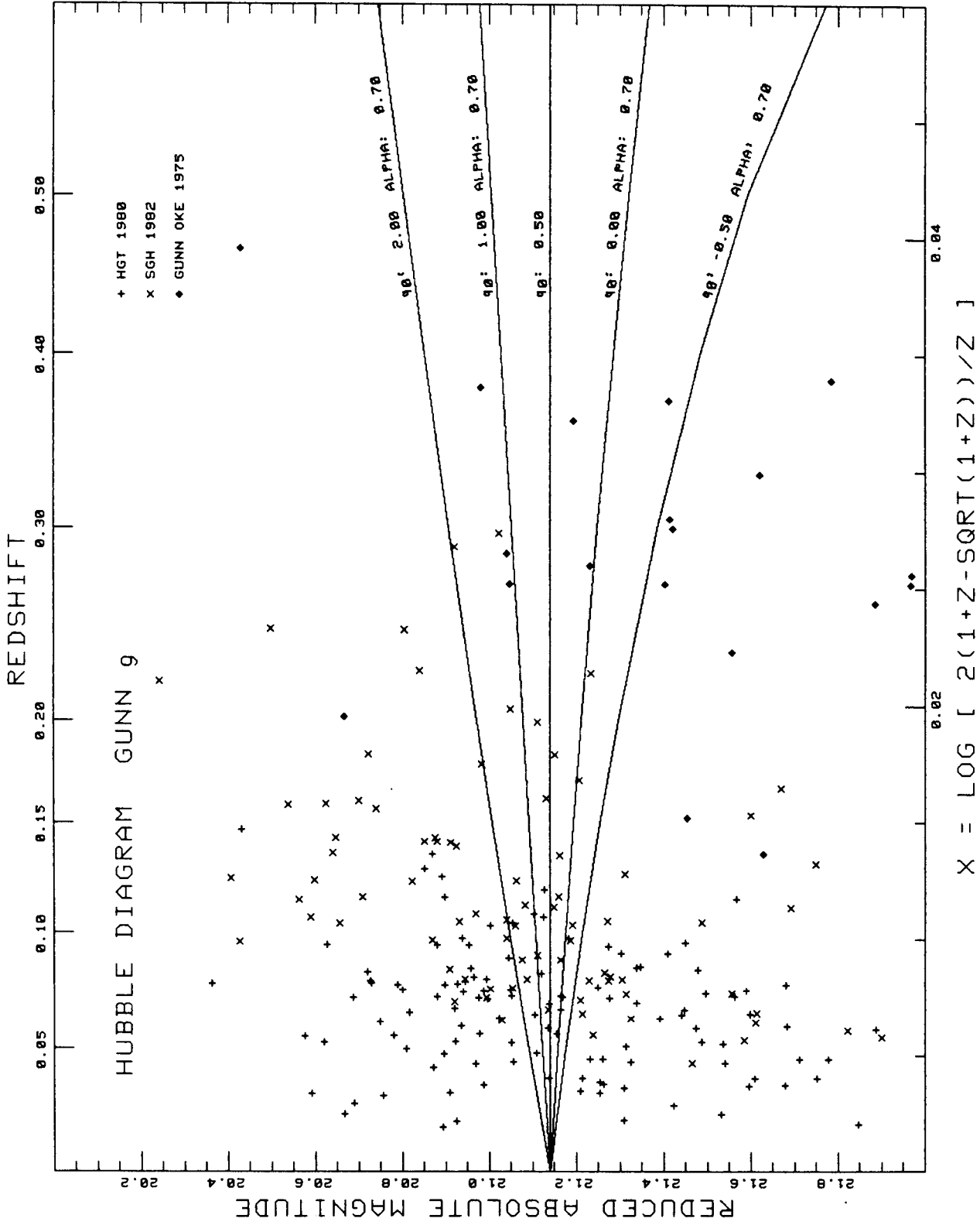
Figure 8

Figure 9

Figure 10

CHAPTER II

SURFACE PHOTOMETRY OF 249 CLUSTER GALAXIES

Authors: Donald P. Schneider, James E. Gunn, and

John G. Hoessel

(Paper II)

I. INTRODUCTION

The best standard candle for observational cosmology
remains the luminosity of the brightest cluster galaxies.
                of
Studies/over 250 relatively nearby clusters ($z < 0.3$) show
that the magnitude of these objects in an aperture of con-
stant metric diameter has a dispersion of only 0.35 mag
(Kristian, Sandage, and Westphal 1978; Schneider, Gunn, and
Hoessel 1982 [hereinafter Paper I]). If this scatter were
the only obstacle confronting cosmologists, the value of
the deceleration parameter, q_o, might now be in hand. Un-
fortunately, galaxies do not have a well-defined cutoff, so
their luminosities depend critically upon the selected
                      metric
aperture. The/aperture size is dependent on q_o, and this
reduces the sensitivity of the test by ~35% (Gunn and Oke
1975). The stellar population of a galaxy will change with
time, which probably leads to a secular decrease of its
luminosity (Tinsley and Gunn 1976). This last effect is
countered to some degree by the likelihood that brightest
cluster galaxies capture other cluster members by dynamical
friction (Ostriker and Tremaine 1975; Hausman and Ostriker
1978; Hoessel 1980).

Hopeful avenues of investigation have been the relation-
ships between the luminosity of the brightest cluster gal-
axy, the cluster morphology, and structure of the brightest
galaxy itself. Sandage and Hardy (1973) found that the

luminosity of the brightest cluster galaxy was very well correlated with Bautz-Morgan type (Bautz and Morgan 1970). In BM I clusters, where there is a very dominant galaxy, the brightest galaxy is considerably brighter than the average first-ranked elliptical, while the second and third brightest members are fainter than their counterparts in BM II and III clusters. In BM III clusters, the brightest galaxy is about 0.5 mag fainter than the typical BM I galaxy. Hausman and Ostriker (1978, hereinafter HO) painted an appealing picture in which dynamical friction plays an important role. Central galaxies which had acquired other cluster members would become more dominant (moving to BM I) and would develop an extended envelope. The investigations of Oemler (1976) and Dressler (1979) found that some aspects of brightest cluster galaxies could be explained by mergers with other cluster members. Hoessel (1980, hereinafter JGH) discovered a good correlation between a galaxy's absolute magnitude and its scale length, and a corresponding BM-size relation. An important result of that investigation was that over one-quarter of the first-ranked galaxies were multiple systems. The high frequency of the multiplicity, together with (uncertain) estimates for the cannibalism time scale, lead to the suggestion that the typical giant has consumed several smaller galaxies, with an average gain in total luminosity of about a tenth of a magnitude per acquisition.

Homologous merger theory (Gunn and Tinsley 1976; HO) pre-
dicts a run of structural length with luminosity very close
to what is observed (JGH), and was able to reduce the cos-
mic dispersion in aperture luminosity to 0.21 magnitude.
These workers argued that the application of this correction gal-
axy by galaxy not only reduces the scatter but corrects in-
dividually for dynamical evolution, so that no uncertain
average correction need be applied.

The small correlation of the luminosity of the brightest
galaxies and of Bautz-Morgan class with cluster richness
(Sandage and Hardy 1973; Sandage, Kristian, and Westphal
1976, and Paper I) might seem at first glance to be difficult
to reconcile with the cannibalism picture, since the densest
clusters would seem likely to have the highest cannibalism
rates. The rates, however, are proportional to the inverse
cube of the velocity dispersion and to only the first power
of the density. For a sequence of clusters of the same
scale and mass-to-light ratio, in fact, the rate decreases
as the inverse square root of the richness. Although the
core radii of clusters are not highly variable (Bahcall 1977),
the frictional rates depend sensitively on them, and it is
not at all obvious which way the effects should go with
richness.

The existence of linear, high-quantum efficiency area
detectors makes these problems much easier to tackle

observationally. Paper I describes a sample of 83 clusters
from Abell's catalog (1958) which are well distributed in
both richness and Bautz-Morgan classes (designated as the
richness sample). This paper will present surface photometry
on the brightest three galaxies within ~250 kpc of the
cluster center. The redshifts for the clusters are given
in Paper I. All dimensions in this paper will be calculated
using $H_O = 60$ km s^{-1} Mpc^{-1} and $q_O = 0.5$. The observations
and reductions, method of fitting the galaxian profiles,
magnitudes of the second and third ranked galaxies in each
cluster, and the results of the profile fitting are pre-
sented in §§ II-V. Section VI compares these results with
previous works and with the cannibalism predictions. The
luminosity functions of the cores of 60 of these clusters
are investigated in Schneider (1982, Paper III).

II. OBSERVATIONS AND REDUCTIONS

All of the data were acquired with the PFUEI (Gunn and
Westphal 1982) operating in its camera mode. The detector
was a low noise Texas Instruments CCD. During the period
of observation (March 1979 to May 1981) the instrumentation
was still in its embryonic stage; as a consequence the quality
of the data differs considerably from cluster to cluster.
Four different CCD's were used; their properties and the number
of clusters taken with each are listed in Table 1. All but
four clusters were done with the Palomar 1.5-m, the others

(410, 777, 1934, and 2125) were obtained on the Hale tele-
scope. The results discussed in this paper are based on a
red exposure (see Paper I for the photometric calibration
procedure) centered on the brightest cluster galaxy (Table 1
in Paper I). The image scales of 0.56"/pixel (1.5-m) and
0.42"/pixel (5-m) yielded pictures which were 4.5' and 3.5'
on a side. The exposures ranged from a low of 300 seconds
on the 1.5-m up to 600 seconds on the 5-m. Attempts were
made to obtain "good seeing" (FWHM = 2.35σ of ~1.5") ex-
posures for each cluster. Half of the clusters had these
pictures taken on non-photometric nights; these were later
tied in by comparison with photometric data (see Paper I).
Comparison of the clusters with multi-night photometry
indicates an internal consistency of 0.04 mag. Figure 1
displays the range of conditions under which the observations
were taken. The horizontal axis is the seeing (FWHM) in
arcseconds, the vertical axis is the seeing disk in kpc at
the cluster. The numbers represent exposure times (not a
linear scale, with 1 the worst and 7 the best, see figure
caption). The two diagonal lines display the z = 0.1 and
z = 0.2 tracks; a given cluster must move on a line roughly
parallel to them. The typical cluster has 1.5" and 3 kpc
seeing.

At the beginning and end of each night a series of out
of focus pictures of the illuminated dome (flat fields) were

taken to allow removal of pixel-to-pixel sensitivity variations. Erase frames were taken throughout the night to monitor the bias levels. The dark emission during our exposure times is negligible. In all cases the Poisson noise from the sky was much greater than the readout noise of the device. The pictures were all reduced on the Space Telescope VAX 11/780 in Pasadena. The erase levels were subtracted from each frame and the cluster data then divided by the mean flat field of that night.

These flattened pictures were then processed by the interactive image processing software package KAREN written by Peter Young, Bob Deverill, and the authors. Minor cosmetic flaws and large scale flat field variations were removed by level fitting (for threshold columns) or interpolation. The seeing was determined from an appropriate star in the field. The seeing profile was constructed using the azimuthally averaged radial profile of the star. This profile was fit to a double gaussian, which has three free parameters: σ_1, σ_2, and the ratio of the power in seeing disks 1 and 2. Tests measuring several stars in the same picture resulted in practically identical seeing parameters, indicating that the focus was nearly constant over the chip. Sky subtraction was accomplished by averaging sky patches around the object. The scatter in these levels indicates accuracies of ~26-27 mag per square arcsecond.

In each cluster we did surface photometry on the
brightest four galaxies within ~250 kpc of the brightest
one. Centering was done for isolated galaxies by peaking
up on the central region. Multiple systems were handled by
finding the 16 kpc radius aperture which contained the
greatest amount of light. Both procedures follow the
definition of the brightest cluster galaxy given in Paper I.
Several galaxies had foreground stars within a few arc-
seconds of the galaxy's center; the stars were removed by
                                    parts of the
interpolating from the surrounding/galaxy. Two clusters,
1235 and 2694, had very bright stars close to the brightest
galaxy; these may significantly affect the deduced profiles.
The azimuthally averaged profile at 0.5 pixel (~0.25")
intervals and the seeing parameters were then deposited onto
a disk file.

III. FITTING PROCEDURE

There have been a number of ways advanced to handle
the effects of seeing on galaxian profiles (for example,
see JGH and Schweitzer [1981]). We have decided
to adopt the following procedure, which we think is well
suited to the CCD data. First, a model was selected which
has an analytic function for the surface brightness (I(r))
as a function of radius, such as those proposed by Hubble
(1930) or de Vaucouleurs (1948). (Hereinafter the latter
will be denoted by GDV models.) This profile is convolved

with the seeing profile, and is then compared with the observations. For a seeing profile composed of a sum of n gaussians

$$I_{obs}(r) = \sum_{i=1}^{n} \frac{A_i}{\sigma_i^2} \int_0^\infty \bar{r} \, I(\bar{r}) \, \exp\left[\frac{-(r-\bar{r})^2}{2\sigma_i^2}\right] \phi\left(\frac{r\bar{r}}{\sigma_i^2}\right) d\bar{r} \qquad (1)$$

where $\phi(x) = \frac{e^{-x}}{2\pi} \int_0^{2\pi} \exp(x \cos \theta) d\theta$

and A_i = the power in the ith gaussian, $\sum_{i=1}^{n} A_i = 1$.

A "quantized" convolved curve was calculated which predicted what one would observe in each radial point. Standard nonlinear least squares techniques which fit to the intensity (not magnitudes) were used to select the best parameters.

This process was subjected to extensive testing. The fitting was done using an interactive program which allowed point editing and evaluation of the fit at various stages. Artificial galaxies with a given I(r) were convolved with typical seeing parameters, then noise was added to simulate our data. Several ways of weighting the points were tried; we chose $\sqrt{r}$ (it made very little difference). Stability of the fitting was tested by deliberately giving the program misleading initial values. For instance, if a and b are two parameters which are correlated as a b^2, we would quadruple a and halve b to see if the program would return to the input values. The final experiment was a blind test,

in which artificial galaxies with size and noise character-
istics of the 1.5-m data were created by one person; another
would attempt to deduce the original profile.

It was discovered quite early that numerically inte-
grating (1) to the desired accuracy (better than 1%) was too
cumbersome, as each fit required over one minute of CPU time.
While this was permissible for this project, it was pro-
hibitive when doing luminosity functions (see Paper III).
This problem was circumvented by creating a two-dimensional
look-up table (all of our selected models have only one
spatial or scale length variable); this reduced the compu-
tational time by an order of magnitude.

Because of the importance of selecting models that fit
the data well, we decided to fit each galaxy with two
different models - one with a core (modified Hubble law)
and one without a core (a GDV model). The Hubble model
(see JGH) falls off as r^{-2} at large radii. This was compared
with the region of interest ($\sim$16 kpc) in our data. For each
brightest cluster galaxy the profile from 11 to 23 kpc was
fit to a power-law (no seeing corrections were made). The
resulting power-law (see § V) had a mean of 1.82 and a
dispersion of 0.49, so we adopted

$$I(r) = \frac{I_o}{[1+(r/a)^2]^{0.9}} \tag{2}$$

as our modified Hubble model. Tests with artificial galaxies generated with the modified Hubble profile showed that the fitting program could reliably solve separately for I_o and a for values of a considerably smaller than the seeing disk. The blind tests indicated that with the 1.5-m data the core radius could be measured to an accuracy of 15% down to 1/20th of the FWHM of the seeing. However, an important caveat must be mentioned - if one fit (2) to an artificially produced GDV galaxy one could find a core that was an appreciable fraction of the seeing disk (also see Schweitzer 1981). Fitting GDV models incurred few problems when the effective radius (R_e) was outside of the seeing disk.

The results of these fits were used to calculate a seeing correction to the magnitudes of each object. Each galaxy was fit with (2) and a GDV model using the radial points from 0 to 16 kpc. For the model there were computed convolved and unconvolved luminosities at 16 kpc. The difference between the two was applied as a seeing correction to the observed 16 kpc luminosity. The largest corrections were ~0.025 mag for the most distant clusters.

IV. PHOTOMETRIC PROPERTIES OF G2 AND G3

One of the most attractive features of area photometers is that while one is obtaining data on a particular source, all objects in its immediate environment are measured

simultaneously at no expense in effort or telescope time.
(There is, of course, the concommitant dramatic increase
in data volume - an aperture photometry measurement pro-
duces two sixteen bit numbers, while one of our frames pro-
duces a quarter of a million, and the difficulty of handling
the data should not be minimized.) By centering the brightest
cluster galaxy in the field, we also acquired photometry on
all objects within 2-3 arcminutes of the center. This
corresponds to a metric radius of ~125 kpc for the nearest
clusters up to 600 kpc for 1018 and 1224. It is here that
the selection problem alluded to in Paper I manifests
itself. In order to have a sample that had a wide range in
richness and with which it would be possible to obtain red-
shift data   in a reasonable period, we ended up with a
very wide range in redshifts (0.044 to 0.30) and a strong
richness-redshift correlation (Paper I). It is clear that
we do not image most of the cluster (at the mean redshift
we have a radius of ~325 kpc), so in order to do a systematic
study a limiting metric radius must be designated. If it is
set small enough to be covered in the nearest clusters, it
encompasses very few galaxies; if it is set larger, the
nearby clusters in the sample do not have enough areal
coverage.

To make the best of this situation, we adopted a cut-
off radius of 250 kpc. This results in 20 of the 83

clusters having pictures with insufficient spatial coverage.
Only five clusters, however, have less than 70% of the re-
quired area (four richness 0 and one richness one clusters).
The brightest four galaxies in this area were selected by
visually examining the data, and the final decisions were
made based on the reductions. In four cases, the original
brightest cluster galaxy was slightly fainter than a
neighbor (Paper I). One cluster (1224) had its originally
chosen second brightest galaxy rejected as a foreground object,/ since it
had a (g-r) color 0.9 mag bluer than the other three.

The colors of the second and third brightest galaxies
(designated as G2 and G3 hereinafter) were compared with the
predicted colors generated by redshifting a standard galaxy
(NGC 4889) through our passbands. Figure 2 displays the
observations and these predicted colors (similar to Figure 5
in Paper I). As for the brightest cluster galaxy (G1), the
agreement is quite good, though there is considerably more
scatter for G2 and G3. For all but the most distant clusters,
the errors in these colors are dominated by systematic errors.
Comparison of 20 clusters with multi-night photometry yield
an internal consistency of ~0.04 mag.

Magnitudes in an aperture of 16 kpc radius were measured
for both G2 and G3. In some cases, an accurate radial pro-
file out to 16 kpc could not be constructed. In these
instances (14 G2's and 27 G3's) an aperture correction was

calculated from the best fitting model, and this was added to the observed luminosity. Figure 3 demonstrates how the magnitudes of the three brightest cluster galaxies are related with Bautz-Morgan type and cluster richness. The bars reflect the one-sigma dispersion of the galaxies in each class; the number of galaxies represented in each class is indicated by the number in parentheses above each set of points. Table 2 lists the mean properties of the galaxies in the richness sample.

The dependence of the luminosity of G1 with Bautz-Morgan type is well documented (Sandage and Hardy [1973] is the classic investigation); it would be desirable for the BM classification to be replaced with an objective, continuous variable. From the results of Sandage and Hardy an obvious candidate quantity would be the magnitude difference between G1 and other cluster members. Figures 4 and 5 show that our adopted quantity, Δ = the magnitude difference between G1 and the mean magnitude of G2 and G3 (see Dressler 1978a), correlates with BM type, richness class, and the luminosity of G1. There appears to be little relationship between Δ and richness (except perhaps that very rich clusters have a smaller Δ) or Bautz-Morgan type (see § VI). In Figure 4 the clusters are coded by richness number. The high degree of mixing (reflecting the small Δ-richness relation in Figure 3) indicates that the effects on this diagram of using an

incorrect value of q_0 to calculate the absolute magnitudes
are very small. The line drawn in Figure 4 is a linear
least squares fit with

$$RAM(1) = 21.32 - 0.24\Delta \ . \tag{3}$$

(RAM is the reduced absolute magnitude, see Paper I.)
The rms scatter is 0.32 magnitude. The point at the lower
right is 2184, which is one of the nearest clusters (only
two have lower redshifts). It was ignored in deriving (3),
as the redshift is suspect (see Paper III).

The equivalent plot for G2 and G3 reveals a very strong
correlation. This is a natural consequence of the nearly
constant luminosity of G1. The best linear fits are

$$RAM(2) = 21.11 + 0.74\Delta$$

$$RAM(3) = 21.41 + 0.92\Delta \ .$$

The rms scatter is 0.37 and 0.41 magnitude, respectively.

V. SURFACE PHOTOMETRY OF THE BRIGHTEST
THREE CLUSTER GALAXIES

As a preparation for the fitting of the Hubble model,
we determined how rapidly the radial profiles of the galaxies
were dropping at the limit of our aperture (see § III).
Since the expected cores are of the order of one kpc (JGH),
by 16 kpc the surface brightness should be falling off as a
power-law. For all 83 brightest cluster galaxies the pro-
file in the range from 11 to 23 kpc was matched to a power-
law relation (linear fit in the magnitude range - log r plane,

no seeing correction). A linear fit was usually a very good representation; the rms errors were typically only ~0.04 mag. The results are displayed in Figure 6. The gaussian with the same mean and dispersion as the data is also plotted. The mean power index (1.82) was then used to get our Hubble model (Eq. [2]). Some indications of the expected GDV parameters can be obtained from this figure. The mean index corresponds to a GDV model at an r/R_e of 0.79, or an effective radius of 20 kpc. An examination of the histogram shows that it can be described as a gaussian with a mean of ~1.65, dispersion of 0.3, and a tail at large power index. This mean indicates a r/R_e of 0.56; or R_e = 28 kpc. The extremes of the histogram correspond to an enormous range in R_e - from about 2 kpc to 100 kpc.

An examination of the data indicates, however, that the extended tail is not due to very compact galaxies. The shaded entries in the histogram in Figure 6 represent multiple systems, i.e., those with more than one local maximum inside a 16 kpc radius. Forty-five percent of our brightest cluster galaxies are multiple (see § VI). Such systems typically have very steep logarithmic surface bright- ness gradients just outside the region containing the nuclei, and it is these systems that are responsible for the tail. The most bizarre multiple systems confuse various of the relations we shall find, but their overall effect is

surprisingly small. There are probably distance-independent ways of recognizing and deleting them from samples with which one is attempting to do cosmology, but until a clear need is present to do that, we prefer to treat them in a homogeneous manner with the other data.

The procedure described in § III was then applied to over 300 cluster galaxies. A few points should be mentioned. First, for the Hubble models the starting value of the core radius was always made comparable to the seeing disk. Tests showed that the program could ferret out the core radius starting from the "outside", but would often get lost if initially placed well inside the seeing disk. The reason is easy to understand. If a $<< \sigma_{see}$, then changing a does very little to the profile until it becomes similar to σ_{see} (it simply adjusts I_o to match the envelope). Second, if the galaxy resembled a GDV model, the initial parameters had very little effect on the final values; but if the radial profile was distorted (usually by bright nuclei) the output was influenced rather strongly by the initial guess. In extreme cases (nuclei separated by the aperture size) the models were very poor representations of the data (see Schneider and Gunn [1982] for an example). The effective radii for these galaxies were very large and ill-determined.

Magnitudes in an aperture of 16 kpc radius were calculated for each galaxy and the brightest three in each

cluster were saved. Table 3 lists the Reduced Absolute Magnitude (RAM), effective radius, and surface brightness at the effective radius for these 249 galaxies. The RAM's are calculated from the definition in Paper I - they are the k-corrected g magnitudes that the galaxies would have if placed at a luminosity distance of one Hubble radius (5000 Mpc or z = 0.866 in our model). The effective radius is in arcseconds and the surface brightness is in r mag per square arcsecond. The latter is the observed value, no corrections for galactic absorption or redshift related effects have been applied.

For most galaxies the GDV model seemed to be a better fit, though the Hubble law did not do too badly. For the normal Gl's the rms errors ranged from 0.03 to 0.15 mag. The second and third brightest galaxies were somewhat less well fit, with residuals of 0.2 and 0.3 mag, respectively. On the distorted systems the Hubble model did considerably better. The fact that both models fit well is not surprising. Kormendy (1977) did an extensive comparison of several models, and found that they all conveyed essentially the same information. Figure 8 displays the similarities of the two models used here. From the fits to all of the galaxies, $\langle \log R_e \rangle - \langle \log a \rangle \sim 1.1$. Using this fact and normalizing the luminosities at 16 kpc, one gets the integrated luminosity curves and the aperture correction factor α. (Kormendy

compares the surface brightnesses of the various models.) We
define $\alpha = \frac{d \ln L}{d \ln r}$ following Gunn and Oke (1975). Since we
are free to chose either model, we selected the GDV model
primarily because it produced, on the whole, better fits.
The relation between R_e and a for galaxies with R_e < 100 kpc
is fairly tight. At a given R_e the scatter in the core
radius is ~40%.

Table 4 lists the structural properties of the brightest
three cluster galaxies. The fact that brightest galaxies
are much bigger in size is clear; the average Gl has an
effective radius over three times larger than G2 and five
times that of G3. While there are definite correlations
between α and richness and BM type for Gl, the second and
third rank galaxies do not show any significant trends.
Figure 9 compares the absolute magnitude of Gl with α (also
see Fig. 8 in JGH). As JGH found, there is a strong cor-
relation, with the largest galaxies being intrinsically
more luminous. Similar plots for G2 and G3 do not display
the effect to nearly the same extent, if at all, but the
much larger scatter in luminosity may serve to mask any
relation present.

Figure 10 shows a most interesting relation. The
effective radius in kpc is plotted as a function of the
corrected surface brightness (see Kormendy [1977] for a
similar plot for some Virgo galaxies). The line is the best

linear fit (ignoring the four objects with R_e > 200 kpc).
The dispersion in log R_e is only 0.10. Similar relations
exist for G2 and G3. Defining SB = $I(R_e)$ -22

$$G1 \quad \log R_e = 1.103 + 0.315 \; SB \quad \sigma = 0.10$$
$$G2 \quad \log R_e = 0.934 + 0.299 \; SB \quad \sigma = 0.12 \tag{4}$$
$$G3 \quad \log R_e = 0.815 + 0.268 \; SB \quad \sigma = 0.13 \; .$$

Kormendy's relation matches G2 and G3 at small R_e ($\sim$ 3 kpc)
and catches up with the G1 curve at around 100 kpc. The
probable explanation is that Kormendy's sample contained a
mix of galaxies with RAM's from $\sim$23 up to $\sim$21 (NGC 4472,
which is the brightest cluster galaxy in Virgo).

VI. DISCUSSION

The measurements in § IV confirm to a large degree the
findings of Sandage and Hardy (1973, hereinafter SH). Com-
parison of their Figure 4 and our Figure 2 show nearly
identical results for the luminosities of the brightest
three cluster galaxies as a function of Abell richness class.
Our brightest galaxy luminosities rise more rapidly with
richness than do those in SH (we have 24 richness 3 and 4
clusters vs. 8 for SH), but the G2 and G3 curves match well.
(Paper III defines cluster richness as cluster luminosity;
the effects of richness on cluster properties is discussed
in that work.) There are some differences with the Bautz-
Morgan data, however. The magnitude dependence of G1 with

BM type is in good agreement. The relationship of Δ with BM class is not as striking in our data. We do see a weak trend, with BM I to I-II having $\Delta \sim 1.3$; the others have $\Delta \sim 1.0$. SH found $\Delta \sim 1.5$ and 0.5 for equivalent types. The most disturbing disagreement is that the luminosities of G2 and G3 in our data are essentially independent of BM classification; in the SH data they are strongly anticorrelated with the brightness of G1.

Both the richness and SH samples have similar number of clusters and distribution in BM class. The procedural differences are 1) we actually photometer the galaxies while SH infer magnitudes from angular sizes, and 2) we are restricted to the core of the cluster while SH are not. Point 1) could explain the slight discrepancy in the Δ relations, as we are measuring luminosities in a relatively small metric radius; therefore galaxies with extended envelopes will appear systematically brighter in the SH measurements – resulting in larger Δ's for BM I clusters (Paper I noted ~ 0.1 mag difference between our BM I corrections and the values found by Kristian, Sandage, and Westphal [1978] using a larger aperture).

The disagreement in the trend of absolute magnitude for G2 and G3 is less easily explained away. One possibility is that the true G2 and G3 are systematically farther from the center of the cluster for BM II to III clusters. This would

not be implausible, as BM I clusters are thought to be the most relaxed and BM III the least relaxed systems. The only serious difficulty lies in the luminosities of G2 and G3 for the BM I clusters. The ones in the richness sample are too bright to be consistent with the measurements of SH.

The other aspect of this work that has been previously investigated is the determination of the aperture correction factor α. From surface photometry of over 100 nearby clusters JGH found $\langle \alpha \rangle = 0.49$. This paper finds $\langle \alpha \rangle = 0.70$. Since the JGH sample was confined primarily to low-richness clusters, an increase in α may be due to the strong α-richness correlation. Direct comparison of our α's with that of the JGH sample reveals, however, that our α's are 30% larger than his at a given richness and BM class. The difference almost certainly comes about from the different fitting functions we have used for the surface brightness distribution. Our modified Hubble law has a slope (-1.8) derived from the mean of the observations, while JGH used a postulated -2.0, which has smaller α's at a given scale radius. The mean value we derive is gratifyingly close to the (in principle unrelated) value of 0.7 from the GDV fits (see Table 4). Both our technique and this agreement suggest that the larger value is the better one in the sense of self-consistency. It also agrees with the directly determined value of 0.7 used in Gunn and Oke (1975).

The frequency of multiplicity in the G1 systems is striking. JGH found 28% of the brightest cluster galaxies in his sample were multiple systems (defined as more than one nucleus in 16 kpc radius aperture). An examination of our G1's found 32 objects with two nuclei, four with three, and one with five - 45% of the sample. The multiple systems are identified in Table 3 by i:Mn where i refers to Gi and n is the number of nuclei.

Since our sample consists of much richer clusters than does JGH's, it can be argued that it is natural to have a higher proportion simply due to projection effects. In the richness 4 clusters 3 of 8 G1's are multiple systems while 10 of 16 of the richness 3's are complex - in total 54% of the "rich" clusters have multiple nuclei. For the richness 0-2 clusters, 41% have more than one nucleus. Since the range in surface density of galaxies over this range in richness class is enormous (a factor of 40, see Paper III), it would appear that projection cannot be primarily responsible for the phenomenon.

To quantify the projection problem, assume the cluster has a surface density profile of

$$\Sigma(r) = \frac{\Sigma_o}{1+(r/a)^2} \quad .$$

Then

$$N(r) = \pi\Sigma_o a^2 \ln [1+(r/a)^2] \quad .$$

The number of galaxies in the core $(r < a)$ is $N_c = 0.69\pi\Sigma_o a^2$. The number of galaxies occurring within a radius r_s is

$$n_s = 1.44 \ N_c \ \ln \ [1+(r_s/a)^2] \quad .$$

The observed core radii of clusters are ~ 250 kpc (Bahcall 1977; Dressler 1978$\underline{b}$). For this calculation $r_s = 16$ kpc $<< a$, so

$$n_s = 1.44 \ N_c \left(\frac{r_s}{a}\right)^2 = 0.0059 \ N_c \quad .$$

A total of 76 galaxies is required to be in the core to yield an average of 0.45 galaxies in the aperture. The results of a study of the luminosity functions of 60 of these clusters based on the same CCD data (Paper III) shows $N_c \sim 15$ galaxies - so 20% of these systems are expected to be projections. This calculation assumes, of course, that the magnitude limit for defining multiplicity is the same as that for determining the number of galaxies in the core. We think that the limits are very similar, although it must be conceded that it is often difficult to estimate the magnitude of a small object embedded in the envelope of a central galaxy. A more telling blow to the projection hypothesis is that the number of multiple systems among G2 and G3 is around an order of magnitude less than that seen in G1. There is a strong bias towards including multiple systems in G2 and G3 - one can often increase the luminosities

by 0.5-0.7 mag if two galaxies are projected onto each other, while in only one case (1689) is a G1 possibly influenced in this manner.

Figure 11 displays the central object in the two most complex clusters in the richness sample - 1689 and 1934. The isophotes are corrected to their rest values and the sizes have been adjusted to place the objects on the same metric scale. In both instances one has the impression that the galaxies are swarming about in an envelope of stripped stars (see also Fig. 2 of Schneider and Gunn [1982]).

The frequency of multiple systems in poor clusters in the richness sample is 50% greater than that determined by JGH. We are currently acquiring CCD data for the galaxies in JGH and will perform an analysis similar to that of this paper to check if differences in the observational material or reduction procedure are responsible for the discrepancy in the fraction of multiple systems.

The ⟨RAM⟩ for the multiple systems is 21.00 ± 0.05 with a dispersion of 0.29 mag, while the numbers for the single systems are 21.13 ± 0.05 and 0.39. (It seems very odd that the dispersion in the multiple systems is lower than the normal G1's.) If these nuclei are, in fact, being consumed frictionally, as the data strongly suggest , then the final product of the merger will be brighter by an amount which must be roughly this magnitude difference, though the fact

that we are discussing aperture magnitudes introduces some uncertainty. The mean evolutionary rate can only be calculated if one knows the frictional lifetimes, and those are very uncertain, but probably are about a billion years (HO; Gunn and Tinsley 1976; Bahcall 1977; White 1978; Schneider and Gunn 1982). The resulting evolutionary correction, if one attempts to apply it in a mean sense, is probably quite large. A change of ~0.13 magnitude in a billion years implies a correction to q_o of +3! This number must be multiplied by something like the fraction of galaxies currently participating in frictional cannibalism, 45% less the projection correction, so the mean evolutionary correction is about unity. The time scale, however, is uncertain by a factor of at least three, and quite apart from questions of principle, which suggest that one cannot ever use the mean dynamical corrections to the Hubble diagram to find q_o, the application of a mean correction to sufficient accuracy is quite hopeless.

A solution to this problem and additional evidence for the whole cannibalism scenario is provided by Figure 9 and the corresponding Figure 8 in JGH. The agreement with the simple theory (Fig. 3 or HO) is exceedingly good; the scatter about the magnitude-α relation is 0.30 magnitude. This latter figure is a little disappointing. JGH found a scatter of only 0.21 magnitude from a sample of comparable size

but considerably less diversity. Cosmological samples,
unfortunately, are likely to be more like the richness sample
than that of JGH. The whole of dynamical evolution is
contained in Figure 9; as galaxies consume others, they move
toward larger α and larger luminosity, but the relationship
is not a function of time. Thus measurement of aperture
magnitude, redshift, and α allow a "dynamical evolutionary
correction" to be made to each system individually, as was
first pointed out in JGH. It can be shown that the appli-
cation of these corrections is itself cosmology-dependent,
and halves the sensitivity of the Hubble test compared with
one made with nonevolving point sources. The decreased
sensitivity just compensates the smaller dispersion using
the α-luminosity relation, so that the statistical situation
with the α correction is the same as without, i.e., the
formal error in q_0 for a given sample size is the same,
but the additional data remove the dynamical evolutionary
effects.

As the giant consumes other cluster members, it should
become bluer as result of the color-magnitude relation for
ellipticals (Gunn and Tinsley 1976; HO). Our data are very
insensitive to this phenomenon - the color (g-r) is not as
good an indicator of galaxy luminosity as the (U-B) used in
HO. Since the other bright galaxies have the same (g-r) as
the brightest cluster galaxy, no strong color evolution in

our observations can be expected or is seen.

Figure 12 is a plot of the observed effective radius as a function of redshift (the x-axis is $x = \log[Z_{1/2}(z)/Z_1(z)]$, for small redshift z ~0.25 log e z ~0.109 z, see Paper I). There is a small increase in size with redshift. This has little use as a cosmological test, as unknown selection effects and the immense scatter overwhelm any contributions of the deceleration parameter.

Attempts to use the surface brightness as a test of stellar evolution (Tinsley 1976 and references therein) run into similar problems. If one compares the corrected surface brightnesses at the effective radius the effects of large scatter with the effective radius-redshift trend in Figure 11 renders interpretation of the $I(R_e) - \log(1+z)$ diagram difficult. We can only make two rather weak statements: 1) there is no evidence of stellar evolution from the colors, and 2) relation (4) works quite well with a correction of $(1+z)^4$ and the result agrees with local measurements (Kormendy 1977). Tired light universes do not reproduce (4); the difference in surface brightness at z = 0.3 is 0.8 mag.

The fact that (4) is such a good correlation leads one to investigate its usefulness as an angular diameter test (see Sandage [1961] for an overview of various cosmological tests). The effective radius for first-ranked galaxies will

be well outside of the seeing disk in good seeing even at a redshift of 0.7. To compare the sensitivity of this procedure to that of the magnitude-redshift test, simply replace the reduced absolute magnitude axis in Figure 8 of Paper I with

$$Y = 5 \log \left[\frac{R_{e}(observed)}{R_{e}(calculated)} \right] . \tag{5}$$

The horizontal "standard line" will be at zero. The dispersion in Y is 0.5 (vs. 0.35 for the magnitudes). However, since there is no aperture correction to worry about, the sensitivity is not reduced by a factor of $(1-0.5\alpha) \sim 0.65$ as it is for luminosities (Gunn and Oke 1975). Any dynamical evolution is self-calibrating - as long as one stays away from very unusual objects with effective radii greater than 200 kpc (like 2125); fortunately, these objects will be easy to recognize at even the highest redshifts. This test is, of course, affected by stellar evolution, since the surface brightness is involved directly.

A little thought will show that this process is simply casting the standard Hubble diagram in a different light. When one envokes surface brightness-scale length relations in this manner one arrives at a quantity related to the aperture magnitude of the model. Since it is hoped that the model bears some resemblance to the observations, in effect one is performing the standard test with model magnitudes.

Relation (4) does say something very fundamental about observational cosmology. One of its direct consequences is that brightest cluster galaxies will have very little dispersion in their aperture magnitudes. For GDV models obeying

$$R_e = A + B \, I(R_e)$$

it is easy to show that the total luminosity is

$$L = L_o \left(\frac{R_e}{r_c}\right)^{[2-0.4/B]} \quad .$$

Let $\gamma = 2 - 0.4/B$. Then the luminosity in a standard aperture of radius r_s is

$$L_s = 0.5 \, L_o \left(\frac{R_e}{r_o}\right)^{\gamma} \left(\frac{r_s}{R_e}\right)^{\alpha}$$

where α is the effective aperture correction factor in the r_s-R_e range. The aperture magnitude is

$$m_s = M_o - 2.5 \, \log[0.5 \, L_o \left(\frac{r_s}{r_o}\right)^{\gamma}] - 2.5 \, \log\left(\frac{r_o}{R_e}\right)^{\alpha-\gamma}$$

or

$$m_s = m_o - 2.5(\gamma-\alpha) \, \log\left(\frac{R_e}{r_s}\right)$$

and

$$\sigma(m_s) = 2.5(\gamma-\alpha)\sigma\left[\log\left(\frac{R_e}{r_s}\right)\right] . \tag{5}$$

For the first-ranked galaxies in this paper, the effective α between r and $\langle R_e \rangle$ (see Fig. 8) ~ 0.6 and $\sigma[\log(R_e/r_s)] \sim 0.5$. Since $B = 0.3$, $\gamma = 0.67$, and $\sigma(m_s) \sim 0.1$. The observed

dispersion is much greater, indicating that the intrinsic scatter in the R_e-$I(R_e)$ relation is the dominant factor. For G2 and G3, $\alpha_{eff} = 0.4$ and the coefficient in (5) becomes 0.7 instead of 0.2. This exercise, while showing that nearly constant aperture magnitudes are a natural result of the way elliptical galaxies are constructed, leaves un-answered the more interesting question of why galaxies follow relation (4) in the first place. The fact that G2 and G3 follow similar relationships lends additional support to the homologous merger picture (HO). Caution must be taken if one tries to fit the inner 50 kpc of G1's with extended envelopes (see Paper III) to a GDV profile. The GDV model is a poor fit to these galaxies, and the effective radius becomes a function of the outermost radius used to determine the optimum model. (This problem will be dealt with in a later paper.)

Our observed radius-surface brightness relation is difficult to reconcile with current notions concerning the dynamics of elliptical galaxies of somewhat lower luminosity. A large body of data now supports the original work by Faber and Jackson (1976) which produced a relation between the luminosity and velocity dispersion in which the luminosity is proportional to the fourth power of the internal velocity dispersion. If the luminosity of a galaxy can be expressed as

$L \propto R^x$ (R is some scale length)

using

$M \propto \sigma_r^2 R$ and assuming constant M/L,

one arrives at the relation

$$L \propto \sigma_r^{\left(\frac{2x}{x-1}\right)} .$$ (6)

(This argument was originally given by Sargent, Schechter, Boksenberg, and Shortridge [1977].) If ellipticals have constant surface brightness, x = 2, and the Faber-Johnson relation is produced. If x = 1, then σ_r is constant. The observed value for x is 0.7 and this requires that $L \propto \sigma_r^{-4.7}$! This result is perhaps not very surprising if the brightest galaxies are merger products, since mergers tend to pre- serve energy per unit mass, i.e., velocity dispersion, and the typical pre-merger piece probably had a much smaller mass than the currently observed Gl's. The calculation also postulates constant M/L along the sequence, and one would expect the giants to have higher M/L's and higher velocity dispersions than one would calculate ignoring this mixing. The dynamics for Gl in Abell 2029 have been investigated in some detail by Dressler (1979) and are consistent with this general picture.

One final note - equation (4) allows a direct test of our infall to the local supercluster (see Kormendy 1977). Transforming Kormendy's GDV parameters for NGC 4472 and

NGC 4486 (scans of four standard galaxies yield r = B - 1.15 ± 0.03)

$$\log\left(\frac{R_e(\text{observed})}{R_e(\text{calculated})}\right) = +0.06 \pm 0.08 \ . \tag{7}$$

Treating the two galaxies as G2's makes (7) larger by ~0.16. Placing this on a velocity scale indicates we are moving away from Virgo with a velocity of +140 km s^{-1} in excess of the Hubble flow; the one-sigma confidence limits are +300 and -50 km s^{-1}. This is the same null result arrived at by Kormendy.

It seems likely that dynamical friction does play an extremely important role in determining properties of brightest cluster galaxies and cluster morphology. Future investigations that seem especially promising are the previously mentioned surface photometry of nearby clusters and dynamical investigations of multiple systems to determine their lifetimes. The dependence of cluster velocity dispersion on overall richness is another interesting quantity. If the velocity dispersions and core radii of clusters of various richnesses indeed correspond to the frictional rates required to explain the richness and BM corrections and statistics, there would be very little room for doubt of the basic cannibalism picture. The current data themselves, without these dynamical constraints, seem almost persuasive enough, but the cosmological interpretation is so dependent

on the correctness of the frictional evolution scenario

that any further confirmation would be extremely valuable.

TABLE 1

CCD Detectors

Chip	Operation	Type	Clusters	Comments
1	Mar 79 - Aug 79	500	20	Cosmetically very flawed, poor g flattening, photometric
2	Sept 79	500	2	Unsatisfactory performance, used on only one run
3	Jan 80 - Mar 81	500	57 (2)	Only ~10 bad columns, good flattening, photometric
4	Mar 81 -	800	(2)	Excellent cosmetics and flattening, photometric

(n) indicates n observations made with the Hale telescope

TABLE 2

PROPERTIES OF THE THREE BRIGHTEST CLUSTER

GALAXIES (RICHNESS SAMPLE)

	G1	G2	G3
⟨RAM⟩	21.07	21.90	22.39
Dispersion	0.35	0.55	0.65
(g-r)	+0.47	+0.46	+0.46
Dispersion	0.06	0.13	0.12

TABLE 3

STRUCTURAL PARAMETERS FOR BRIGHTEST THREE CLUSTER GALAXIES

Abell	G1 RAM	G1 Log(Re)	G1 I(Re)	G2 RAM	G2 Log(Re)	G2 I(Re)	G3 RAM	G3 Log(Re)	G3 I(Re)	Comments
22	20.88	1.46	25.27	21.24	0.79	23.34	21.84	0.39	22.36	1:M2 log a=0.42 I(0)=20.42
42	20.97	2.27	27.03	21.30	0.45	21.56	22.21	0.53	22.84	1:M2 Eq gal sep by 15 kpc
43	21.69	0.31	21.49	21.86	0.45	22.02	22.14	0.55	22.74	
77	20.99	1.44	24.11	21.51	0.68	22.11	22.61	0.53	22.53	
98	21.06	0.74	22.36	21.40	0.47	21.74	22.05	0.46	22.28	
136	20.74	1.08	24.06	22.64	-0.02	21.75	23.01	-0.09	21.68	1:M2
140	20.63	0.74	22.81	21.82	0.25	21.98	21.80	0.31	22.29	1:M2
160	21.47	1.80	24.78	23.14	0.72	22.76	23.67	0.17	20.73	1:M2
186	20.59	1.14	23.35	22.51	0.05	20.96	22.72	0.04	21.15	1:M2
279	20.94	1.18	23.33	21.79	0.78	22.65	21.98	0.14	20.18	
326	21.24	1.40	23.98	22.33	0.58	22.00	23.85	0.43	22.78	1:M3 Eq gal sep by 8 kpc
410	22.04	0.61	22.69	22.42	0.39	22.32	22.57	0.68	23.55	
423	21.30	1.14	23.70	21.97	0.43	21.60	22.77	0.28	21.71	1:M2
458	20.93	1.03	23.29	21.58	0.39	21.54	22.38	0.21	21.39	
545	21.60	0.05	21.45	21.66	-0.01	21.10	21.78	0.11	22.02	
655	20.41	1.13	23.36	21.59	0.53	22.55	22.54	0.20	22.01	
665	21.15	1.08	24.70	21.47	0.57	23.25	21.74	0.66	23.91	3:M2
733	20.71	1.21	23.77	21.79	0.59	22.74	22.24	0.39	22.31	
777	21.23	0.41	22.93	21.47	0.29	22.75	22.00	0.57	23.84	
819	21.05	0.97	22.71	21.55	0.56	21.72	21.84	0.74	22.62	1:M2
858	21.17	0.81	22.45	21.58	0.81	22.95	21.75	0.43	21.59	
882	20.91	0.67	22.59	21.34	0.70	23.10	22.22	0.56	23.45	
910	21.05	0.84	24.12	21.70	0.64	24.07	21.94	0.53	23.88	
1018	21.02	0.55	23.89	21.11	0.58	24.06	21.32	0.27	23.09	
1081	20.54	0.88	23.05	21.99	0.50	23.03	22.60	0.30	22.89	
1123	21.06	0.85	23.05	21.87	0.16	21.33	22.84	0.21	22.31	1:M2 log a=-0.10 I(0)=18.74
1149	21.21	0.80	22.23	22.31	0.43	21.63	22.74	0.56	22.54	1:M2
1155	21.56	0.76	22.34	22.86	0.15	21.10	23.96	0.40	23.22	
1169	21.82	0.63	21.67	22.08	0.38	20.84	23.15	0.60	22.64	
1170	21.13	0.47	22.35	21.98	0.22	22.09	22.00	0.13	21.75	1:M2 Complex of 4
1190	21.23	1.03	23.03	21.28	1.15	23.62	21.67	0.41	21.08	1:M2
1224	20.92	0.29	22.74	21.23	0.31	23.05	21.42	0.39	23.64	
1227	21.15	1.26	24.31	21.73	0.47	22.03	22.21	0.49	22.61	
1235	21.19	1.51	24.92	22.30	0.42	22.32	22.31	0.03	20.58	
1264	21.31	1.35	25.00	22.29	0.40	22.64	23.08	0.23	22.66	
1346	21.19	1.27	24.15	21.74	0.65	22.50	22.03	0.66	22.90	1:M2
1373	21.75	1.01	24.45	22.03	1.69	26.85	22.07	0.97	24.70	2:M2
1401	21.67	1.00	24.79	21.99	0.62	23.87	21.90	0.88	24.67	1:M2 Chain of bright galaxies
1413	20.65	1.54	25.02	21.99	0.25	21.99	22.04	0.13	21.50	1:M2
1461	21.58	0.81	21.99	22.84	1.33	24.92	23.70	0.81	24.06	
1514	21.11	0.97	24.53	21.30	1.07	24.98	21.93	0.48	23.55	1:M2
1548	20.70	1.06	23.94	22.26	0.12	21.99	22.43	0.10	21.94	

TABLE 3 (Continued)

STRUCTURAL PARAMETERS FOR BRIGHTEST THREE CLUSTER GALAXIES

Abell	G1 RAM	G1 Log(Re)	G1 I(Re)	G2 RAM	G2 Log(Re)	G2 I(Re)	G3 RAM	G3 Log(Re)	G3 I(Re)	Comments
1559	20.66	1.71	25.35	22.09	0.16	20.94	22.26	0.33	21.96	
1589	20.92	0.94	22.30	21.76	0.58	21.60	22.01	0.70	22.37	
1630	21.21	0.63	21.35	21.90	0.87	22.81	22.77	0.54	22.38	
1674	21.27	1.63	25.54	22.62	0.31	22.14	22.85	0.31	22.42	1:M2
1689	20.98	1.18	25.11	21.06	1.31	25.24	21.07	1.29	25.73	1:M2
1738	20.56	1.27	23.79	21.25	2.00	26.78	21.53	0.79	23.23	1:M2 3:M2 Spectacular cluster
1785	21.27	0.34	20.50	22.41	0.61	22.56	23.64	0.39	22.79	2:M2 Eq gal sep by 15 kpc
1825	21.32	0.87	22.25	21.43	0.02	22.18	21.99	0.71	22.30	1:M2
1827	21.14	1.88	26.05	21.93	0.30	20.84	22.25	0.32	21.15	1:M2
1880	20.88	1.42	25.10	22.65	0.01	21.62	23.19	-0.21	21.07	1:M2 log a=0.32 I(0)=20.19
1918	20.85	1.54	25.20	22.15	0.50	22.00	22.20	0.07	21.35	1:M3 Eq gal sep by 10 kpc
1921	21.16	0.74	22.97	21.43	1.09	24.32	21.45	0.17	20.99	
1934	20.24	1.72	26.26	21.34	0.23	22.24	21.60	0.23	22.44	1:M5 Central obj has 8-10 galaxies
1940	20.92	0.91	23.36	22.65	0.41	23.16	23.05	-0.01	21.66	
1984	20.82	2.20	27.11	21.96	0.95	24.56	22.44	0.21	21.80	1:M2 Eq gal sep by 15 kpc
2036	21.16	0.59	22.24	21.33	0.26	20.97	21.73	1.60	26.40	1:M2 3:M2
2110	21.04	0.89	22.82	22.70	0.46	22.86	22.66	0.45	22.64	
2125	20.50	2.41	27.54	21.25	0.31	22.76	22.09	0.26	23.36	1:M3 3 eq gal sep by 20 kpc
2184	21.90	0.66	21.70	24.37	0.51	23.37	24.53	-0.04	21.31	
2218	21.21	1.74	26.36	21.71	0.88	24.50	22.29	0.16	22.21	1: Very extended low sur bright
2244	20.87	1.58	24.74	21.68	0.52	22.08	22.41	0.28	21.65	
2246	20.84	0.97	24.48	21.36	0.48	23.30	22.08	0.42	23.84	
2263	21.49	1.41	24.96	22.08	0.49	22.27	22.61	0.09	21.25	1: log a=0.13 I(0)=19.74
2283	20.72	0.68	23.00	21.97	0.10	21.92	22.26	0.00	21.75	
2377	21.28	1.03	23.21	21.31	1.18	23.76	21.79	0.46	21.55	
2388	21.61	1.21	23.73	22.74	0.15	20.55	23.35	0.33	22.00	
2400	21.08	1.24	23.85	22.33	0.32	21.80	22.65	0.17	21.24	1:M2
2420	20.91	1.53	24.46	21.79	0.67	22.42	22.23	0.30	21.39	
2440	21.11	1.46	24.57	21.67	0.50	21.72	22.08	0.52	22.24	
2459	21.31	0.68	21.81	21.32	0.67	21.78	22.85	0.71	23.41	
2462	21.00	0.71	21.64	22.14	0.55	22.10	22.72	0.81	23.75	1:M2
2469	21.61	0.92	22.86	21.88	2.13	26.64	23.34	0.39	22.28	2:M2
2496	20.60	1.33	24.20	22.06	0.16	21.44	22.74	0.34	22.94	1:M3 log a=-0.21 I(0)=18.04
2521	20.64	1.81	25.91	21.47	1.53	26.02	21.79	0.37	22.19	1:M2 Eq gal sep by 15 kpc
2554	21.04	1.28	24.23	21.24	0.51	21.81	21.82	0.34	21.58	1:M2
2559	21.09	1.24	23.73	22.22	0.01	19.94	22.11	0.88	23.61	
2597	21.26	1.34	24.26	22.73	0.29	21.89	23.03	0.51	22.88	
2622	21.03	1.26	23.41	21.80	1.03	23.40	22.35	0.24	20.57	1:M2
2645	20.81	2.00	27.07	21.40	0.51	23.76	21.79	0.00	21.99	1:M2 Eq gal sep by 10 kpc
2686	21.08	0.88	23.05	21.95	0.72	23.31	22.28	0.52	22.88	1:M2
2694	20.43	1.05	22.83	21.51	1.13	24.04	23.18	-0.20	20.25	1:M2

TABLE 4

MEAN STRUCTURE PARAMETERS

	G1	G2	G3
$\langle \log Re \rangle$	1.45 ± 0.05	0.93 ± 0.05	0.74 ± 0.04
Dispersion	0.47	0.42	0.32
$\langle \log a \rangle$	0.33 ± 0.04	-0.14 ± 0.04	-0.32 ± 0.04
Dispersion	0.40	0.40	0.40
$\langle \alpha \rangle$	0.70 ± 0.03	0.40 ± 0.03	0.30 ± 0.02
Dispersion	0.27	0.23	0.16
Richness (α)			
0	0.54 ± 0.04	0.32 ± 0.03	0.31 ± 0.05
1	0.64 ± 0.05	0.36 ± 0.06	0.28 ± 0.03
2	0.75 ± 0.06	0.47 ± 0.07	0.27 ± 0.03
3	0.83 ± 0.06	0.42 ± 0.04	0.29 ± 0.04
4	0.85 ± 0.15	0.50 ± 0.08	0.44 ± 0.08
Bautz-Morgan (α)			
I	0.84 ± 0.07	0.52 ± 0.09	0.27 ± 0.04
I-II	0.68 ± 0.07	0.30 ± 0.03	0.28 ± 0.03
II	0.75 ± 0.06	0.43 ± 0.05	0.25 ± 0.02
II-III	0.71 ± 0.08	0.41 ± 0.05	0.38 ± 0.06
III	0.57 ± 0.05	0.36 ± 0.05	0.32 ± 0.04

REFERENCES

Abell, G. O. 1958, Ap. J. Suppl., 3, 211.

Bahcall, N. A. 1977, Ann. Rev. Astr. Ap., 15, 505.

Bautz, L. P., and Morgan, W. W. 1970, Ap. J. (Letters), 162, L149.

de Vaucouleurs, G. 1948, Ann. d'Ap., 11, 247.

Dressler, A. 1978a, Ap. J., 222, 23.

_____. 1978b, Ap. J., 226, 55.

_____. 1979, Ap. J., 231, 659.

Faber, S. M., and Jackson, R. E. 1976, Ap. J., 204, 668.

Gunn, J. E., and Oke, J. B. 1975, Ap. J., 195, 255.

Gunn, J. E., and Tinsley, B. M. 1976, Ap. J., 210, 1.

Gunn, J. E., and Westphal, J. A. 1982, preprint.

Hausman, M. A., and Ostriker, J. P. 1978, Ap. J., 224, 320 (HO).

Hoessel, J. G. 1980, Ap. J., 241, 493 (JGH).

Hoessel, J. G., Gunn, J. E., and Thuan, T. X. 1980, Ap. J., 241, 486.

Hubble, E. 1930, Ap. J., 71, 231.

Kormendy, J. 1977, Ap. J., 218, 333.

Kristian, J. A., Sandage, A., and Westphal, J. A. 1978, Ap. J., 221, 383.

Oemler, A. 1976, Ap. J., 209, 693.

Ostriker, J. P., and Hausman, M. A. 1977, Ap. J. (Letters), 217, L125.

Ostriker, J. P., and Tremaine, S. D. 1975, Ap. J. (Letters), 202, L113.

Sandage, A. 1961, Ap. J., 133, 355.

Sandage, A., and Hardy, E. 1973, Ap. J., 183, 743 (SH).

Sandage, A., Kristian, J. A., and Westphal, J. A. 1976, Ap. J., 205, 688.

Sargent, W. L. W., Schechter, P. L., Boksenberg, A., and Shortridge, K. 1977, Ap. J., 212, 326.

Schneider, D. P. 1982, preprint (Paper III).

Schneider, D. P., and Gunn, J. E. 1982, Ap. J., in press.

Schneider, D. P., Gunn, J. E., and Hoessel, J. G. 1982, preprint (Paper I).

Schweizer, F. 1981, Ap. J., 246, 722.

Tinsley, B. M. 1976, Ap. J. (Letters), 210, L49.

Tinsley, B. M., and Gunn, J. E. 1976, Ap. J., 203, 52.

White, S. D. M. 1978, M.N.R.A.S., 184, 185.

FIGURE CAPTIONS

Fig. 1. - The conditions under which the observations were made. Each point represents a cluster, the number indicates the quality of the data based on the exposure time. Number code: 1 = 300, 2 = 500, 3 = 1300, 4 = 1500, 5 = 2000, 6 = 3300, 7 = 6600; the units are seconds of exposure on the Palomar 1.5-m. The axes are the seeing (FWHM) in arcseconds and kpc. The two diagonal lines represent z = 0.1 and z = 0.2.

Fig. 2. - A plot of the observed (g-r) colors (+) and the colors predicted from a standard galaxy for G2 (top) and G3 (bottom). As was the case for G1 (Paper I), the agreement is quite good.

Fig. 3. - The absolute magnitude of the brightest three cluster galaxies as a function of richness and Bautz-Morgan class. The number of galaxies represented in each class is given in parentheses above each set of points. The dispersion of galaxies in each point is indicated by the associated bar.

Fig. 4. - The magnitude difference between the brightest cluster galaxy and the mean of the second and third ranked ones. Notation is the same as in Figure 3.

Fig. 5. - The absolute magnitude of the brightest cluster galaxy as a function of Δ = mag $\langle 2+3 \rangle$ - mag 1. The best

fitting line is RAM(1) = 21.32 - 0.24Δ; the dispersion is reduced to 0.32 mag. The clusters are coded by Abell richness class. Since the luminosity of G1 is nearly constant, there is a very strong correlation between the magnitudes of G2 and G3 and Δ; the dispersion for these objects is reduced to 0.37 and 0.41 mag, respectively (vs. an uncorrected dispersion of 0.55 and 0.65 mag).

Fig. 6. - A histogram for the power-law index of the envelope of the brightest cluster galaxy. The index (β) represents the best fit of $I(r) \propto r^{-\beta}$ in the 11-23 kpc region (no seeing corrections have been made). The shaded galaxies are multiple nucleus systems; the objects with sharp cutoffs (large β) are usually systems with roughly equal components separated by 5 to 10 kpc. The line represents the gaussian with the same mean (1.82) and dispersion (0.49) as the data.

Fig. 7. - Radial profiles of two brightest cluster galaxies. The dots represent observations, the crosses the best fitting GDV model (fit from 0-16 kpc). The seeing profile is plotted in the lower left; the FWHM's are 1.47 and 1.26 arcsec. The rms error in the fits is 0.07 mag in both cases. Abell 1413 is a classic cD in a BM I cluster, its effective radius is 96 kpc. Abell 1514 has an effective radius of 33 kpc, very near the mean (28 kpc). Both galaxies have a small galaxy within 16 kpc of the center of the brightest galaxy, but they may be due to projection as both are quite rich (class 3) clusters.

Fig. 8. - A comparison of Hubble and GDV models. The shift between the models was determined by (1) $\langle \log r \rangle$ - $\langle \log a \rangle$ ~1.1 for the galaxies studied, and (2) normalizing $L(r)$ at 16 kpc. The GDV model has a total magnitude of 0.0, the Hubble model has $L(r) \propto r^{0.2}$ at large radii. Over the range in scale factors (roughly a factor of 3) the difference in the model α's is at most 15%.

Fig. 9. - A plot of the effect of the structure of brightest cluster galaxies on their luminosity. The horizontal axis is the aperture correction factor $\alpha = \frac{d \ln L}{d \ln r}$ at 16 kpc for first-ranked cluster galaxies. The clusters are coded by richness class. Similar graphs for G2 and G3 do not reveal such a strong relationship.

Fig. 10. - The effective radius in kpc of the best fitting GDV model as a function of the corrected red surface brightness at R_e for brightest cluster galaxies. The line is $\log R_e = 1.103 + 0.315(I(R_e)-22)$, which is a linear fit to the points with effective radii less than 200 kpc. (Clusters 42, 1984, 2125, and 2645 were ignored.) The 1σ error in predicting $\log R_e$ is 0.10.

Fig. 11. - Contour maps of the central objects in clusters 1689 and 1934. The contours represent constant surface brightness corrected to the rest frame, the brightest is 19.0 mag per square arcsec, the faintest 23.5, and the

interval is 0.5. Each picture is 240 kpc on a side. Both maps are based on red exposures with the Hale telescope. The most striking feature is the extended envelope surrounding the inner core of galaxies.

Fig. 12. - A plot of effective radius vs. redshift for the brightest cluster galaxies in this sample. (X ~0.11 z, see text). The distant clusters have slightly larger R_e's which indicate higher luminosities. The trend in the figure is almost certainly due to selection effects - the distant clusters tend to be richer (points are coded by richness).
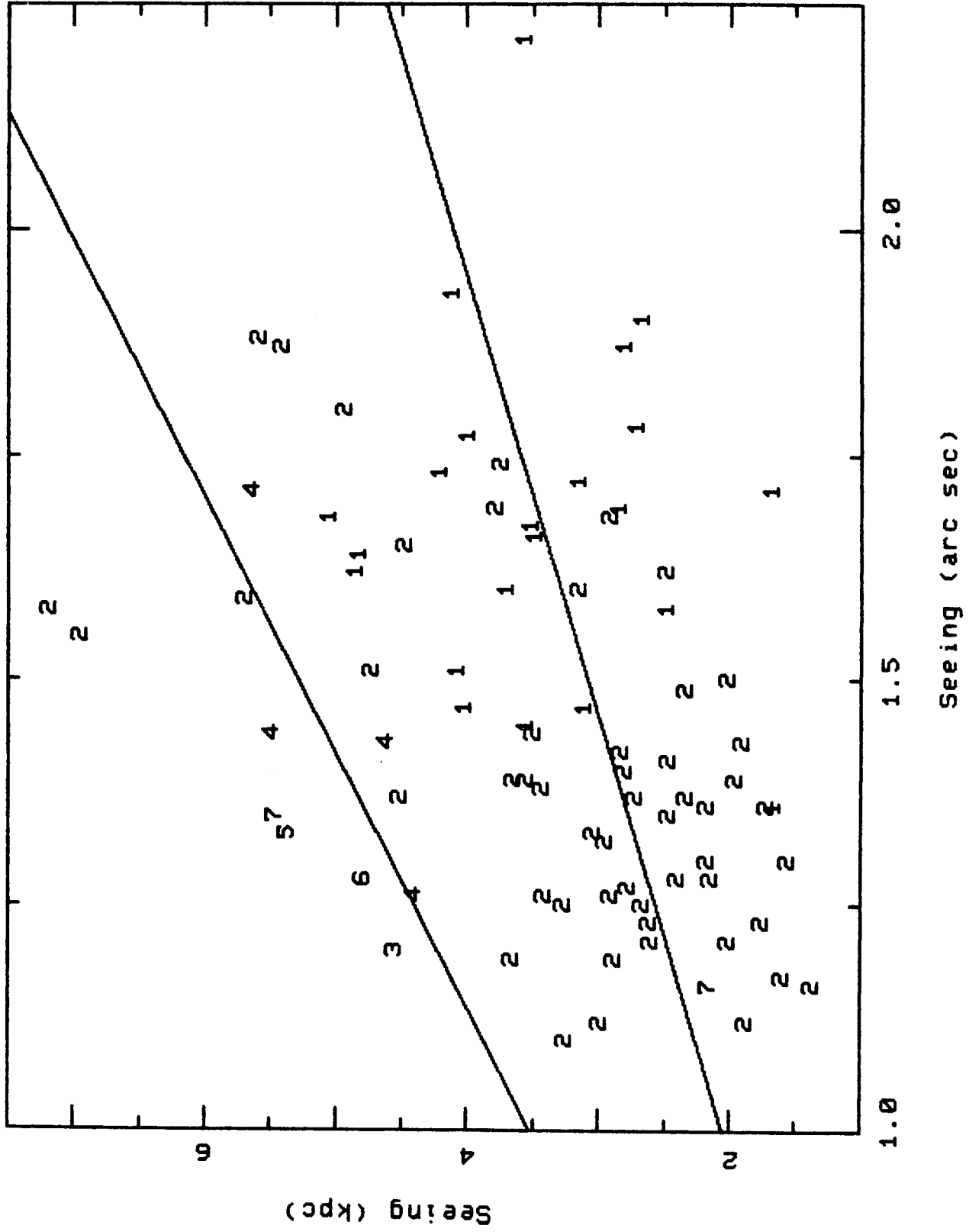
Figure 1
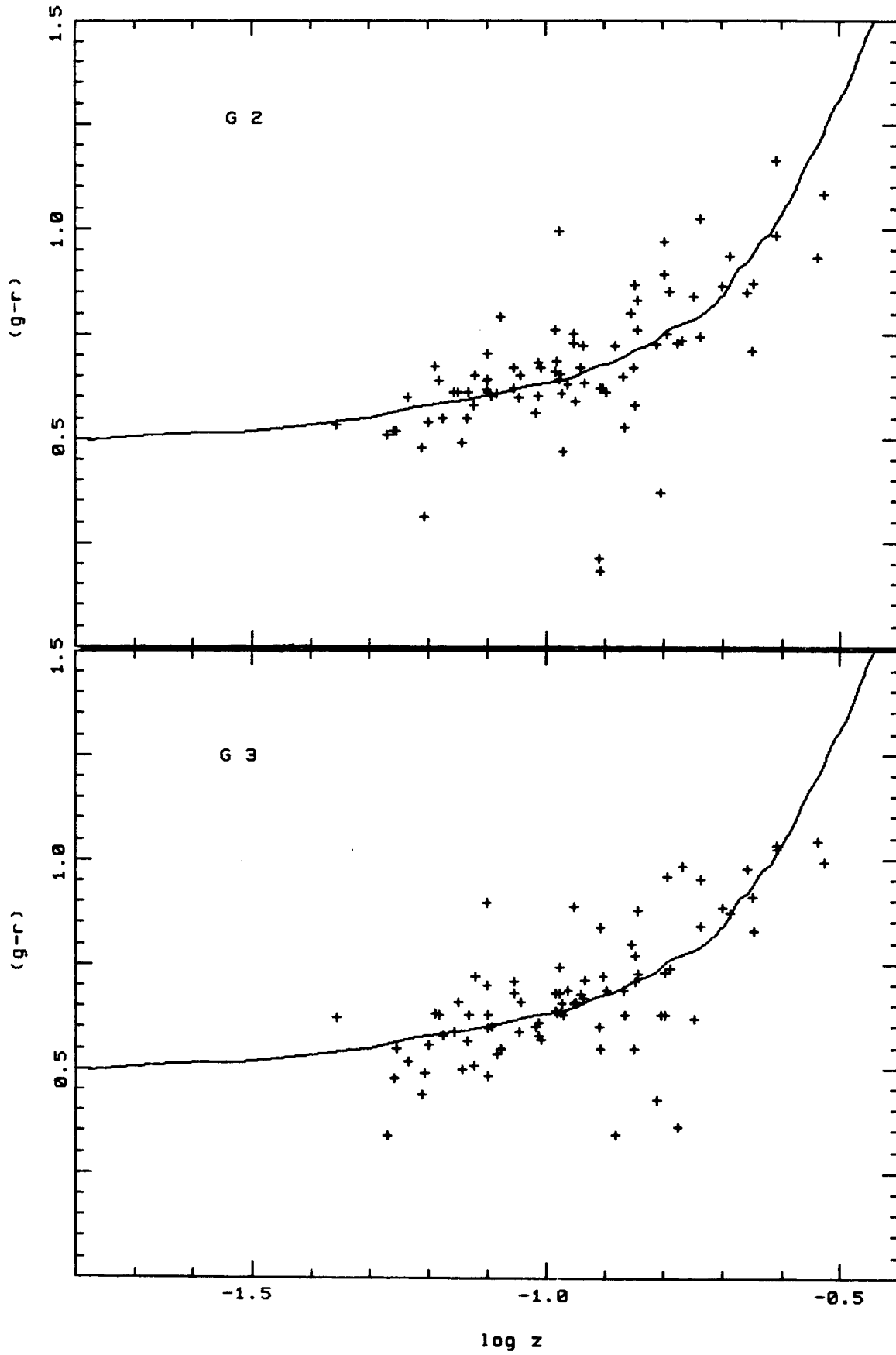
Figure 2
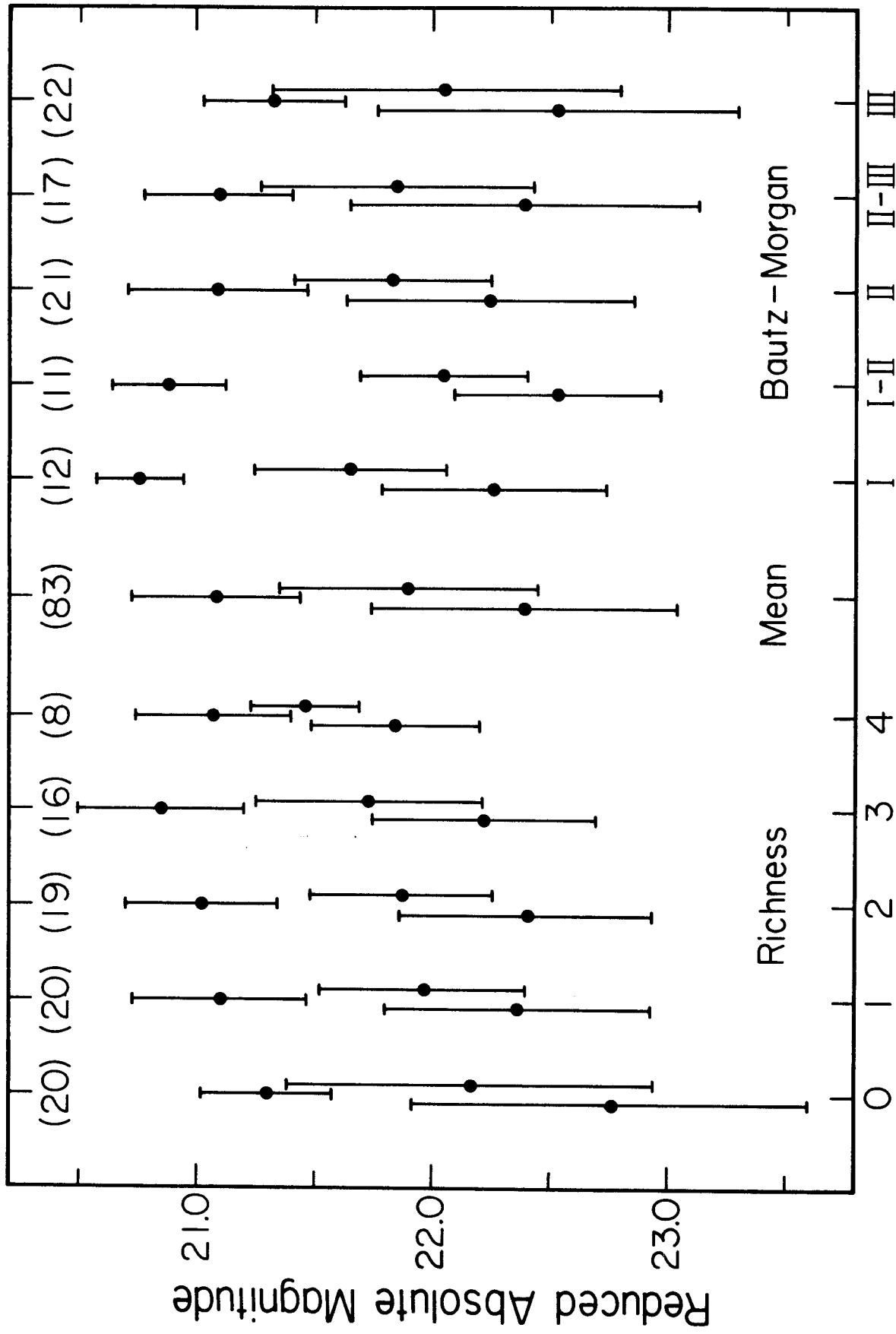
Figure 3
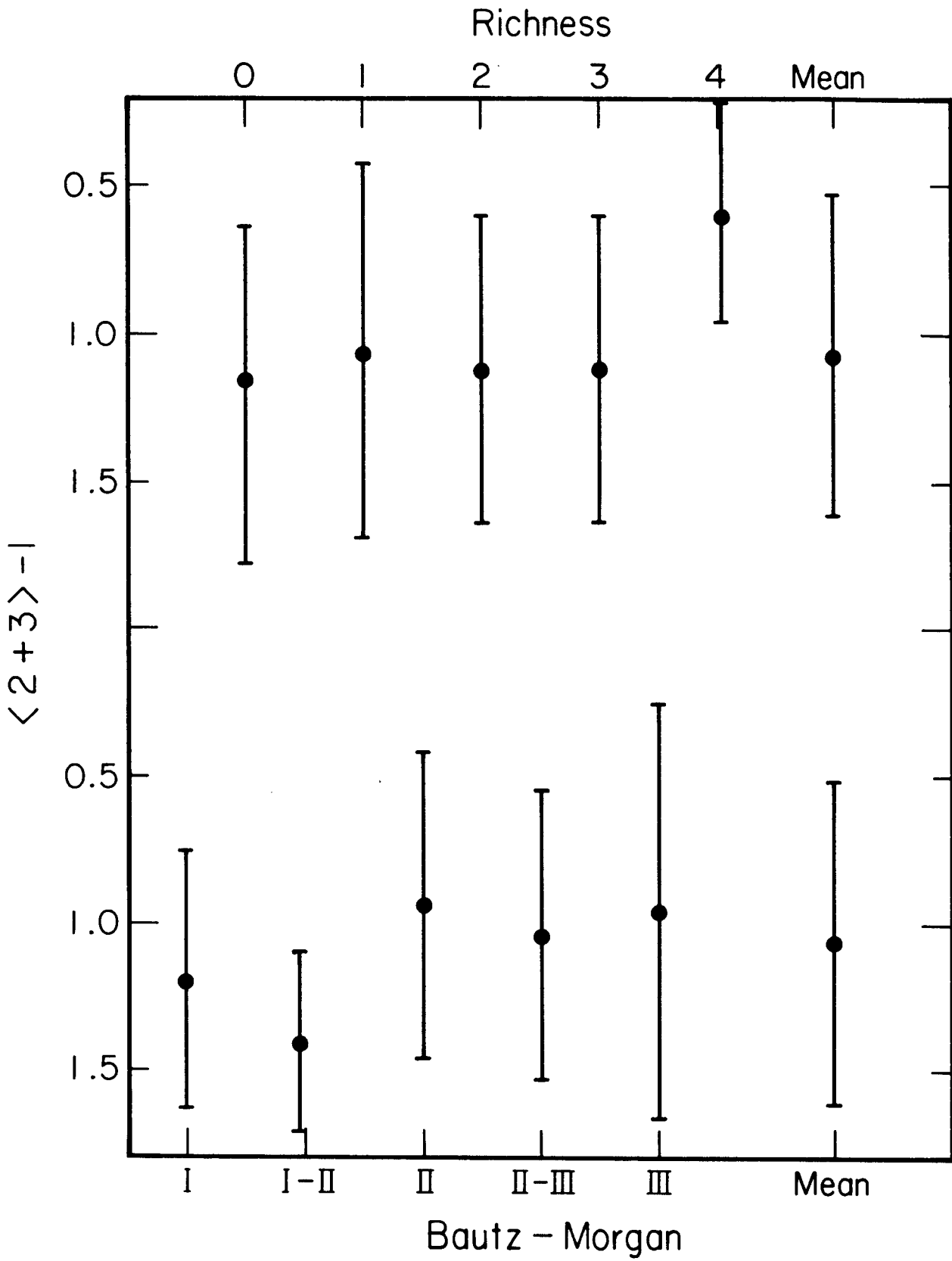
Figure 4

Figure 5

Figure 6

Figure 7

Figure 8

Figure 9

Figure 10

A 1689

A 1934
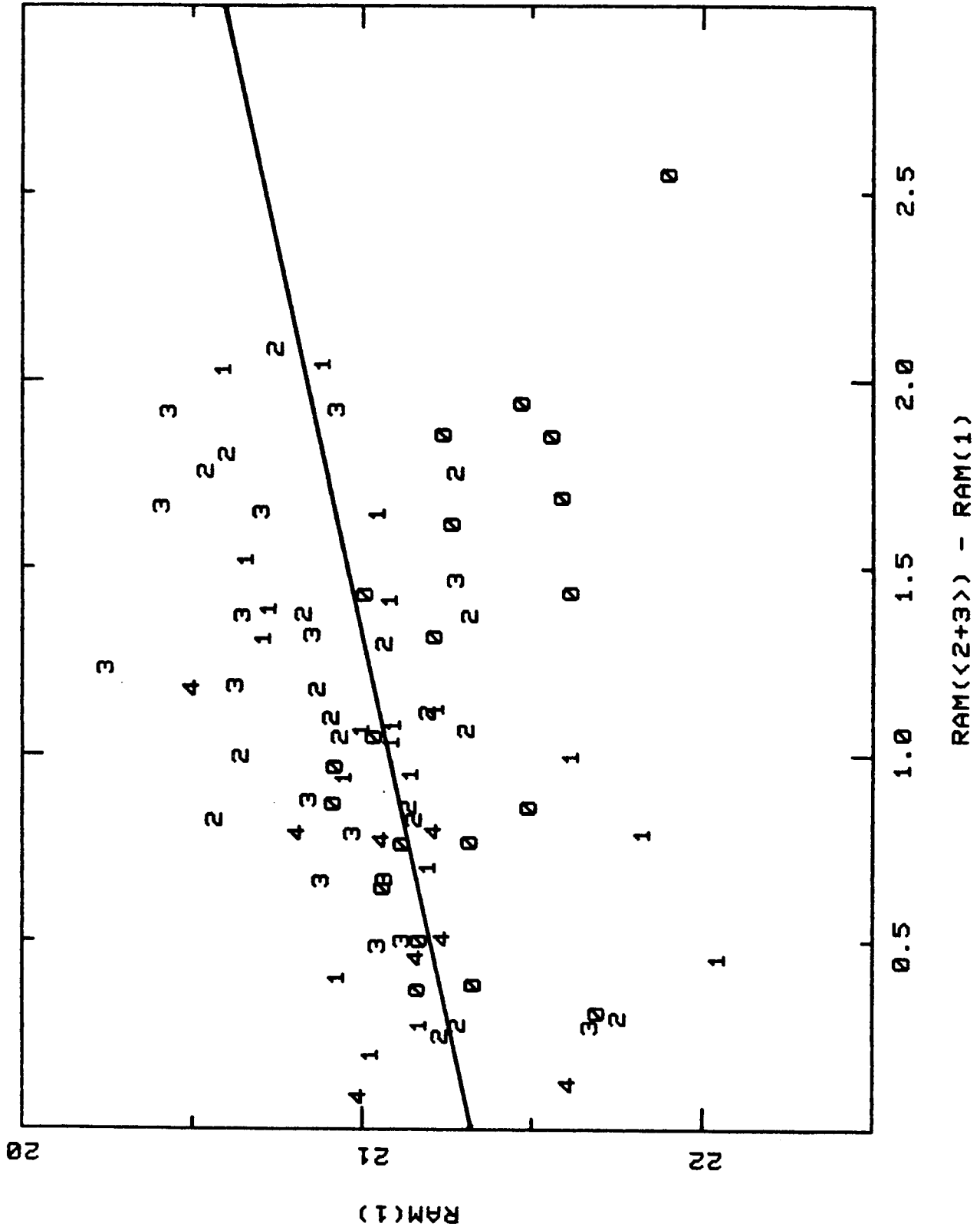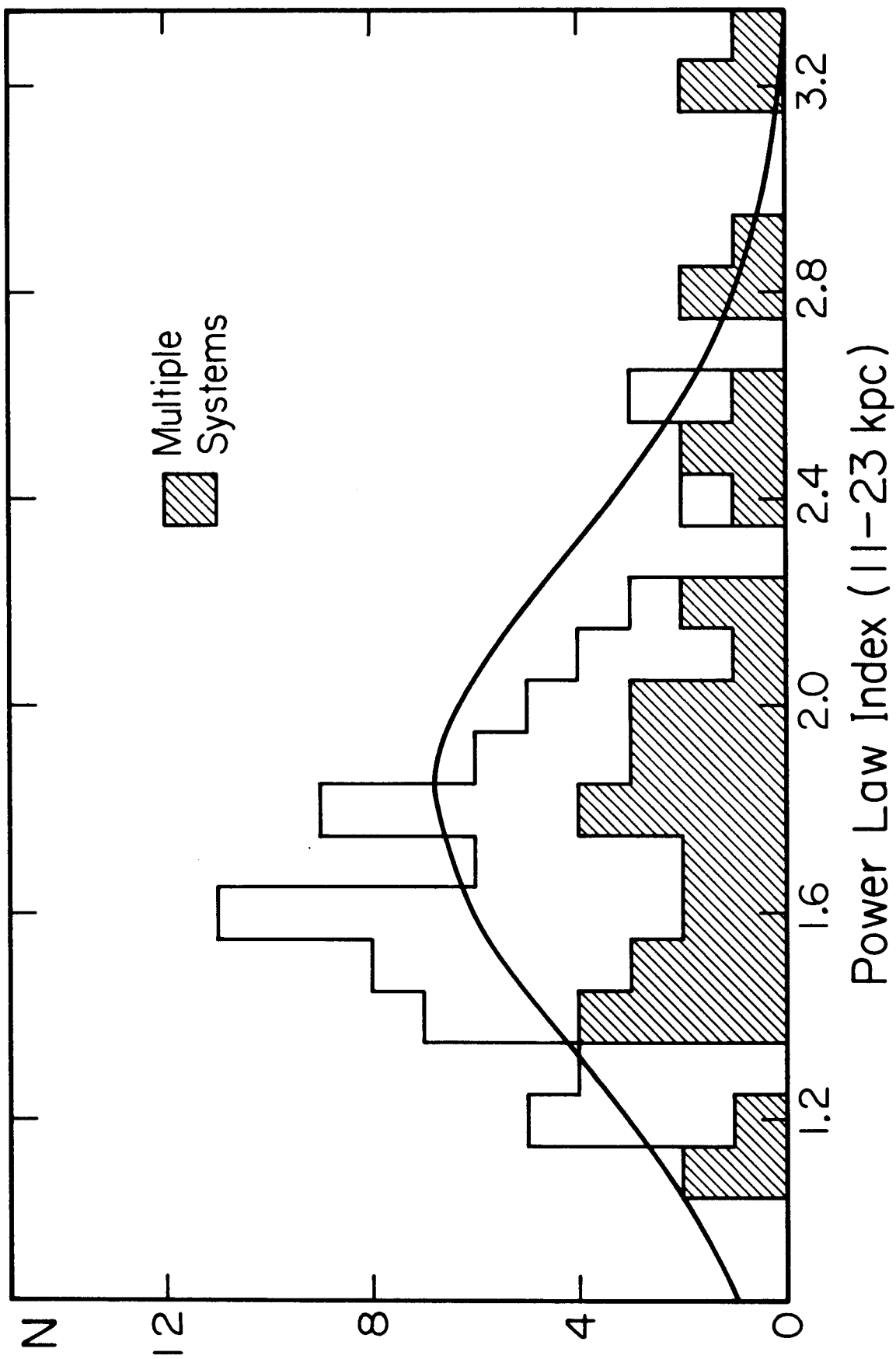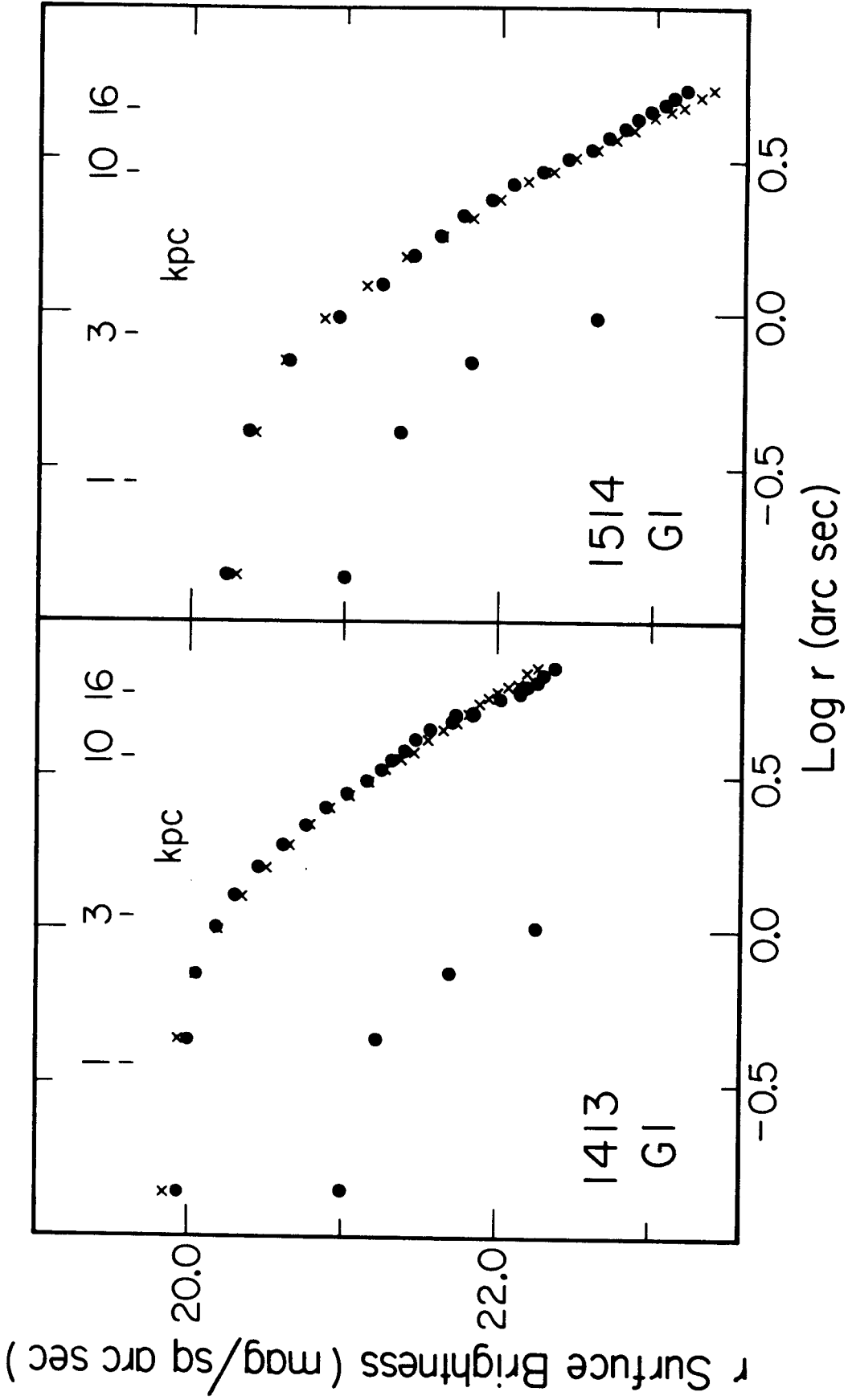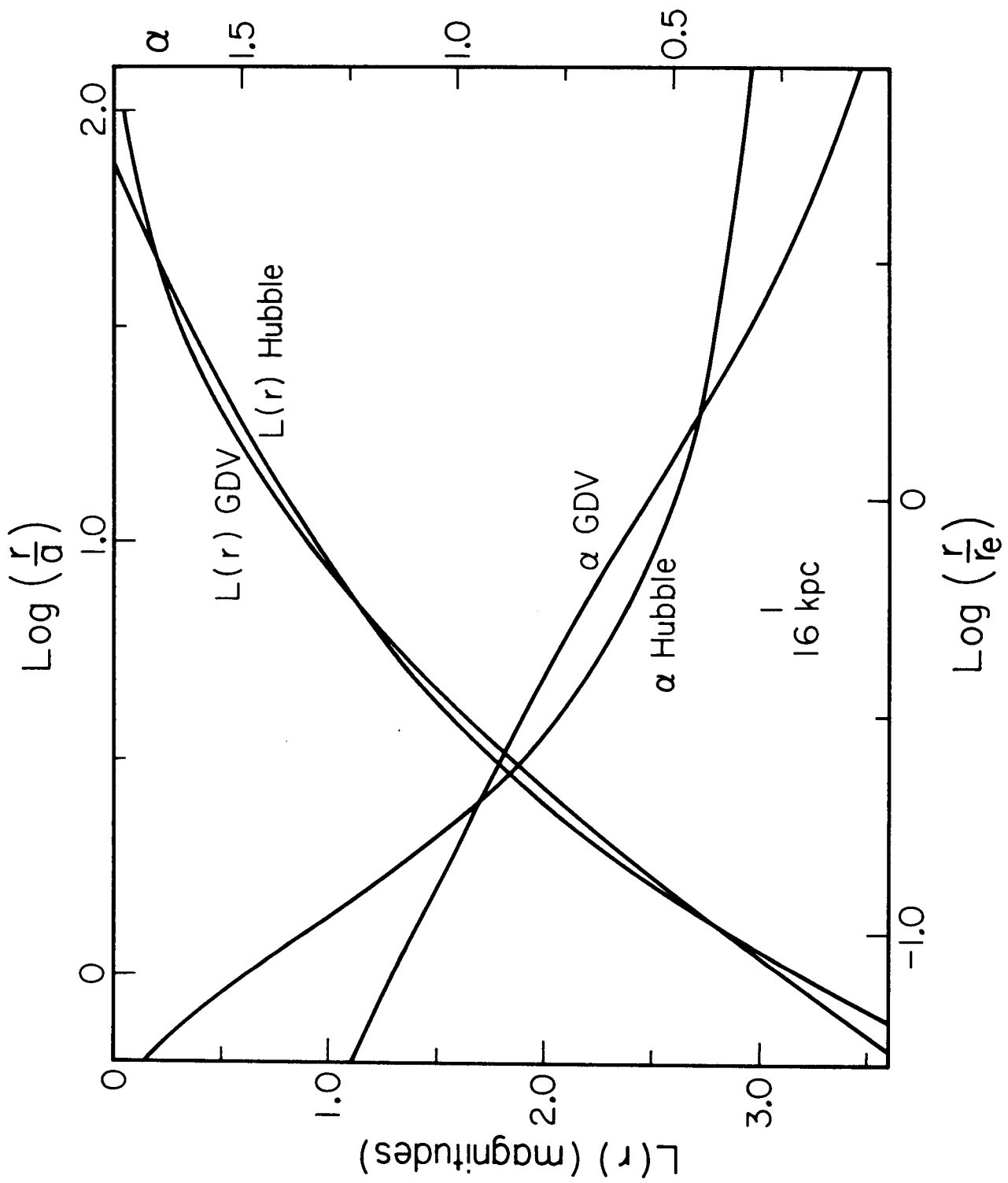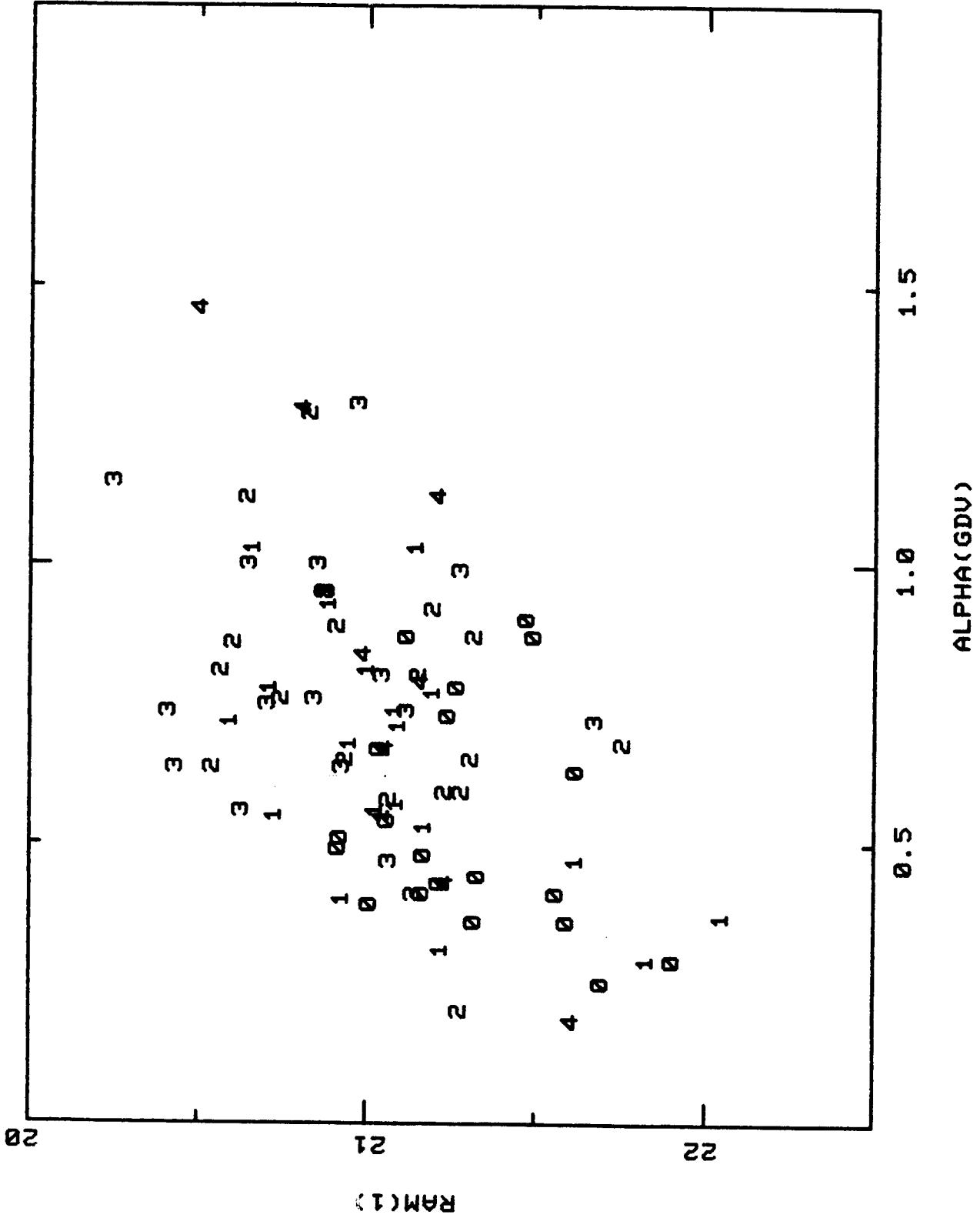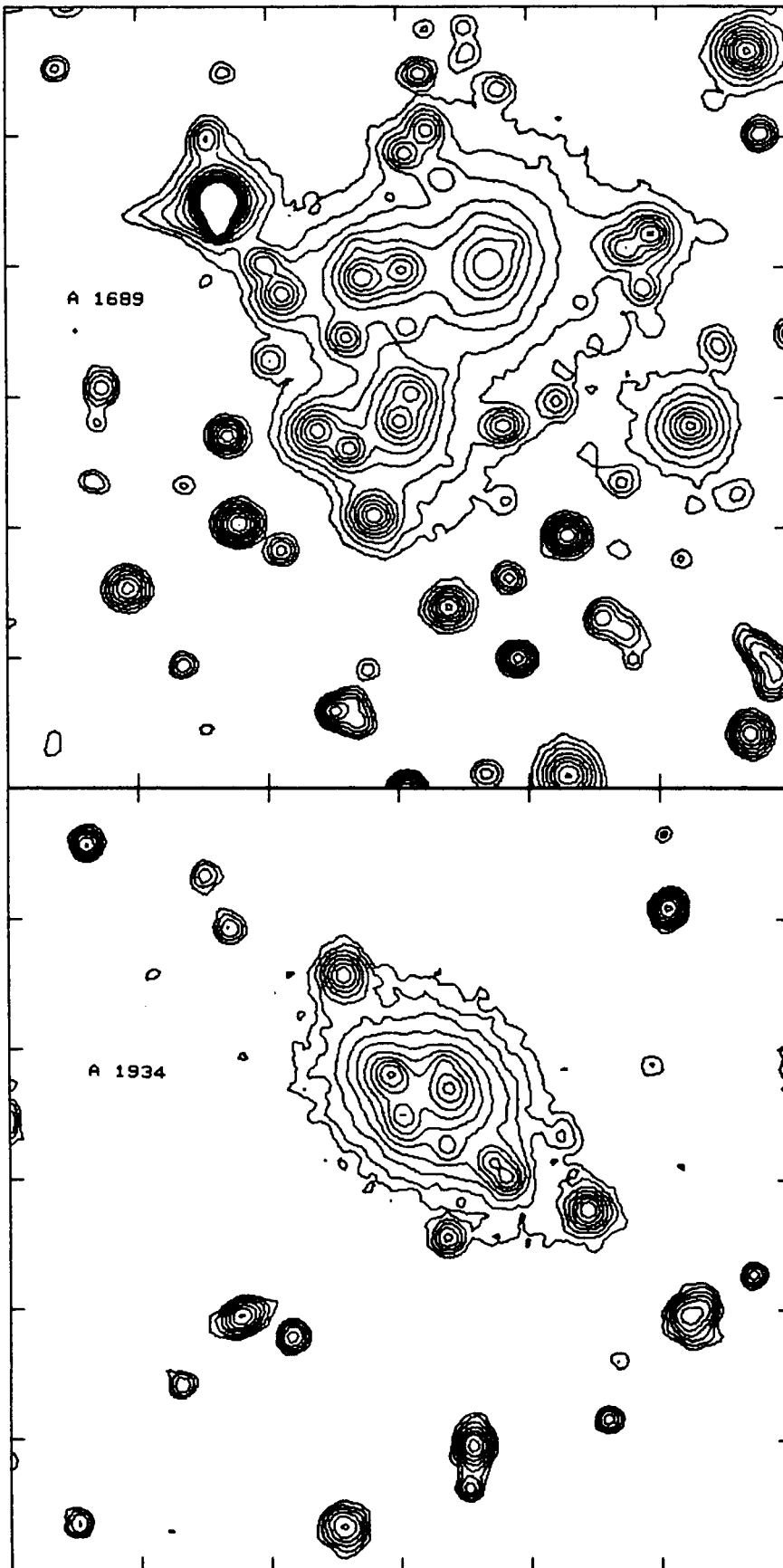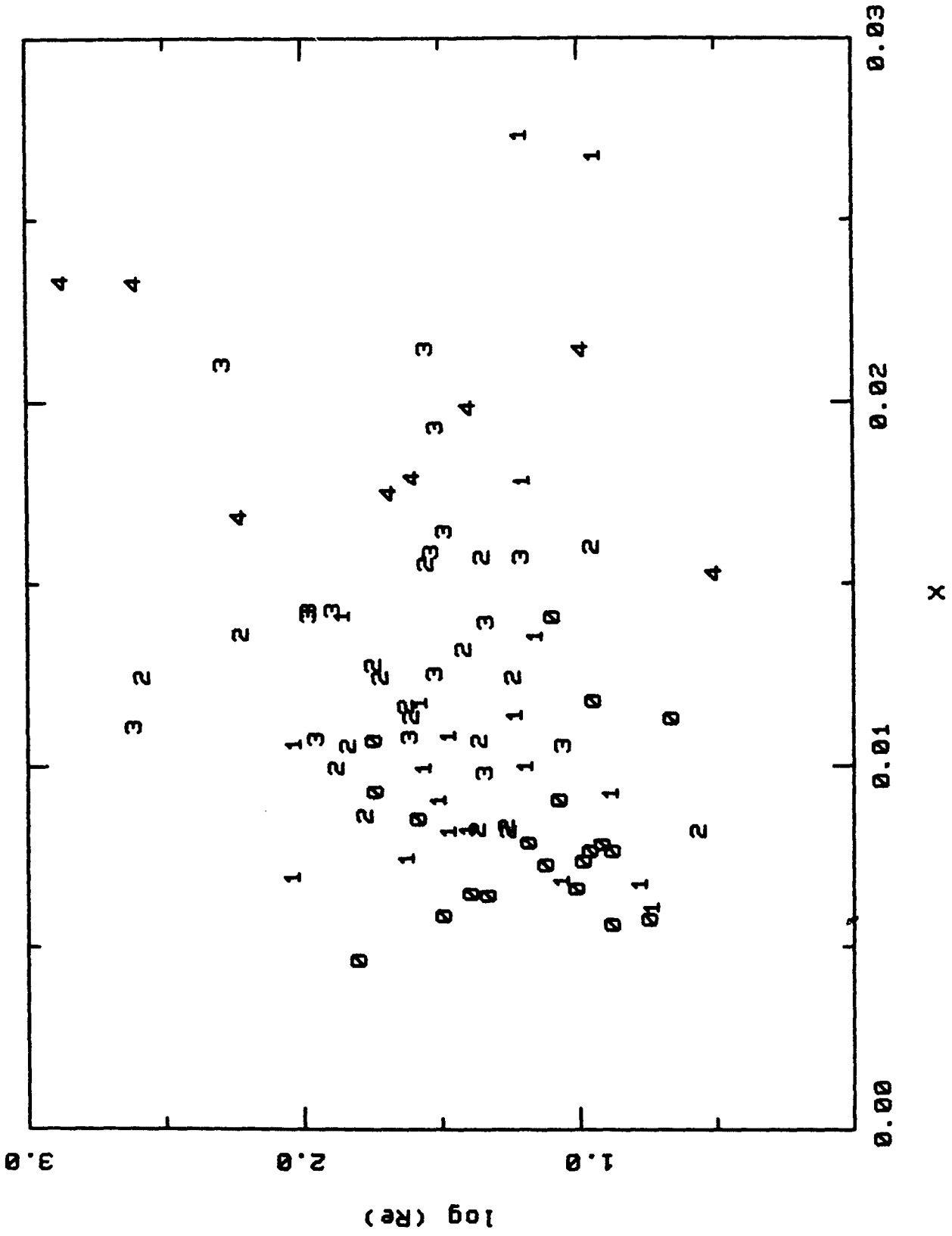
Figure 11

Figure 12

CHAPTER III

LUMINOSITY FUNCTIONS FOR 60 CLUSTERS

To be submitted to <u>The Astrophysical Journal</u>.

Author: Donald P. Schneider

(Paper III)

I. INTRODUCTION

The luminosity function for galaxies has long been a subject of interest and has recently been an area of intense investigation (for reviews see Schechter [1976] and Dressler [1978$\underline{b}$]). The most widely used representation of the luminosity function was proposed by Schechter (1976):

$$n(L) \, dL = n_* \left(\frac{L}{L_*}\right)^\alpha e^{-L/L_*} \frac{dL}{L_*} \quad . \qquad (1)$$

From a sample of 14 Abell (1958) clusters, Schechter found $\alpha = -5/4$ and M_* (= absolute magnitude of a galaxy of luminosity L_*) = -21.1 on the B_T system. For small groups (~10 members) Turner and Gott (1976) found a M_* similar to Schechter's measurement but a value of α (the power-law slope at the faint end) of ~-1. Investigations of the luminosity function of field galaxies have recently been completed by Kirshner, Oemler, and Schechter (1979) and Sandage, Tammann, and Yahil (1979).

Luminosity functions of rich clusters are especially interesting, because of their possible use as cosmological probes (Abell 1965). Schechter found a dispersion of 0.25 mag in M_*, which indicates M_* is a better standard candle than the commonly used luminosity of the brightest cluster galaxy (Gunn and Oke 1975; Sandage, Kristian, and Westphal 1976). The study of luminosity functions of rich clusters by Dressler (1978$\underline{b}$), however, cast suspicions as to the

usefulness of M_* as a cosmological test and presented some evidence that the functional form of the luminosity function varied from cluster to cluster. Using statistical arguments, Tremaine and Richstone (1977) found that the brightest cluster galaxies (denoted in this paper by G1) are "special objects", i.e., they are not drawn from the general luminosity function. Dressler (1978a) showed that three aspects of clusters are difficult to reconcile with a universal luminosity function - the low disperion in the luminosities of brightest cluster galaxies (most recent studies are Kristian, Sandage, and Westphal [1978] and Schneider, Gunn, and Hoessel [1982a], hereinafter Paper I), the small correlation of richness with the luminosity of the first-ranked galaxy (Sandage and Hardy 1973; Sandage, Kristian, and Westphal 1976; and Paper I), the relative fractions of morphological types (catalog of Lier and van den Berg 1977). A piecewise power-law form (Geller and Peebles 1976) does reproduce the observed distributions in BM class (Bautz and Morgan 1970), but fails the first two tests. The Schechter function predicts the properties of G1 by having a steep cutoff at high luminosity, but predicts that only one in 30 clusters will be of type BM I, contrasted with the observed 15%.

Hausman and Ostriker (1978) propose that these features are due to dynamical friction (Ostriker and Tremaine 1975).

Numerical simulations of the consequences of a brightest cluster galaxy accreting its neighbors match the observations quite well (Dressler 1979; Hoessel 1980). Cluster morphology (central galaxies growing at the expense of other members) is readily explained.

The number of moderately distant clusters ($z > 0.05$) that have been investigated in detail is only ~20 (Oemler 1974; Schechter 1976; Dressler 1978b,c). The introduction of high efficiency area photometers renders this problem much more tractable. This paper presents the luminosity functions in the cores (inner 250 kpc) of 60 Abell clusters. Despite the small region covered (a few percent of the cluster area) these data may reveal a great deal about cluster properties. Formation and evolutionary processes are probably very sensitive to the core conditions (primarily density and velocity dispersion). The observations and reductions are discussed in § II, and surface photometry of the galaxies in each cluster in § III. Sections IV and V deal with the fitting and results of the luminosity functions, and a discussion is given in § VI. In this paper all absolute dimensions refer to a $H_o = 60$ $q_o = 0.5$ universe.

II. OBSERVATIONS AND REDUCTIONS

a) Observations

The clusters in this study were selected from the rich-
ness sample described in Paper I. Briefly, 83 clusters
were taken from the catalog of Leir and van den Bergh (1977)
with emphasis on a wide range of richness. All clusters of
Abell richness classes 3 and 4 are included, as well as 20
each from richness classes 0, 1, and 2. Abell 545, at
lower latitude, was added due to the scarcity of rich
clusters. The observations were performed primarily with
the Palomar 1.5-m using the PFUEI (Gunn and Westphal 1982)
coupled to a low noise Texas Instruments 500 x 500 CCD.
The photometric calibrations and initial reductions are pre-
sented in Schneider, Gunn, and Hoessel (1982b, hereinafter
Paper II).

A relatively homogeneous set of high-quality data were
obtained for 61 or the 84 clusters. These exposures were of
at least 500 seconds duration in the r filter (Thuan and
Gunn 1976) in fairly good seeing using CCD's with very few
cosmetic flaws (see Fig. 1 of Paper II for the observing
conditions, the clusters in this paper are represented by
the symbols 2-7). The 1.5-m pictures had a field 4.7' on
a side. Four clusters were observed with the Hale telescope;
the field size of those pictures was 3.5'. The two clusters
acquired with the 800 x 800 CCD had their pictures reduced

to the same size as 500 x 500 data for convenience in re-
duction. One of the clusters, 2694, had to be rejected for
this work as a very bright nearby star made working on even
the brightest galaxies difficult. The remaining 60 clusters
(listed in Table 1) are well distributed in richness (0-4)
and redshift (0.05-0.30). A listing of the cluster proper-
ties can be found in Paper I.

b) Object Selection

To allow rapid processing of the data it was decided
to select objects based on their rest frame isophotes.
Tests on the most distant clusters showed that reasonably
accurate (~10%) photometry could be done on all objects
which possessed isophotes brighter than 22 r mag per square
arcsec (throughout this paper surface brightnesses will be
given in these units). This criterion has two unfortunate
side effects:

1. It discriminates against large, low-surface bright-
ness galaxies.

2. Object selection becomes seeing dependent. If the
same cluster is observed under different seeing conditions
one will go further down in the luminosity function in better
seeing. Another aspect of this effect is the redshift
dependence of object selection. If a set of clusters is
observed under identical conditions, the reductions will
find intrinsically fainter galaxies in the low-redshift

clusters. These problems can be handled in a consistent manner, and the practicality of the method is a strong positive factor. Since both the intrinsic luminosity and the photometric limits are determined by the most distant clusters, all clusters will be at least as complete at the faint end as the distant clusters. The determinations of the luminosity function will deal with the incompleteness by adopting an appropriate cutoff (§ V).

Contour maps of the central 480 x 480 area of each picture were generated displaying the 22nd, 21st, and 20th isophotes. Each object was labeled and its position recorded. About 5% of the objects were flaws or cosmic rays and were removed by inspecting the frame. Obvious foreground galaxies (large spirals) were also eliminated. Overlapping objects were also checked to make certain all objects had been found.

The latter point presents a dilemma - how to deal with complex objects. Paper I presented an unambiguous, easy to implement definition of a galaxy - the region of maximum light enclosed in an aperture with a metric radius of 16 kpc. This became necessary because of the high frequency of multiple systems - over 40% of the Gl's in the richness sample were multiple! While forming luminosity functions it seems more reasonable to treat the nuclei individually, as each nucleus represents a galaxy formed from the initial

luminosity function. The price one pays is some ambiguity

in comparing the magnitudes of the brightest cluster gal-

axies found in Paper I with the total luminosities in this

paper, as fitting each nucleus splits up a galaxy (as

defined in Paper I) into several components. Only a few

Gl's are strongly affected - those composed of several

roughly equal nuclei (1934 is a classic example of this,

see Fig. 11 of Paper II).

c) Object Reduction

The flattened data frames were processed by the inter-

active image processing program KAREN (see Paper II). Sky

subtraction for small objects was performed using a 2 pass 2σ

rejection procedure in a surrounding annulus. The sky level

for large galaxies was formed by averaging patches sur-

rounding the galaxy. On each frame a seeing star was

selected and the seeing profile found by fitting a double

gaussian to the stellar profile. Star/galaxy classification

was accomplished using the method described by Sebok (1979).

If the object was designated as a galaxy, then a

de Vaucouleurs (1948) model convolved with the seeing was

fit to the observed profile. (See Paper II for a description

of the convolution method . In this paper de Vaucouleurs

models will be denoted by GDV models.) Small objects could

be processed in a little less than a minute. The total

luminosity function could be completed in one to three hours,

depending on the cluster richness.

Several points should be noted:

1. All objects were assumed to be symmetric, as azimuthally smoothed radial profiles were created.

2. Complex objects were treated by ignoring pie-shaped regions where objects overlapped. When forming the radial surface brightness profile of an object, areas which were confused with other objects (or CCD flaws) were handled by rejecting points in a region bounded by two limiting radii and two angles (using the center of the object as the reference point) selected from visual inspection. This also assumes object symmetry.

3. The GDV model fit the majority of the galaxies quite well. The magnitudes in this paper refer to the total integrated magnitudes found from the models. The magnitudes should be reasonably accurate, as the region enclosed in a typical fit represented ~80% of the model luminosity.

4. Some brightest cluster galaxies did not fit GDV models when traced out to ~50 kpc. In general the envelopes of these galaxies were much more extended than those of the models. This caused the effective radius and the total luminosity to be dependent on what parts of the radial sur-face brightness profile were used to determine the model. Since the primary subject of this work is the luminosity function, it was decided that an accurate estimate of the

total luminosity was of primary importance. The surface
brightness profile was measured as far out as possible (out
to radii of ~50 to 90 kpc). The effective radius of the
model was fixed and the program adjusted the total lumi-
nosity. Several different R_e's were tried until a) the
model luminosity enclosed at the limit of the radial surface
brightness profile equaled the observed luminosity, and b)
at this point the surface brightness of the model and the
observed surface brightness were equal. For very extended
systems this resulted in an extrapolation of a factor of two
to three to the total luminosity.

5. Spiral galaxies (or, at high z, presumed spirals)
were also very poor fits to the GDV profile; they were
treated the same way as the Gl's.

After a model was accepted, the object's name,
position, effective radius, and magnitude were stored on a
disk file. The number of galaxies on a frame varied from
~10 for the poorest clusters to 135 for 1689.

III. SURFACE PHOTOMETRY OF CLUSTER GALAXIES

Surface photometry of roughly 2000 galaxies was per-
formed using the methods described in § II. All clusters
were searched for radial luminosity or size segregation,
but none were found in the regions covered by the data
(within 160 to 600 kpc of the central galaxy). Since only
the cores of the clusters were imaged and the Gl's roughly

centered, the center of the clusters were adopted to be at the position of the brightest cluster galaxy. All distances in this paper are defined in this manner.

Kormendy (1977) and Paper II found a very strong relationship between the effective radius (R_e) and surface brightness at the effective radius [$I(R_e)$] for elliptical galaxies. The data fit the relation

$$\log R_e = A + B\ (I(R_e) - 22) \tag{2}$$

remarkably well; for brightest cluster galaxies the dispersion in $\log R_e$ is only 0.1. The values A and B vary slightly depending on the class of galaxy (G1, G2, or G3); approximate values are 1.0 and 0.3, respectively, (R_e in kpc). This relation results in a luminosity-size relation ($L \propto R_e^{0.7}$) for bright ellipticals which has interesting cosmological and dynamical implications (Paper III). If all ellipticals had the same total luminosity, B would be 0.2.

Figure 1 displays the R_e-$I(R_e)$ relation for four clusters. Two of the clusters are among the richest (1689 and 2645); the other two are of richness classes 3 (42) and 2 (1785). Also plotted are the best linear fits.

This exercise was performed on all sixty clusters and their values for A and B are given in Table 1. A few brief comments should be made.

1. The rest frame surface brightnesses were calculated

using the k-corrections for ellipticals given in Paper I.

2. The brightest cluster galaxies all fall well above the mean relation. The average cluster galaxy with $I(R_e) =$ 22 has an R_e of 3 kpc, while a similar G1 has an R_e of 10 kpc - a factor of ten in luminosity.

3. For a given cluster the average dispersion about the line is 0.2 in log R_e.

4. The value of A for 2184 is abnormally low.

5. Lines of constant luminosity have slope of 0.2 in this diagram, which is very close to the average value of B.

6. As one moves to higher redshift the A's become larger (corresponding to a factor of two in R_e from the nearest to the most distant cluster).

The last feature sounds very ominous. This is precisely the effect one would expect if the deconvolution was incorrectly done. The critical factor is the ratio of R_e to the seeing disk; if the value of $R_e(cal)/R_e(true)$ is related to this ratio these results would have to be viewed with suspicion. The size of the effective radius at $I(R_e) =$ 22 is ~3 kpc, which would give a galaxy at z = 0.2 the same size as a 1.5" seeing disk.

Extensive tests of the profile program were performed and showed no systematic bias (Paper II), but then the real world is rarely as well behaved as the models. To check the deconvolution the clusters were binned into four redshift

groups and their values of A were compared to the seeing (FWHM). Figure 2 presents the results; no obvious trend is present.

Another test of the deconvolution is to follow the behavior of B with redshift. If the size of a galaxy is overestimated as the effective radius approaches the seeing disk, the R_e-$I(R_e)$ diagram for a given cluster should be distorted. As one moves to smaller galaxies in a cluster, they become systematically larger relative to the largest galaxies, which would lower the value of B. The nearest clusters should be relatively free of this effect as the effective radii of even the small galaxies are large compared to the seeing disk, while the distant ones would suffer a flattening of the relation. The observed values of B increase slightly with redshift, however; which contradicts the poor deconvolution hypothesis. (Of course, one could argue that there is a richness effect that overwhelms the seeing problem, but that would be as interesting as the observed increase in A with richness/redshift.)

The fact that the mean slope is so similar to the lines of constant luminosity causes one to wonder if this entire relation is merely an artifact of the selection process. Assume that there is no effective radius-luminosity relation for cluster galaxies and that the galaxies are uniformly distributed in luminosity. The points in the

R_e-$I(R_e)$ diagram would then be uniformly distributed below a line corresponding to the maximum luminosity present in the cluster. If the critical factor in object selection is luminosity, the observed distribution will be uniform between the maximum and minimum luminosity lines - and the best linear fit in the R_e-$I(R_e)$ plane would have a slope of 0.2. The same cluster observed at a larger redshift and reduced with the same methods would almost certainly have a cutoff at higher intrinsic luminosity. This would reduce the dispersion (σ_I) and raise the intercept in the R_e-$I(R_e)$ diagram. To get a rough idea of the expected effect, if the width of the relation was four-sigma, then the change in A would be

$$A(\text{distant}) - A(\text{nearby}) \sim 2(\sigma_I(\text{nearby}) - \sigma_I(\text{distant})).$$

The data do show this trend. The dispersion decreases with increased redshift, for the nearby clusters $\sigma_I \sim 0.27$, while for the distant clusters $\sigma_I \sim 0.18$. This corresponds to a change in the intercept (or A) of ~ 0.2, which is comparable to the observed change of 0.25-0.3. There is no doubt that there are incompleteness problems. The luminosity functions show the nearby clusters are complete down to 4-5 magnitudes fainter than M_*, whereas the distant clusters are complete only to ~ 3 magnitudes fainter than M_*. Also, the galaxies are clearly not uniformly distributed in luminosity; faint

galaxies are much more common (see Eq. [1]). Raising the lower luminosity limit in a cluster with a Schechter distribution of luminosities will cause the intercept of the mean relation to rise more than for a cluster with a uniform distribution in luminosity.

Before the R_e-$I(R_e)$ relation for cluster galaxies is dismissed as a selection effect, two points should be considered. First, brightest cluster galaxies, which all fall well above the cluster line (Paper II), have greatest influence in poor clusters. Excluding G1 in all clusters will reduce the observed σ_I and cause the values of A to drop more in poor clusters than in rich ones. This reduces the dependence of σ_I on redshift and causes an increase in the difference in A between near and distant clusters. Second, the objects are not selected on basis of luminosity, but on rest frame isophote levels. At a given luminosity, this clearly discriminates against galaxies with large effective radii if there are no seeing effects. The introduction of a seeing profile allows large galaxies to compete more favorably with compact ones, but the compact galaxies still win out for the observing conditions and object sizes present in this study. This should lead to a decrease in B with increasing redshift. Still, considering all the evidence, it appears that the process used in selecting the galaxies is the primary cause of the R_e-$I(R_e)$ relation for

cluster galaxies. Clearly, more work in this area is necessary.

Another point to consider is the effect of the presence of field galaxies. Their movement in the R_e-$I(R_e)$ diagram can be easily visualized from Figure 3. Assume a field galaxy of redshift z_f intrudes on a cluster at redshift z_c. Drawing a vector in Figure 3 from the point corresponding to z_c to z_f will show the error introduced. Note that for nearby field galaxies the motion is practically perpendicular to the line of constant luminosity, and at high redshift it becomes flat (the angular size changes slowly with redshift for $z > 0.25$ while the k-correction and the $(1+z)^4$ factor rapidly dim the surface brightness). Nowhere does it mimic the slopes found from the data. Inclusion of field galaxies will increase the dispersion about the observed relation.

Figure 4 compares the 16 kpc radius aperture measurements of G1 (Paper I) with the total magnitudes formed from the reductions in § II. RAM is the reduced absolute magnitude, which is the k-corrected magnitude an object would have if placed at a luminosity distance of one Hubble radius. The magnitudes are reduced to the g passband of Paper I. The lower line in Figure 4/equal magnitudes (no luminosity
represents
outside of 16 kpc); the upper line corresponds to a galaxy with an effective radius of 28 kpc (average R_e for brightest

cluster galaxies, see Paper II). A point of concern is that three galaxies fall below the lower line - 1880, 1934, and 1984. This is a consequence of the fitting procedure in § II. All three G1's are composed of at least two objects separated by < 20 kpc. The aperture magnitudes enclose all of the objects, whereas the total magnitudes were calculated for each individual nucleus. The brightest nucleus becomes the brightest cluster galaxy for the total luminosities; thus the appearance of several galaxies near the lower line. On average the total luminosities are about one magnitude brighter than those measured through the standard aperture.

IV. LUMINOSITY FUNCTIONS VIA MAXIMUM LIKELIHOOD

Previous investigations of cluster luminosity functions (Schechter 1976; Dressler 1978b) determined the luminosity function using standard non-linear least squares analysis. The advantages of using maximum likelihood techniques were reviewed by Sarazin (1980). In order to obtain the maximum amount of information from the data in this paper a maximum likelihood algorithm was developed that fit a Schechter function and a background. If the background has the form

$$\log N(r) = N_O + a \, r \; ,$$

(3)

where

$$N(r) = \text{number of galaxies per square degree between}$$
$$\text{magnitudes } r - 0.5 \text{ and } r + 0.5 \; ,$$

then

$$N(L)dL = \frac{\gamma}{L} \left(\frac{L}{L_s}\right)^\beta dL \quad .$$

Here

$$\beta = -2.5 \, a \quad ,$$

$$\gamma = 2.5 \log e \, \text{Area} \, 10^{(N_o + ar_s)} \quad ,$$

$$r_s = \text{arbitrary fiducial magnitude} \quad ,$$

and

$$L_s = \text{luminosity of a galaxy with magnitude } r_x \quad .$$

The number of background galaxies brighter than L_o is

$$n_b = \frac{\gamma}{\beta} \left(\frac{L_o}{L_s}\right)^\beta \quad .$$

The normalized probability density $p(L)$ is

$$p(L) \, dL = \frac{n_{cl} \, e^{-L/L_*} \left(\frac{L}{L_*}\right)^\alpha \frac{1}{L_*} + \frac{\gamma}{L}\left(\frac{L}{L_s}\right)^\beta \, dL}{\int_{L_o}^\infty n_{cl} \, e^{-L/L_*} \left(\frac{L}{L_*}\right)^\alpha \frac{1}{L_*} + \frac{\gamma}{L}\left(\frac{L}{L_s}\right)^\beta \, dL} \quad ,$$

where

$$L_o = \text{minimum observed luminosity} \quad ,$$

$$n_{obs} = \text{number of observed galaxies} \quad ,$$

$$x_o = L_o/L_* \quad ,$$

$$n_{cl} = \frac{n_{obs} - n_b}{\int_{x_o}^\infty x^\alpha e^{-x} dx}$$

and

$$\ln \mathcal{L} = \sum_{i=1}^{n_{obs}} \ln p(L_i) \quad .$$

No attempts were made to determine the value of α because of the difficulties with faint galaxies mentioned in § II. Maxmizing $\ln \mathcal{L}$ by varying L_* leads to

$$\sum_{i=1}^{n_{obs}} \frac{e^{-x_i} x_i^{\alpha} (x_i - \alpha)}{n_{cl} e^{-x_i} x_i^{\alpha} + \frac{\gamma}{x_i}\left(\frac{L_i}{L_s}\right)^{\beta}} = \int_{x_o}^{\infty} e^{-x} x^{(\alpha+1)} dx - \alpha \int_{x_o}^{\infty} e^{-x} x^{\alpha} dx \quad (4)$$

where $x_i = L_i / L_*$. If $\gamma = 0$ (no background) then (4) reduces to

$$\sum_{i=1}^{n_{obs}} x_i = n_{obs} \frac{\int_{x_o}^{\infty} e^{-x} x^{(\alpha+1)} dx}{\int_{x_o}^{\infty} e^{-x} x^{\alpha} dx} \quad .$$

The program was extensively tested using Monte Carlo simulations. Approximately 15,000 clusters of galaxies were created using the Schechter function with different m_*'s (apparent magnitude of L_*) and richnesses. Both $\alpha = -5/4$ and $\alpha = -1$ models were generated. A background area was then assigned and field galaxies were drawn from (3) with $N_o = -3.92$ and $a = 0.35$ (see Kristian, Young, and Westphal 1980). Any field galaxy brighter than the brightest cluster galaxy was rejected (this is, after all, what happens in practice). The models were submitted to a program which solved (4) to find the optimum Schechter function. The fitting program fit two models ($\alpha = -5/4$ and -1) to each cluster. The tests revealed a small L_*-richness bias in the

fit (underestimation of m_* by ~0.1 mag in poor clusters) which was empirically removed. The accuracy was not affected by the choice of the cutoff [x_o in (4)] except in the poorest clusters. Figure 5 shows a typical distribution of the likelihood found from this fitting procedure.

The most intuitive representation of cluster richness would seem to be total luminosity, or the integration of the Schechter function. (Integrating (1) gives 1.225 L_* and 1.0 L_* for α = -5/4 and -1, respectively.) For example, a cluster with 100 galaxies brighter than 0.01 L_* has a total luminosity of 15.7 L_* (α = -5/4) or 24.8 L_* (α = -1). This total magnitude will be denoted by m_{clus} (apparent) and M_{clus} (absolute). The quantity M_*-M_{clus} is directly related to the number of galaxies in a cluster.

In order to test the validity of the Schechter function, clusters with properties similar to the observational data were constructed. The simulations were divided into seven "richness classes" spanning the observed range (number of galaxies brighter than 0.01 L_* from 5 to 240). Representative values for the background area and m_* were selected (poor clusters had brighter m_*'s than rich ones). Eight hundred models in each class were created and then fitted with the maximum likelihood algorithm. The results for α = -1 models are listed in Table 2. As one moves to richer clusters the brightest three galaxies become more luminous (two magnitudes

from poor to rich) and the dispersion decreases (influence
of the exponential cutoff). The practical use of M_* as a
standard candle appears to be confined to clusters with
luminosities brighter than ~6 L_* (similar conclusions were
arrived at by Dressler [1978b]).

V.   LUMINOSITY FUNCTION DATA

The limited size of the field (~ 20 square arcminutes)
greatly restricts the region of the clusters that can be
investigated. It will be impossible to construct the total
cluster luminosity functions as did Schechter (1976) and
Dressler (1978b). An attractive alternative is the concept
of a limiting metric radius (R_L); this would allow the
clusters in this sample to be treated consistently. The core
radii of clusters are about 250 kpc (Bahcall 1977; Dressler
1978c); since this is representative of the region covered in
the data it is an obvious number to adopt. Several clusters
are at relatively high redshift and therefore can have larger
areas included in the luminosity function. A survey of the
available data found that an appreciable number could be done
using a radius of 400 kpc.

The center of each cluster was defined as the position
of the brightest cluster galaxy (§ III). If the circle with
a radius of 250 (or 400) kpc was completely contained on the
frame, the reduction was straightforward. If this was not
the case (due either to too low a redshift or improper

centering of G1) the following procedure was carried out:

1. The "radius" of a frame (R_f) was defined as the radius of the circle which contained the same area as the entire observed frame.

2. All galaxies on the frame were used in forming the luminosity function.

3. A luminosity correction factor f was determined assuming the spatial cluster luminosity profile was similar to the surface density of galaxies and that the surface density of galaxies was adequately represented by a modified Hubble law with a core radius of 250 kpc. The value of f for a limiting radius R_L is

$$f = \frac{\ln [1 + (R_L/250 \text{ kpc})^2]}{\ln [1 + (R_f/250 \text{ kpc})^2]} .$$

The luminosity correction factor is proportional to R_f^{-2} for small R_f (constant surface density of clusters in the core) but falls off less steeply at large R_f. (If $R_L = 250$, the f($R_f = 400$ kpc) is 0.55 instead of 0.39). There are several problems associated with this method. If there is any luminosity segregation, the equal area argument is not valid. The second and third brightness galaxies found in this manner may not be the same as the actual ones (and there are no systematics in this since in practice f goes from less than one to greater than one). The most serious objection is that the brightest cluster galaxy is

automatically included in all luminosity functions. This will cause M_* to become fainter as R_L is increased (fainter cluster members dilute Gl's effect), which would normally be interpreted as luminosity segregation.

All 60 clusters were analyzed using an R_L of 250 kpc. Twenty-nine clusters required corrections due to improper spatial coverage (f ranged from 0.68 to 1.71). Twenty clusters could be properly studied using R_L = 400 kpc; their f's varied from 0.74 to 1.03 (only one cluster, 910, needed a correction greater than 15%).

These luminosity functions were processed by an inter-active fitting program which employed the maximum likelihood technique described in § IV. Equation (4) was solved, which yielded an initial value of m_*. Then the galaxies within 2.5 mag (rich clusters) and 3 mag (poor clusters) of m_* were used to determine the final parameters. This usually resulted in a limiting fitted magnitude about one magnitude above the faintest measurement, but a few clusters used nearly all of the galaxies. No corrections for incomplete-ness were made, and there is some evidence that it is pre-sent (the faint end of some luminosity functions turn down). The magnitude limits used in fitting nearly all the clusters, however, are probably brighter than the luminosity where incompleteness becomes a problem.

The models for ten of the poorest clusters were very

poor fits to the data, undoubtedly due to the small number
of galaxies present. The m_*'s for these clusters were very
bright (11-13 magnitude), thus only a few galaxies were used
in the final iteration. These clusters were reprocessed
using a magnitude cutoff 4 magnitudes fainter than m_*; the
resulting models were much better representations of the data.

The adopted level of the background is considerably
greater than that used by Dressler (1978b). The CCD data,
however, are fairly impervious to background problems.
Since only the cores are measured, the ratio of cluster
galaxies to field galaxies is very high (only 5-10% of the
galaxies arise in the field while Dressler's sample suffered
a contamination of 25%). The field galaxies are heavily
weighted at the faint end (they have a Schechter α of -1.88).
The rich clusters have no problem with the background as they
dominate it at all levels. The poor clusters are consider-
ably brighter in apparent magnitude (since there is a strong
richness-redshift correlation in this sample), thereby
avoiding most of the background. Tests were run on several
clusters of different richness; to get noticeable effects
one had to increase the background by ~40%, this caused the
m_*'s to brighten by ~0.1 mag.

Problems with this scheme became apparent upon studying
the deduced Schechter functions. The values of M_*'s for the
20 distant clusters were systematically dependent on

$R_L(\langle M_*(250)\rangle = \langle M_*(400)\rangle - 0.4)$. The $\langle M_*(250)\rangle$ was about one magnitude brighter than the M_*'s found by Schechter and by Dressler. Poor clusters had M_*'s which were a magnitude brighter than that of the rich clusters.

All this can be traced to the influence of the brightest cluster galaxy. At small radii (or poor clusters) G1 dominates the fit. Not only that, but if G1 is not drawn from a general luminosity function (Tremaine and Richstone 1977) then it is not clear how useful the fits are.

When the observed M_*-G1, M_*-G2, and M_*-G3 for each cluster were compared to the predictions in Table 2, the second and third brightest galaxies were in good agreement with the hypothesis that they are drawn from a Schechter function. The brightest cluster galaxy matched the simulations in a third of the cases, but the rest of the G1's were one or two magnitudes too bright.

The luminosity functions were all redone ignoring the brightest cluster galaxy (although its position still defined the cluster center). This method avoids one of the previous pitfalls - the old second brightest member (new G1) is not automatically included in the innermost radius. If there is no luminosity segregation the derived M_* should be independent of the limiting radius used to construct the luminosity function.

The results of these fits are given in Tables 3 (250 kpc)

and 4 (400 kpc). Also listed are the magnitudes of the brightest three galaxies (G1 refers to the brightest cluster galaxy, the one ignored when determining the cluster luminosity function). The m_*'s are the observed r mag, while M_*, M_{clus}, G1, G2, and G3 are the reduced absolute magnitude in the g band. The k-corrections for ellipticals of Paper I were used in calculating the absolute magnitudes, and the rest color of +0.47 (average G1, G2, and G3 from Paper I) was assumed. Figure 6 displays four examples of the luminosity function fits. There is a remarkable contrast in cluster luminosities inside of 250 kpc (which is a measure of the central density). The richest (1689, see Fig. 12 in Paper II) is nearly four magnitudes brighter than the least luminous clusters.

Dressler found that the luminosity function of clusters became very flat at low luminosities and the data in this work suggests the same. Only the $\alpha = -1$ models are listed in Tables 3 and 4. The $\alpha = -1$ models described the data slightly better than did the $\alpha = -5/4$ ones. This is a very tentative conclusion, as α is primarily determined by the faint cluster galaxies which are most subject to incompleteness and background problems. Another reason for selecting the $\alpha = -1$ model was the instability of the $\alpha = -5/4$ models. The fits using the latter value were much more sensitive to the cutoff luminosity than the $\alpha = -1$

models.

Figure 7 compares the M_*'s found using different R_L's
for the 20 distant clusters. There is still a slight trend
with limiting radius ($\langle M_*(250)\rangle = \langle(M_*(400))\rangle -0.19$), but
overall the agreement is quite good. The cluster luminosities
in both radii for these 20 clusters are plotted in Figure 8.
If the assumptions about core radii and luminosity are cor-
rect, then the clusters should brighten by 0.66 mag when the
limiting radius is changed from 250 to 400 kpc. The observed
difference is 0.64 mag. Remember that these luminosities
are the integrated Schechter function determined without Gl
and not the sum of the observed luminosities. That is why
one cluster, 1401, is practically on the line of $M_{clus}(250) =$
$M_{clus}(400)$. This cluster has a concentration of bright
galaxies in the center, so the 250 kpc model luminosity
function is much higher than the observations for faint
galaxies. The 400 kpc data fills in this "hole" while
adding very few luminous members, thus changing the model
very little. This is an illustration of the fact that M_*
is determined primarily from the bright galaxies (Dressler
1978b).

VI. DISCUSSION

It was decided to only use 59 of the 60 clusters in the
analysis based on evidence presented in Paper II and this
work. One of the clusters, 2184, has very unusual properties.

It manages to isolate itself in the $\langle 2+3 \rangle - 1$ aperture magnitude relation (Fig. 5 of Paper II). A cluster member in 2184 with $I(R_e) = 22$ has an effective radius of only 1 kpc, whereas galaxies with $I(R_e) = 22$ in other clusters at that redshift have R_e's of 2.3 $\pm$ 0.35. The luminosity function yields a M_* (Table 3) over a magnitude fainter than the next faintest one (1785). All of this would be rectified if the cluster redshift was ~0.1 instead of 0.055, suggesting that the adopted G1 is a foreground object. In any case, it is so unusual that it will be excluded in the following discussion.

First let us return to the $R_e - I(R_e)$ data on the cluster members presented in § III. Figure 9 shows A as a function of redshift (actually as a function of x, which is 0.11 z at small redshifts, see Paper I) and Figure 10 depicts the dependence of A on cluster richness. (Unless otherwise stated, all remarks concern the 59 member 250 kpc sample.) The A-redshift plot is most compelling, and, unless selection effects are very strong, hard to explain. If it is attributed to surface brightness evolution, a change of one mag per square arcsec is required in order to move A by 0.2. This is ruled out by a) no color evolution in giant ellipticals back to redshifts of 0.3, and b) the strong $R_e - I(R_e)$ relation for giant ellipticals. The effect is not likely to be due to use of an incorrect world model in

calculating the effective radii, as one needs a q_o of ~8 to reproduce the observations. The A-richness correlation is strong, but the scatter is 50% greater than in Figure 9. Whatever the resolution of this problem (is this effect real or due to seeing/selection uncertainties?) it appears that this may be a very powerful angular diameter test/ evolutionary probe. If the A-redshift relation is caused by selection effects, a cosmological test may be possible using the cluster members. One interpretation of Figure 9 is that the mean luminosity of cluster galaxies with luminosities within a given factor (~0.1) of the luminosity of Gl is remarkably constant. Further investigations are required to determine if this is practical.

The interpretation of the other surface photometric coefficient, B, is likewise difficult. Figure 11 displays its relationship to cluster richness. The constant luminosity value (0.2) is drawn in. The only trends with richness are a reduction in the scatter in rich clusters and a tendency of poor clusters (especially richness class 0) to fall below the B = 0.2 line. Perhaps we are viewing different populations (stripping vs. non-stripped galaxies, spirals vs. ellipticals?). In any case, the cluster members fall well below the relation for the luminous cluster galaxies (B ~0.3), although B does systematically decline from Gl to G3 (see Paper II). This aspect of clusters seems

ideally suited for investigation with the Space Telescope.

Returning to the luminosity functions, Table 5 lists the M_*, M_{clus}, and G1 magnitudes binned by Abell richness class and BM type. There is very strong correlation between richness class and M_{clus} (clusters with a larger number of total galaxies have high central densities), but as can be seen from Figure 10 the relation is not perfect (some richness 0 clusters have higher central surface densities than some richness 3 clusters). The luminosity of the brightest cluster galaxy has roughly the same relation to richness as for Abell richness class (see Paper I). Note that in poor clusters G1 on average contributes nearly as much light as do the rest of the cluster core members. (Perusal of Table 3 will reveal several clusters with G1's that outshine the rest of the core!) The sigmas of M_* decrease with increasing richness, as predicted by Table 2.

The Bautz-Morgan table is rather uninformative. If one bins the I and I-II's together and compares them with the combined II, II-III, and III's, one finds that the brightest cluster galaxies in the first group are slightly brighter and their M_*'s slightly fainter than those in the second group. This is the effect one would expect if the BM I and I-II clusters were more evolved and the giant had consumed other bright members, but the difference in the observed M_*'s is only marginally significant.

One interesting entry in Table 5 is the intrinsic dispersion of 0.61 mag in the total luminosity of the brightest cluster galaxy. It appears that the conjecture of Paper II/ — is correct — the small dispersion in the aperture magnitudes (0.35 mag) is due to the structural relation and not to the luminosity. It is clear that brightest cluster galaxies are impossible to explain using any type of general cluster luminosity function. There must be a sharp cutoff in order to produce the small cluster richness-Gl luminosity relation. The cutoff must be steeper than a Schechter function (see Table 2). At the same time, however, the dispersion in luminosity must remain large (0.6 mag), and a steeper cutoff will produce a smaller dispersion than the Schechter function (0.35 mag).

If the brightest cluster galaxy is ignored, can the rest of the cluster be explained by a Schechter function with a universal M_*? Table 5 gives an average M_* of 22.07 and a dispersion of 0.51 mag. To compare this with the results of Schechter and of Dressler, this mean will be placed on the B_T and M_F systems using the photometric transformation given in Paper I:

$$B = g + 0.68 \pm 0.03 \quad \text{and} \quad F = g - 1.05 \pm 0.10 \ .$$

The distance modulus of one Hubble radius for $H_o = 50$ is 43.89. Thus,

$M_*(B_T,$ this paper$) = -21.14 \pm 0.08$ $M_*($Schechter$) = -21.1$

$M_*(M_F,$ this paper$) = -22.87 \pm 0.12$ $M_*($Dressler$) = -22.6$.

Dressler used isophotal magnitudes instead of total magnitudes and a value of one (instead of 0.5) for q_0. Approximately 0.1-0.2 mag should be subtracted from his result for direct comparison with this work. The dispersion in M_* in the richness sample is similar to that found by Schechter (0.50) and Dressler (0.45).

Figure 12 compares M_* with the cluster richness. The solid line is the mean, and the dashed lines the expected dispersion. The evidence for a universal M_* seems well justified. The poor clusters have a smaller dispersion than predicted, but this is undoubtedly due to the fitting program "getting lost" while finding M_* (see § V). Using roughly the same luminosity cutoff for the poor and rich clusters resulted in unsatisfactory fits for ~30% of the poor clusters. The final models for the badly fit clusters were determined by lowering the luminosity cutoff to include more galaxies in the fit. Since the poor clusters tend to be at low redshift, incompleteness should not be serious at levels used in the final model. In the simulations, however, the poor fits were included (each cluster was not inspected to see how well the model represented the data). The dispersions for the poorest clusters given in Table 2 should be viewed as upper limits.

If one requires the clusters to have core luminosities (RAM) brighter than 20, one has a standard candle that is at least as good as the aperture magnitude of G1. While M_* gives up ~25% to the aperture magnitude in the dispersion, it recovers the loss with a gain in sensitivity to q_0. A test using M_* is not afflicted with an aperture correction factor, unless it is shown that M_* changes systematically with limiting radius (and there is some evidence of weak luminosity segregation, as the $\langle M_*(400) \rangle$ is fainter than the $\langle M_*(250) \rangle$).

Figure 13 shows that if one ignores the brightest cluster galaxy the other bright members fit a Schechter function quite well. Plotted for each cluster is M_*-G1 (the galaxy ignored in the fit), M_*-G2, and M_*-G3 as a function of M_*-M_{clus} (the number of galaxies in the core). The solid line is the mean and the dashed lines the expected dispersions from Table 2 (the low richness errors are uncertain). The middle panel has the M_*-G1 relation of Table 3 plotted, while the lower graph shows the M_*-G2 curve. Once again the use of the Schechter function for all but the brightest galaxy seems justified. It is easy to see that the G1's are out of place - the $\langle M_*$-G1$\rangle$ is 1.84 mag, with a few instances of M_*-G1 > 3 mag. The brightest G1's have total luminosities of ~19.2, which corresponds to a B_T magnitude of -23.6 or 4.4 x 10^{11} $L_\odot$ for H_0 = 60.

Cluster core luminosities range from ~4 x 10^{10} $L_\odot$ to 1.2 x 10^{12} $L_\odot$.

The strong relationship between the luminosities of G2 and G3 and cluster richness seen in Figure 13 is not as prominent when the magnitudes are divided into Abell richness classes. Table 6 lists M_*-G1, M_*-G2, and M_*-G3 for the clusters broken down by Abell richness class and BM type. As was found in Paper II, the luminosities of G2 and G3 rise by roughly the same amount as G1 from richness class 0 to richness class 3. In richness 4 clusters, G2 and G3 are considerably brighter than their counterparts in class 3 cluster, whereas G1 drops slightly in magnitude from richness 3 to 4. (Remember the measurements in Paper II are aperture magnitudes while this paper presents total luminosities.) This suggests (not unexpectedly) that estimates of cluster richness based on measurements of the central density are more indicative of cluster properties than Abell richness class.

This returns us to one of the motivating factors of this work - attempts to calibrate the luminosity of the brightest cluster galaxy. Figure 14 shows how the aperture magnitudes of G1, G2, and G3 (Paper II) change as function of cluster richness. There is very little relationship between the luminosity of G1 and cluster richness. This graph conveys about the same information as Table 5 - a

brightening of 0.4 mag from the poorest to the richest clusters. The results for G2 and G3 are striking; there is a very steep relationship. The second-ranked galaxy brightens by 1.5 mag and G3 2 mag over the range of cluster richness. If one applies a richness correction to G2 and G3, they become decent cosmological probes in their own right (dispersions of 0.34 and 0.40 mag, respectively). Tests based on this will not be practical, however, at least until richness can be determined using a larger fraction of the cluster. Richness in this paper is effectively the aperture magnitude of the cluster, and thus is subject to the same systematic effects as the aperture magnitudes of brightest cluster galaxies (see Gunn and Oke 1975). The problem is especially acute for cluster richness because the aperture correction factor (α, see Gunn and Oke 1975) is over one (vs. 0.7 for brightest cluster galaxies). The large α is due to the aperture size being roughly equal to the core radius.

A final calibration attempt is to compare the aperture magnitude with the difference between the aperture magnitude and M_* (if M_* were constant, then the relation would be a straight line). Figure 15 shows the resulting curve. The dispersion in the aperture magnitude after this correction is 0.29 mag. The same accuracy can be achieved by applying

a Bautz-Morgan correction or using the aperture correction factor (Paper II); each requires far less work than the luminosity functions, and the latter corrects for dynamical evolution automatically.

TABLE 1

GDV FITS TO CLUSTER GALAXIES

$$\log(Re) = A + B \; (I(Re)-22)$$

Abell	z	A	B	Abell	z	A	B
22	0.1432	0.61	0.24	1880	0.1413	0.47	0.23
42	0.1087	0.51	0.19	1918	0.1415	0.62	0.15
43	0.1114	0.47	0.17	1921	0.1352	0.47	0.22
77	0.0719	0.42	0.27	1934	0.2195	0.52	0.22
140	0.1591	0.64	0.26	1940	0.1393	0.48	0.19
186	0.1066	0.55	0.11	1984	0.1231	0.53	0.29
279	0.0797	0.51	0.11	2036	0.1163	0.46	0.16
410	0.0897	0.38	0.22	2110	0.0978	0.39	0.22
545	0.154	0.60	0.19	2125	0.2465	0.60	0.21
665	0.1832	0.61	0.25	2184	0.0550	0.06	0.23
777	0.224	0.57	0.20	2218	0.1710	0.61	0.21
910	0.2055	0.63	0.29	2244	0.0970	0.45	0.19
1018	0.297	0.72	0.23	2246	0.225	0.61	0.22
1081	0.1588	0.69	0.09	2263	0.1051	0.47	0.19
1169	0.0582	0.48	0.08	2283	0.1830	0.62	0.24
1190	0.0794	0.42	0.09	2377	0.0808	0.45	0.24
1224	0.2897	0.70	0.15	2388	0.0615	0.36	0.23
1227	0.1117	0.51	0.17	2400	0.0881	0.43	0.17
1264	0.1267	0.49	0.19	2420	0.0838	0.48	0.24
1346	0.0970	0.53	0.14	2440	0.0904	0.43	0.21
1373	0.1314	0.54	0.21	2459	0.0736	0.53	0.09
1401	0.1670	0.64	0.18	2462	0.0755	0.38	0.16
1461	0.0538	0.49	0.01	2469	0.0656	0.30	0.21
1514	0.1995	0.57	0.19	2496	0.1233	0.47	0.23
1674	0.1055	0.46	0.15	2521	0.1359	0.57	0.22
1689	0.1784	0.57	0.23	2554	0.1060	0.54	0.21
1738	0.1146	0.56	0.17	2559	0.0796	0.46	0.30
1785	0.0792	0.32	0.18	2597	0.0826	0.37	0.22
1825	0.0632	0.48	0.04	2622	0.0621	0.33	0.20
1827	0.0668	0.44	0.10	2645	0.246	0.61	0.22

TABLE 2

SCHECHTER FUNCTION SIMULATIONS

	M* − Mclus						
	0.24	0.99	1.44	2.19	2.93	3.68	4.44
M*-G1	-0.71	-0.28	0.08	0.52	0.79	1.03	1.25
SIGMA	1.24	0.96	0.79	0.48	0.39	0.33	0.30
M*-G2	-1.61	-0.97	-0.50	0.07	0.42	0.71	0.97
SIGMA	1.61	1.09	0.78	0.38	0.29	0.24	0.22
M*-G3	-2.22	-1.48	-0.93	-0.28	0.17	0.52	0.81
SIGMA	1.79	1.25	0.83	0.38	0.26	0.21	0.18
1(SIGMA)	0.99	0.80	0.63	0.53	0.43	0.38	0.33
*(SIGMA)	1.83	1.42	1.10	0.63	0.41	0.28	0.19

TABLE 3

LUMINOSITY FUNCTION DATA FOR R = 250 KPC

Abell	m*	M*	Mclus	G1	G2	G3
22	16.97	21.43	19.19	20.78	20.91	21.65
42	16.65	21.76	19.55	20.23	21.01	21.32
43	15.58	20.61	20.86	21.38	21.53	21.68
77	15.69	21.68	20.35	19.49	21.16	22.59
140	18.10	22.30	19.19	19.71	21.56	21.58
186	17.38	22.51	20.92	19.70	22.48	22.59
279	16.18	22.01	19.26	19.84	21.28	21.69
410	16.37	21.81	20.16	21.63	22.23	22.29
545	18.36	22.17	18.69	21.50	21.64	21.66
665	18.02	21.82	19.01	19.76	20.84	21.17
777	18.64	21.97	19.31	20.74	21.18	21.81
910	18.86	22.36	19.81	19.83	21.42	22.12
1018	18.99	21.53	18.93	19.87	20.11	21.72
1081	17.79	22.00	20.49	19.81	21.57	22.39
1169	15.84	22.40	20.03	21.43	21.82	22.95
1190	15.98	21.84	19.56	20.05	20.56	21.49
1224	18.58	21.20	19.96	20.26	21.43	21.46
1227	17.24	22.31	19.77	19.89	21.38	21.86
1264	16.40	21.15	20.82	20.09	22.07	22.95
1346	17.03	22.40	19.91	19.97	21.26	22.34
1373	17.68	22.32	20.14	20.69	22.75	22.83
1401	17.40	21.50	19.09	20.29	21.02	21.16
1461	15.13	21.87	21.03	21.17	22.23	23.74
1514	18.60	22.20	19.33	19.73	21.80	21.82
1674	17.23	22.42	20.61	20.60	22.68	22.98
1689	17.75	21.66	17.96	20.28	20.86	20.90
1738	17.02	22.03	19.55	19.30	21.54	21.73
1785	17.54	23.39	20.72	21.19	21.98	22.98
1825	15.47	21.82	19.67	20.82	20.98	21.66
1827	14.90	21.13	19.95	20.72	21.79	22.11
1880	18.35	22.84	21.23	21.14	21.56	23.22
1918	17.24	21.75	21.54	19.42	22.97	23.24
1921	17.68	22.27	19.14	19.91	20.87	21.26
1934	19.02	22.40	18.95	20.51	21.28	21.39
1940	17.52	22.06	19.82	19.60	21.05	22.27
1984	17.00	21.80	19.71	20.92	21.15	21.71
2036	16.50	21.43	19.64	20.26	21.18	21.97
2110	17.43	22.77	20.22	20.02	22.38	22.51
2125	18.42	21.46	18.98	19.78	19.84	21.25
2184	17.69	24.38	21.80	21.47	24.44	24.54
2218	18.28	22.28	18.62	19.49	21.02	21.54
2244	17.02	22.37	19.09	19.16	21.07	21.34
2246	18.74	22.04	19.47	19.82	20.79	22.19
2263	17.26	22.39	20.42	20.11	21.67	22.41
2283	18.50	22.28	19.73	19.87	21.69	22.14
2377	16.50	22.26	19.45	20.28	20.51	21.59
2388	16.65	23.00	20.84	20.67	22.76	23.19
2400	16.73	22.29	19.96	19.83	22.10	22.27
2420	16.75	22.42	19.47	19.47	21.25	22.08
2440	16.87	22.36	19.88	19.95	21.39	21.75
2459	16.09	22.05	20.21	20.90	20.99	22.69
2462	16.70	22.62	20.29	20.28	21.84	22.55
2469	16.67	22.87	20.71	21.10	21.55	21.85
2496	17.79	22.58	19.95	19.21	21.99	22.33
2521	17.09	21.66	18.91	20.44	21.13	21.57
2554	16.47	21.63	19.40	19.74	20.77	21.55
2559	16.55	22.37	20.54	19.77	21.57	22.09
2597	17.15	22.89	21.24	20.36	22.66	22.87
2622	15.28	21.62	19.96	20.11	21.58	22.24
2645	18.91	21.95	18.66	20.63	20.66	21.21

TABLE 4

LUMINOSITY FUNCTION DATA FOR R = 400 KPC

Abell	m*	M*	Mclus	G1	G2	G3
22	17.21	21.67	18.69	20.78	20.91	21.43
140	17.97	22.17	18.50	19.71	20.79	21.41
545	18.26	22.07	18.23	21.50	21.62	21.64
777	19.02	22.35	18.53	20.74	21.18	21.27
910	18.72	22.22	18.76	19.83	20.92	21.42
1018	18.73	21.27	18.54	19.87	20.11	20.79
1081	17.62	21.83	19.60	19.81	21.57	22.03
1224	19.01	21.63	18.84	20.26	20.92	21.43
1401	17.46	21.56	19.05	20.29	21.02	21.16
1514	18.65	22.25	18.57	19.73	20.18	21.62
1689	18.02	21.93	17.62	20.28	20.86	20.90
1880	18.87	23.36	20.99	21.14	21.56	22.73
1918	18.12	22.63	19.80	19.42	20.53	21.76
1921	18.20	22.79	18.76	19.91	20.87	21.26
1934	18.83	22.21	18.54	20.51	21.15	21.28
1940	17.99	22.53	18.99	19.60	21.05	21.66
2125	18.86	21.90	18.62	19.78	19.84	21.11
2218	18.20	22.20	17.90	19.49	21.02	21.35
2246	19.15	22.45	18.89	19.82	20.79	21.87
2645	19.15	22.19	18.08	20.63	20.66	21.21

TABLE 5

LUMINOSITY FUNCTION RELATIONS (250 KPC)

Class	N	M*	SIGMA	Mclus	SIGMA	G1	SIGMA
Richness							
0	11	22.06	0.70	20.37	0.56	20.55	0.47
1	16	22.15	0.54	20.06	0.62	20.28	0.68
2	13	22.16	0.53	19.82	0.59	20.04	0.66
3	11	21.95	0.36	19.65	0.77	20.02	0.46
4	8	21.96	0.31	18.88	0.54	20.25	0.67
autz-Morgan							
I	7	21.89	0.36	19.53	0.45	19.94	0.56
I-II	8	22.48	0.50	20.20	0.79	19.86	0.66
II	16	22.08	0.47	19.75	0.63	20.24	0.59
II-III	13	22.04	0.45	19.78	0.88	20.22	0.44
III	15	21.96	0.60	19.89	0.85	20.55	0.65
Total	59	22.07	0.51	19.83	0.75	20.23	0.61
00 kpc	20	22.16	0.47	-	-	-	-

TABLE 6

MAGNITUDES OF THE BRIGHTEST THREE GALAXIES (250 KPC)

Class	N	M*-G1	SIGMA	M*-G2	SIGMA	M*-G3	SIGMA
Richness							
0	11	1.51	1.01	0.35	0.61	-0.37	0.68
1	16	1.86	0.83	0.57	0.66	-0.05	0.57
2	13	2.13	0.80	0.71	0.74	0.10	0.70
3	11	1.92	0.60	0.51	0.71	0.03	0.68
4	8	1.71	0.71	1.03	0.35	0.50	0.26
autz-Morgan							
I	7	1.95	0.84	0.65	0.24	0.03	0.47
I-II	8	2.62	0.46	0.60	0.81	0.14	0.72
II	16	1.84	0.82	0.69	0.71	0.28	0.58
II-III	13	1.82	0.58	0.64	0.63	-0.14	0.70
III	15	1.40	0.85	0.49	0.73	-0.21	0.65
Total	59	1.84	0.81	0.61	0.66	0.01	0.65

REFERENCES

Abell, G. O. 1958, Ap. J. Suppl., 3, 211.

_____. 1965, Ann. Rev. Astr. Ap., 3, 1.

Bahcall, N. A. 1977, Ann. Rev. Astr. Ap., 15, 505.

Bautz, L. P., and Morgan, W. W. 1970, Ap. J. (Letters),
162, L149.

de Vaucouleurs, G. 1948, Ann. d'Ap., 11, 247.

Dressler, A. 1978a, Ap. J., 222, 23.

_____. 1978b, Ap. J., 223, 765.

_____. 1978c, Ap. J., 226, 55.

_____. 1979, Ap. J., 231, 659.

Geller, M. J., and Peebles, P. J. E. 1976, Ap. J., 206, 939.

Gunn, J. E., and Oke, J. B. 1975, Ap. J., 195, 255.

Gunn, J. E., and Westphal, J. A. 1982, preprint.

Hausman, M. A., and Ostriker, J. P. 1978, Ap. J., 203, 297.

Hoessel, J. G., Gunn, J. E., and Thuan, T. X. 1980, Ap. J.,
241, 486.

Kirshner, R. P., Oemler, A., and Schechter, P. L. 1979,
A. J., 84, 951.

Kormendy, J. 1977, Ap. J., 218, 333.

Kristian, J. A., Sandage, A., and Westphal, J. A. 1978,
Ap. J., 221, 383.

Kristian, J. A., Young, P. J., and Westphal, J. A. 1980,
preprint.

Leir, A. A., and van den Bergh, S. 1977, Ap. J. Suppl.,
34, 381.

Oemler, A. 1974, Ap. J., 194, 1.

Ostriker, J. P., and Tremaine, S. D. 1975, Ap. J. (Letters),
202, L113.

Sandage, A., and Hardy, E. 1973, Ap. J., 183, 743.

Sandage, A., Kristian, J. A., and Westphal, J. A. 1976,
Ap. J., 205, 688.

Sandage, A., Tammann, G., and Yahil, A. 1979, Ap. J., 232,
352.

Sarazin, C. L. 1980, Ap. J., 218, 75.

Schechter, P. L. 1976, Ap. J., 203, 297.

Schneider, D. P., Gunn, J. E., and Hoessel, J. G. 1982a,
preprint (Paper I).

_____. 1982b,
preprint (Paper II).

Sebok, W. L. 1979, A. J., 84, 1526.

Thuan, T. X., and Gunn, J. E. 1976, Pub. A.S.P., 88, 543.

Tinsley, B. M., and Gunn, J. E. 1976, Ap. J., 203, 52.

Tremaine, S. D., and Richstone, D. O. 1977, Ap. J., 212, 311.

Turner, E. L., and Gott, J. R. 1976, Ap. J., 209, 6.

FIGURE CAPTIONS

Fig. 1. - Surface photometry of the galaxies in four moderate to rich clusters. The ordinate is the effective radius in kpc, the abcissa the surface brightness in r mag per square arcsec. The best linear fit for each cluster is plotted. The slopes for 42, 1689, 1785, and 2645 are 0.19, 0.23, 0.18, and 0.22, respectively. Lines of constant luminosity have a slope of 0.2. The 1σ dispersion about the line is ~0.2 in $\log(R_e)$.

Fig. 2. - The clusters have been grouped into four redshift bins to compare the dependence of A ($\log(R_e)$ for a galaxy with $I(R_e)$ of 22 r mag per square arcsec) on the seeing. It appears that the deconvolution works fairly well.

Fig. 3. - The movement of a field galaxy in the $\log(R_e)-I(R_e)$ plane. The curve was calculated using the k-corrections for ellipticals given in Paper I. The line with a slope of 0.2 represents constant luminosity. See text for explanation.

Fig. 4. - A comparison of the total luminosity of G1 (integrated GDV model) with the 16 kpc radius aperture magnitude (see Paper I). The clusters are coded by Abell richness class. The lower line represents RAM(tot) = RAM(16); the upper line RAM(tot) = RAM(16) - 1.13 (from extrapolation of a GDV model with an R_e of 28 kpc, see Paper II). Three galaxies fall below the lower line. Each is a multiple

system in which there are at least two nuclei of comparable luminosity within the 16 kpc aperture.

Fig. 5. - The distribution in $\langle \ln(\text{Likelihood}) \rangle$ from 600 simulations of a cluster with $m_* = 16$, $m_{clus} = 14.6$, $\alpha = -1.00$, and a background area of 19.6 square arcmin. The bin size is 0.2σ. The gaussian has the same mean and dispersion as the simulations.

Fig. 6. - Luminosity functions for the four clusters in Figure 1. The bin size is 0.5 mag. The $\alpha = -5/4$ fits are denoted by *'s, the $\alpha = -1.00$ fits by x's, and the +'s represent the background. The best fitting m_*'s are marked by the arrows. The brightest cluster galaxy is plotted but was not used in determining the luminosity function parameters.

Fig. 7. - A comparison of the M_*'s derived from the galaxies inside of 250 and 400 kpc. The bars in the lower right represent the one-sigma dispersions expected for a typical cluster in this sample of 20. The mean M_* found from the 400 kpc data is 0.19 fainter than the 250 kpc M_*.

Fig. 8. - The relation of the cluster luminosity inside of 250 and 400 kpc. The solid lines are $M_{clus}(400) = M_{clus}(250)$ and $M_{clus}(400) = M_{clus}(250) - 0.66$. The latter relation would hold if the cluster luminosity surface density went as the observed number counts.

Fig. 9. - The Hubble diagram for A (=log R_e of a galaxy with $I(R_e)$ = 22 r mag per square arcsec). The dispersion at a given redshift is only 0.06 (=15%). The tightness of this relation leads one to suspect that the seeing was improperly handled or redshift related selection effects are operating. If this slope is due solely to geometrical effects, q_o's of ~8 are required. The numbers represent Abell richness class.

Fig. 10. - The same as Figure 9 but using cluster richness as the abcissa. Rich clusters have larger values of A. Making a richness correction (solid line) yields a dispersion in A of 0.09 (22%). The strong redshift-richness correlation makes interpretation difficult.

Fig. 11. - The slope of the R_e-$I(R_e)$ diagram (B) as a function of cluster richness. Rich clusters have a slope of ~0.22 which implies $L \propto R_e^{0.2}$.

Fig. 12. - Dependence of M_* on the total cluster luminosity for the 250 kpc data. The solid line is the mean (22.07) and the dashed lines are the expected dispersion assuming a universal M_* and α = -1 (Table 2).

Fig. 13. - The observed M_*-G1, M_*-G2, and M_*-G3 magnitudes as a function of the number of galaxies in the cluster for the 250 kpc data. For G2 and G3 the solid line is the mean and the dashed lines the expected one-sigma dispersion from

simulations of Schechter functions. The plotted relation in
the M_*-G2 graph is actually the M_*-G1 curve from Table 2,
while the M_*-G3 panel uses the M_*-G2 points from Table 2.
The observed luminosities of brightest cluster galaxies are
too bright to be drawn from a Schechter function. The
clusters are coded by BM class.

Fig. 14. - The relation of the aperture/of the three bright-
est cluster galaxies and cluster richness. The clusters are
coded by Bautz-Morgan class (1 = I, 5 = III). While there
is a definite relationship between the aperture magnitude
and the total cluster richness (Paper I), the core richness
(density) has little effect on the luminosity of G1. From
the figure it is clear that BM class is a better indicator
of luminosity. The second and third ranked galaxies rapidly
brighten with increasing cluster richness. The dispersions
in their magnitudes are 0.34 and 0.40 mag after application
of a richness correction.

Fig. 15. - A comparison of the aperture magnitude of the
brightest cluster galaxy with the difference between the
aperture magnitude and the cluster M_*. If M_* were constant,
then the points would fall on a straight line. The dispersions
in the aperture magnitudes is reduced to 0.29 mag. The
numbers represent BM type.

Figure 1

Figure 2

Figure 3

Figure 4

⟨ln(Likelihood)⟩

Number
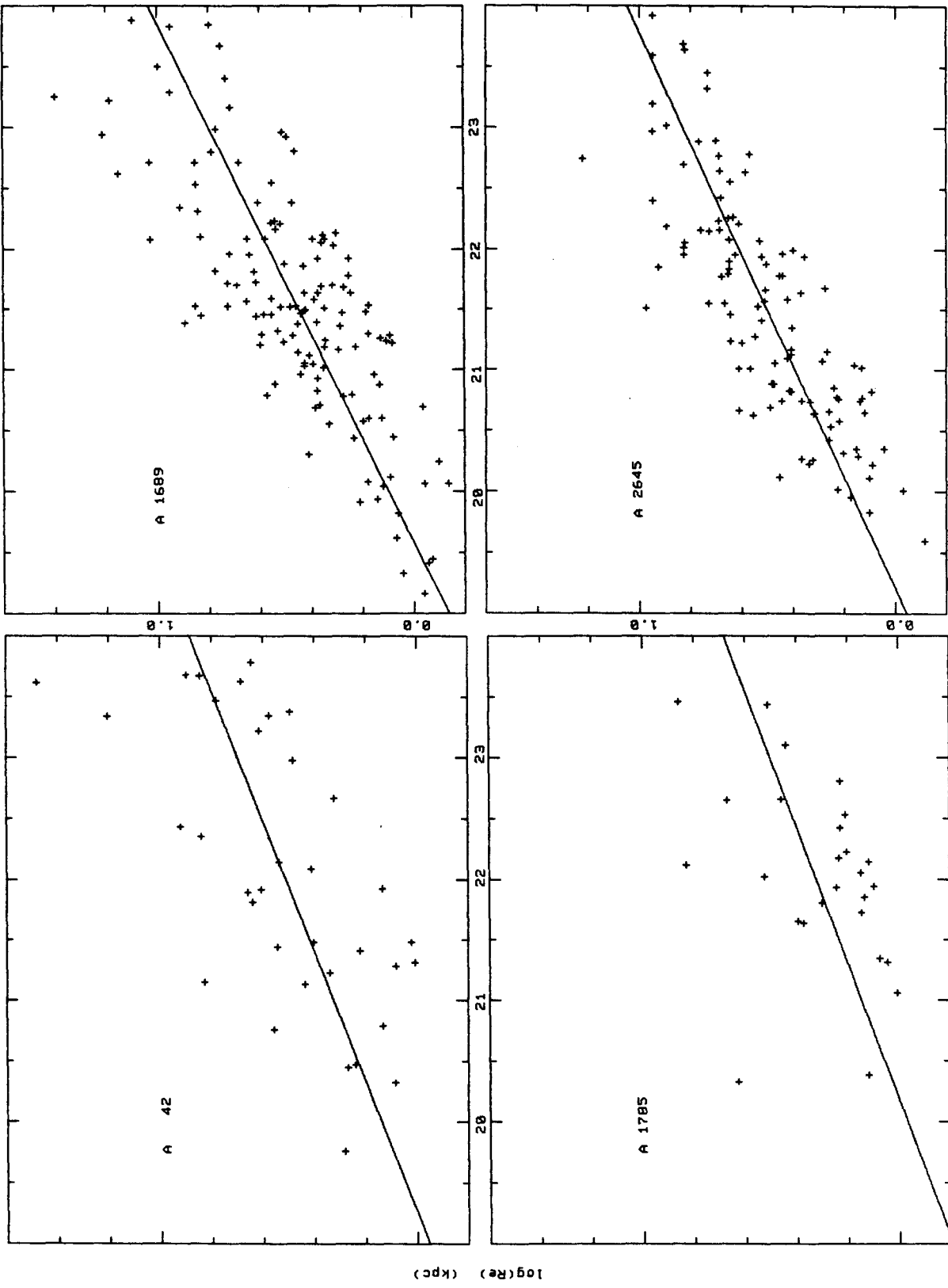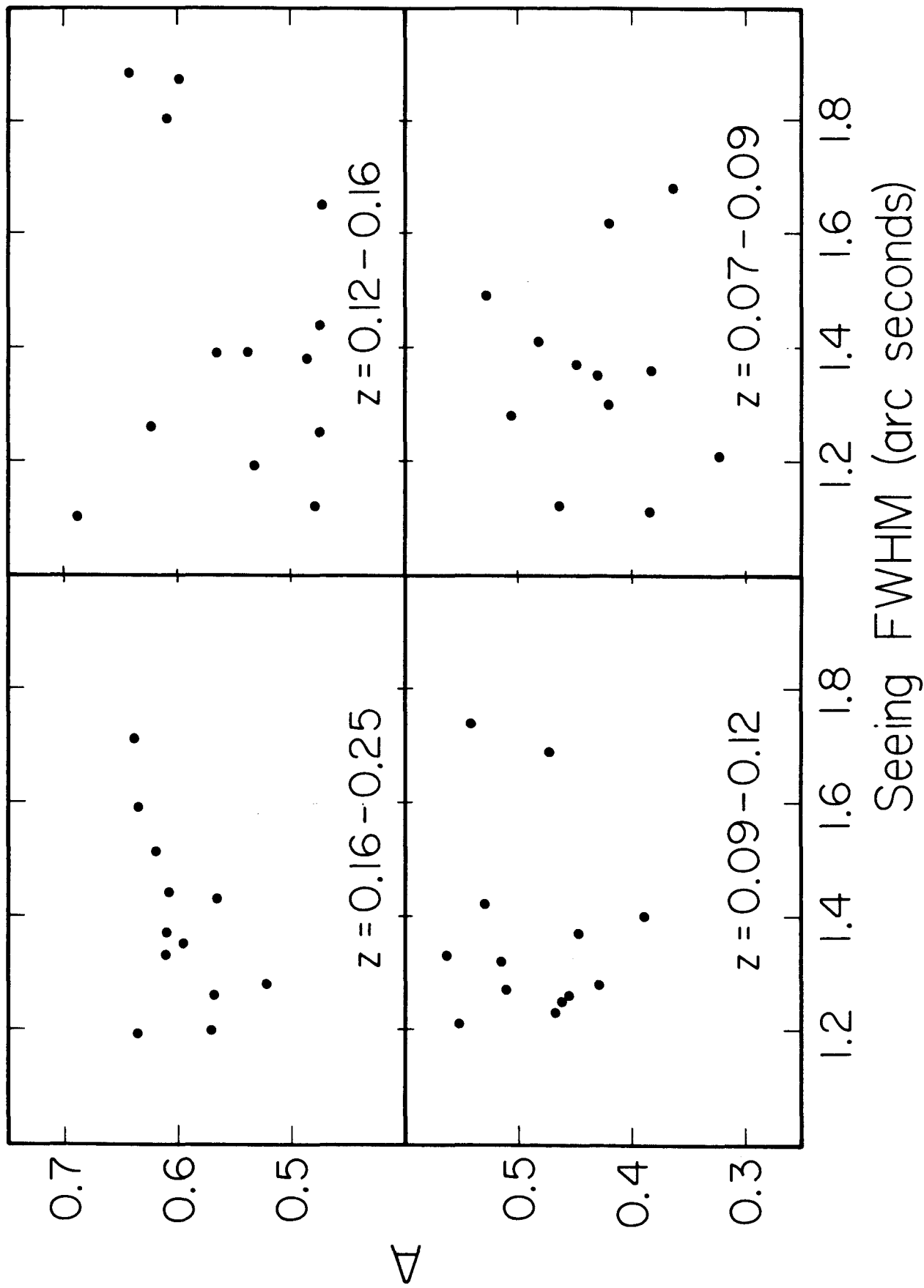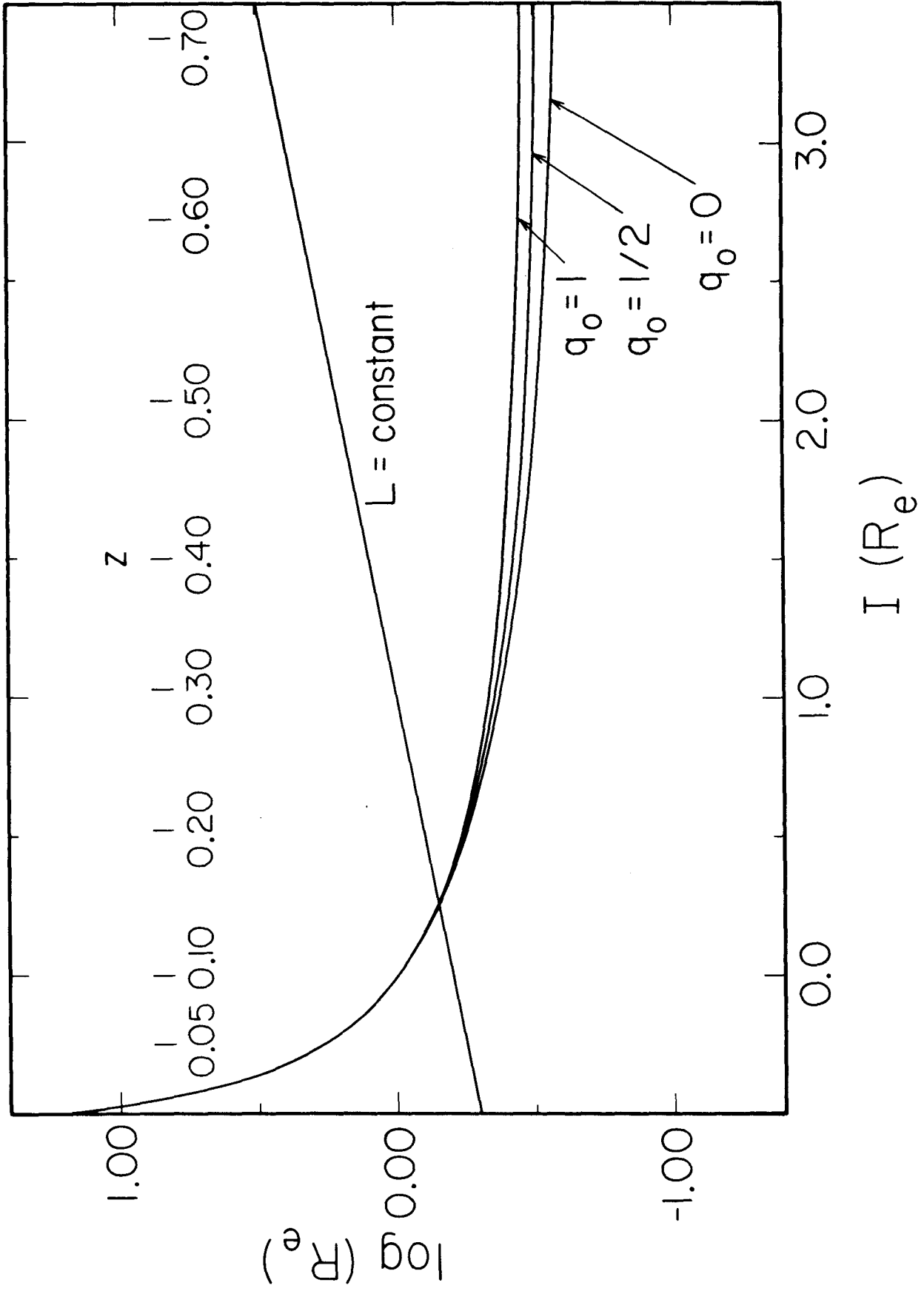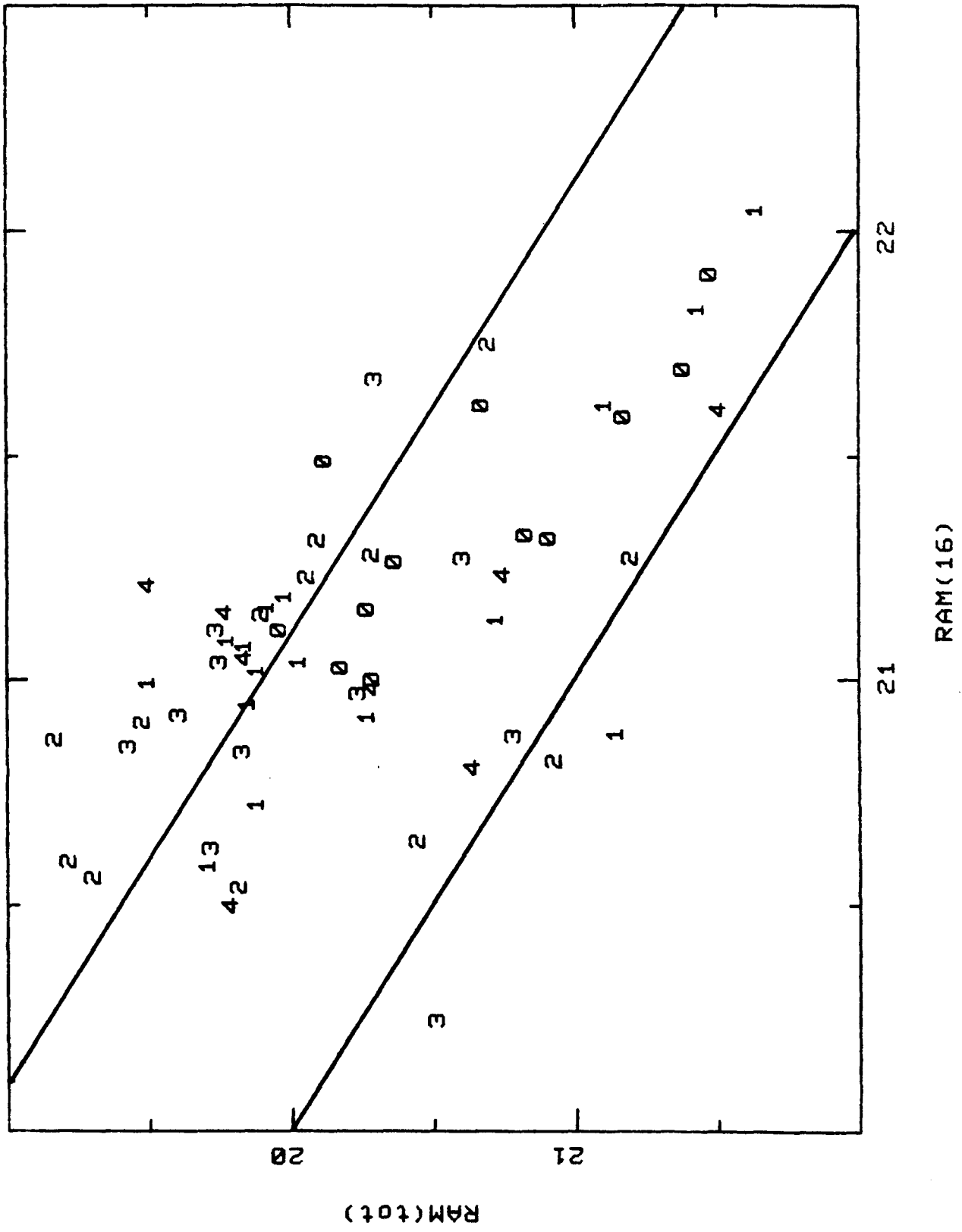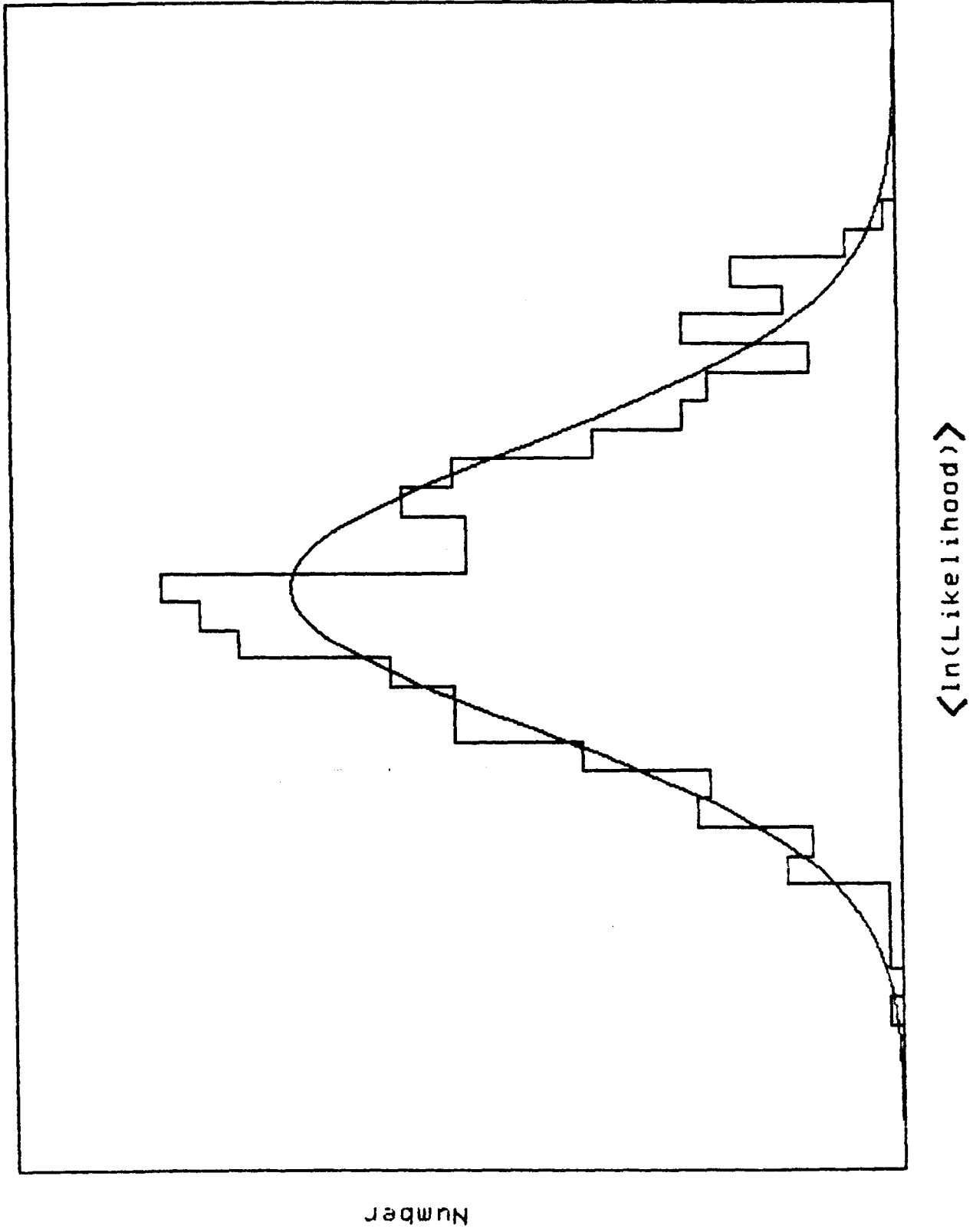
Figure 5
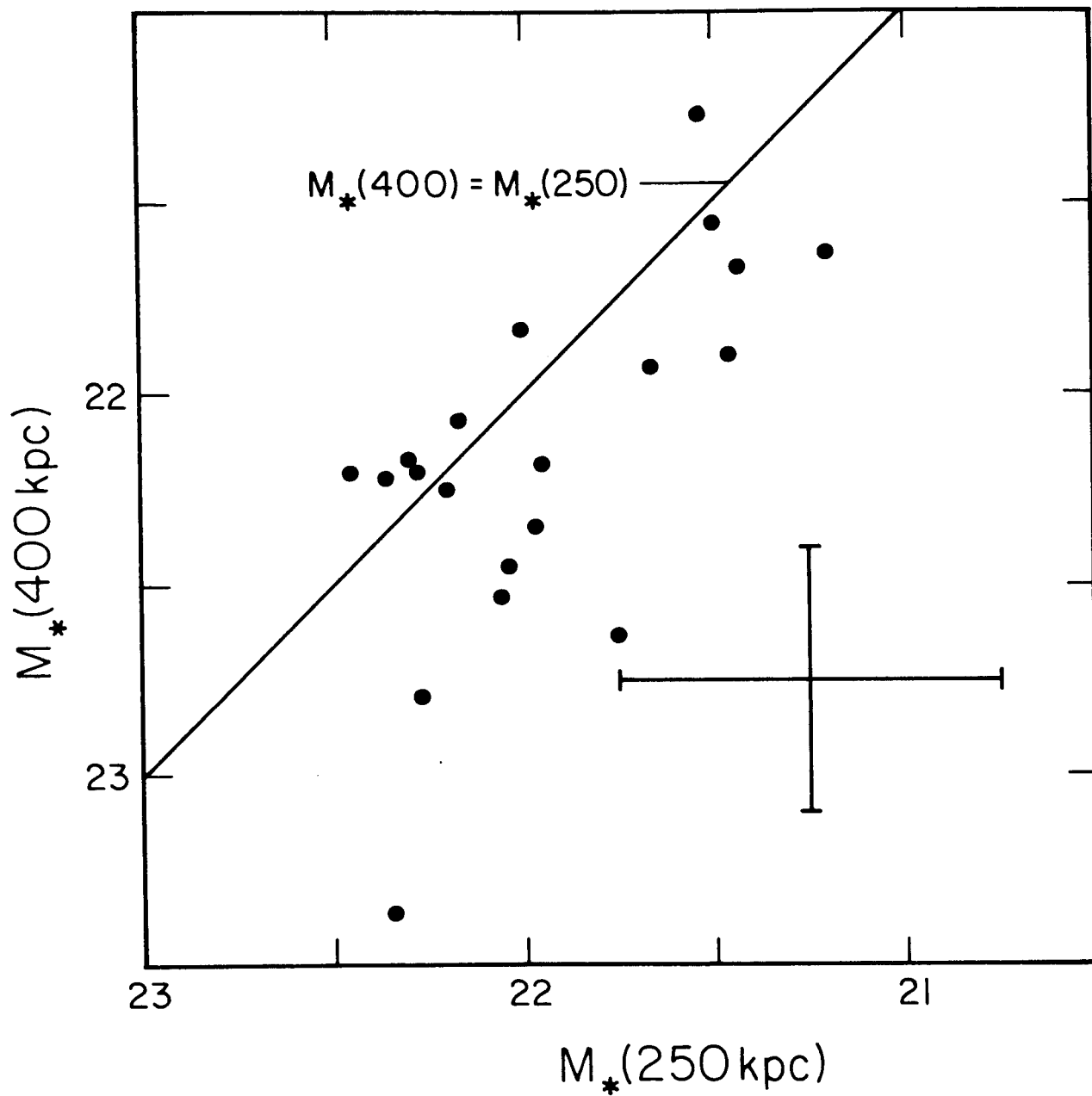
Figure 6
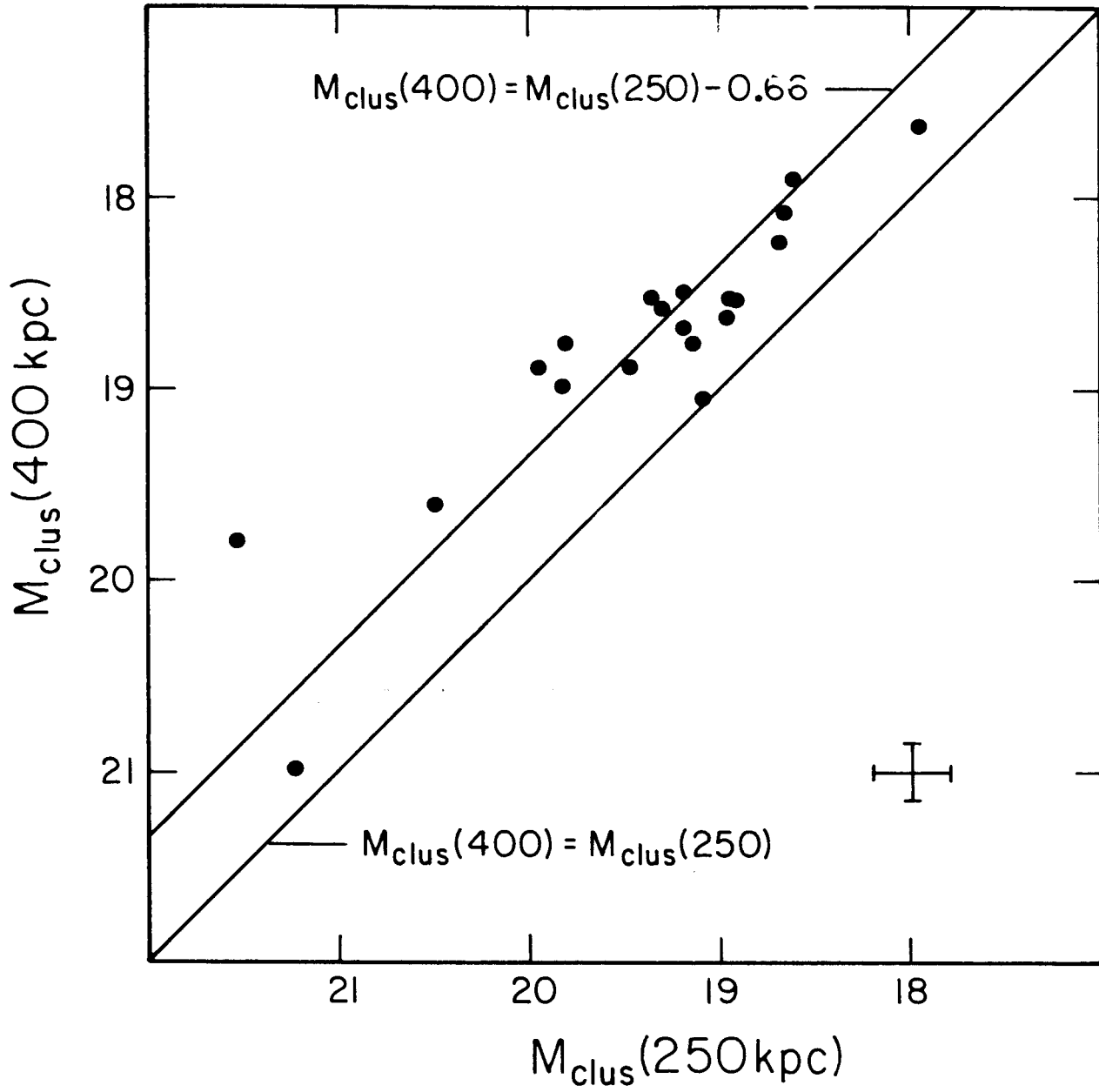
Figure 7
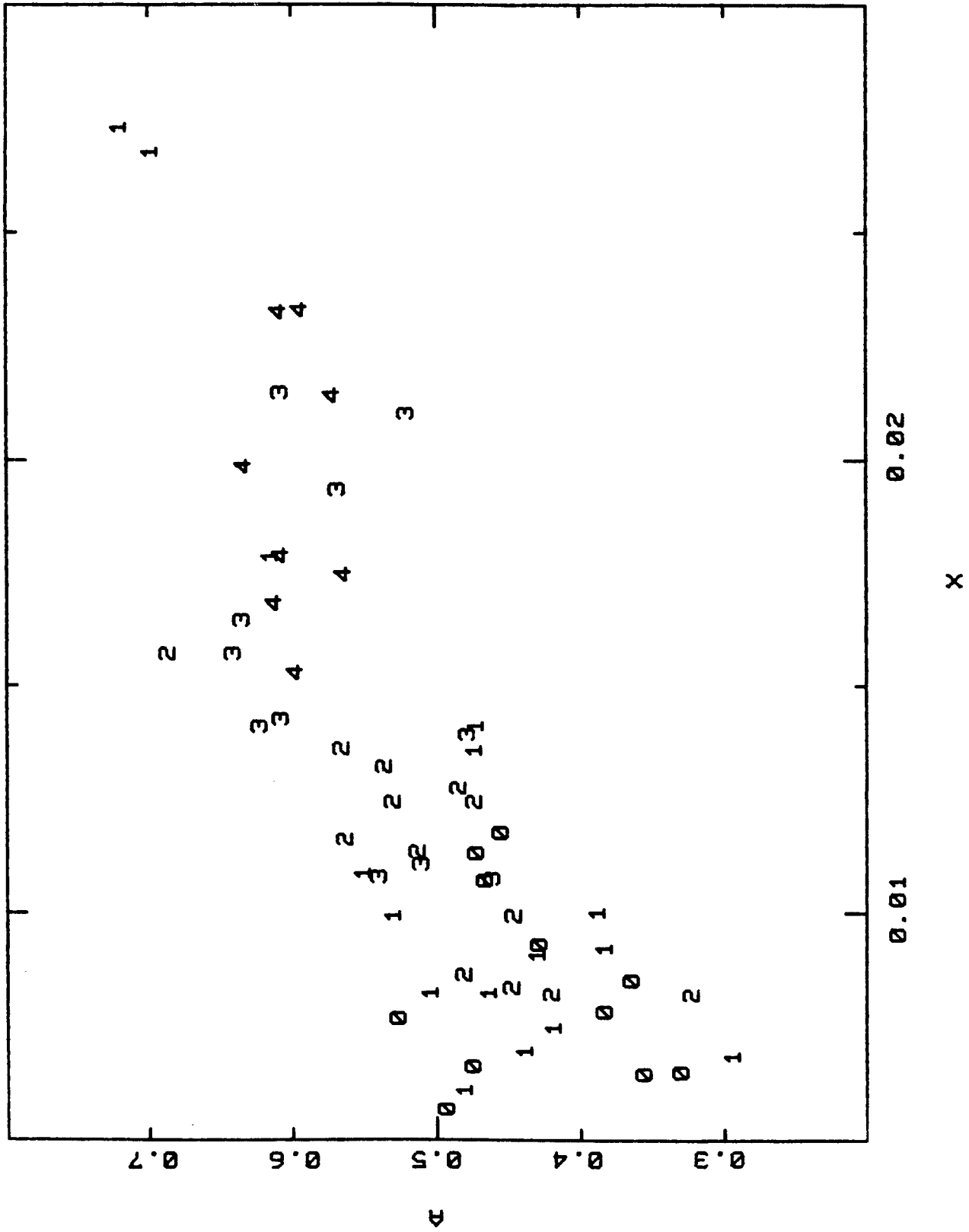
Figure 8
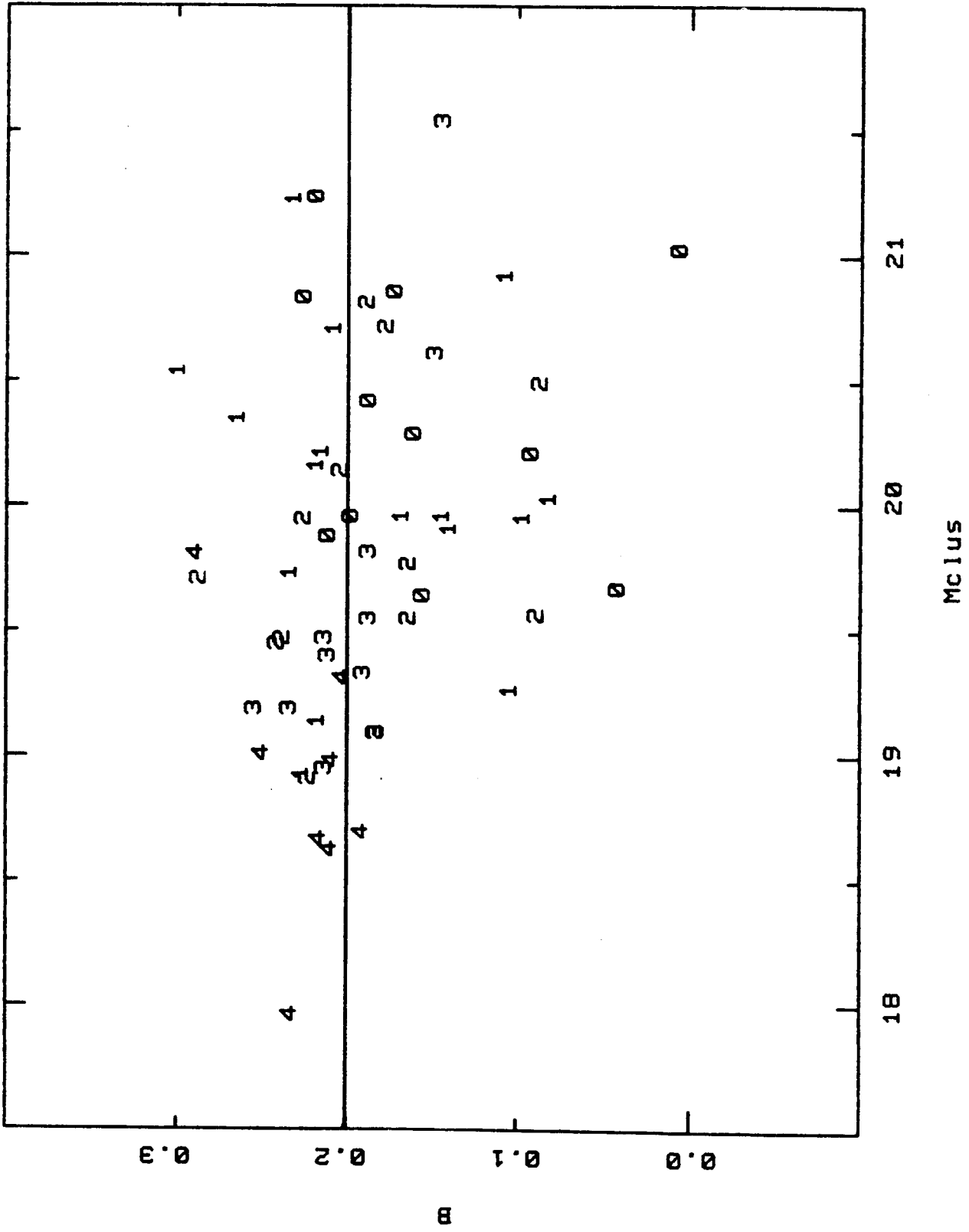
Figure 9
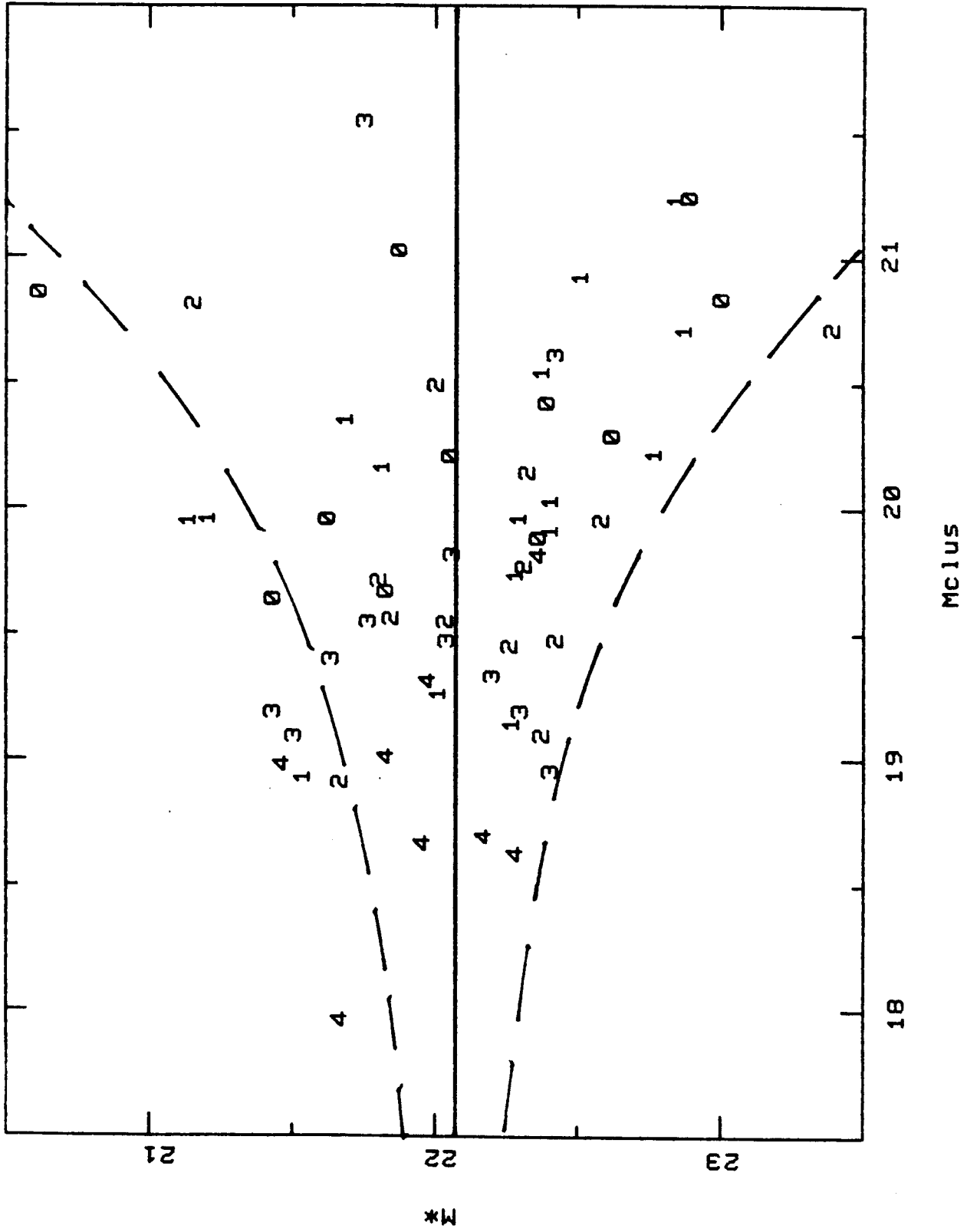
Figure 18
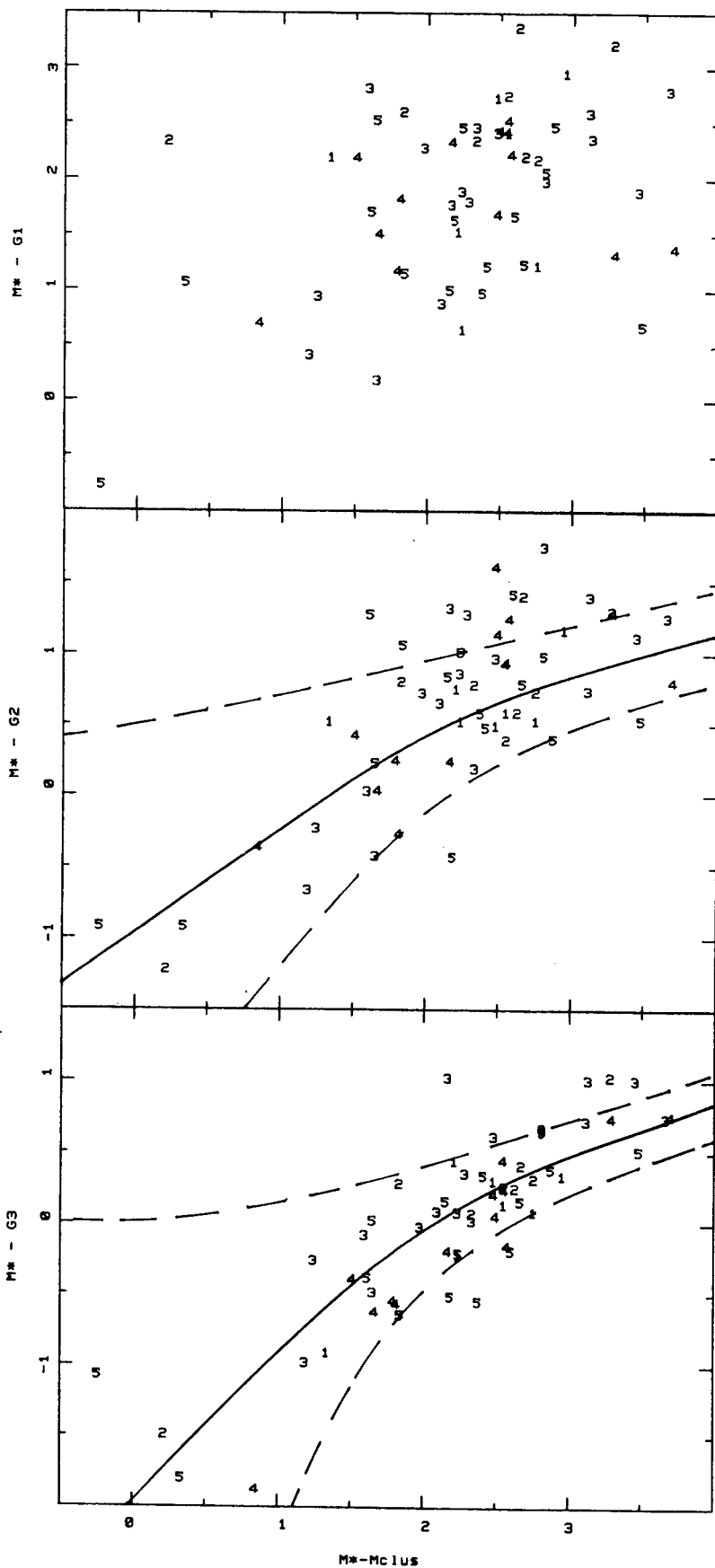
Figure 11

Figure 12

Figure 13
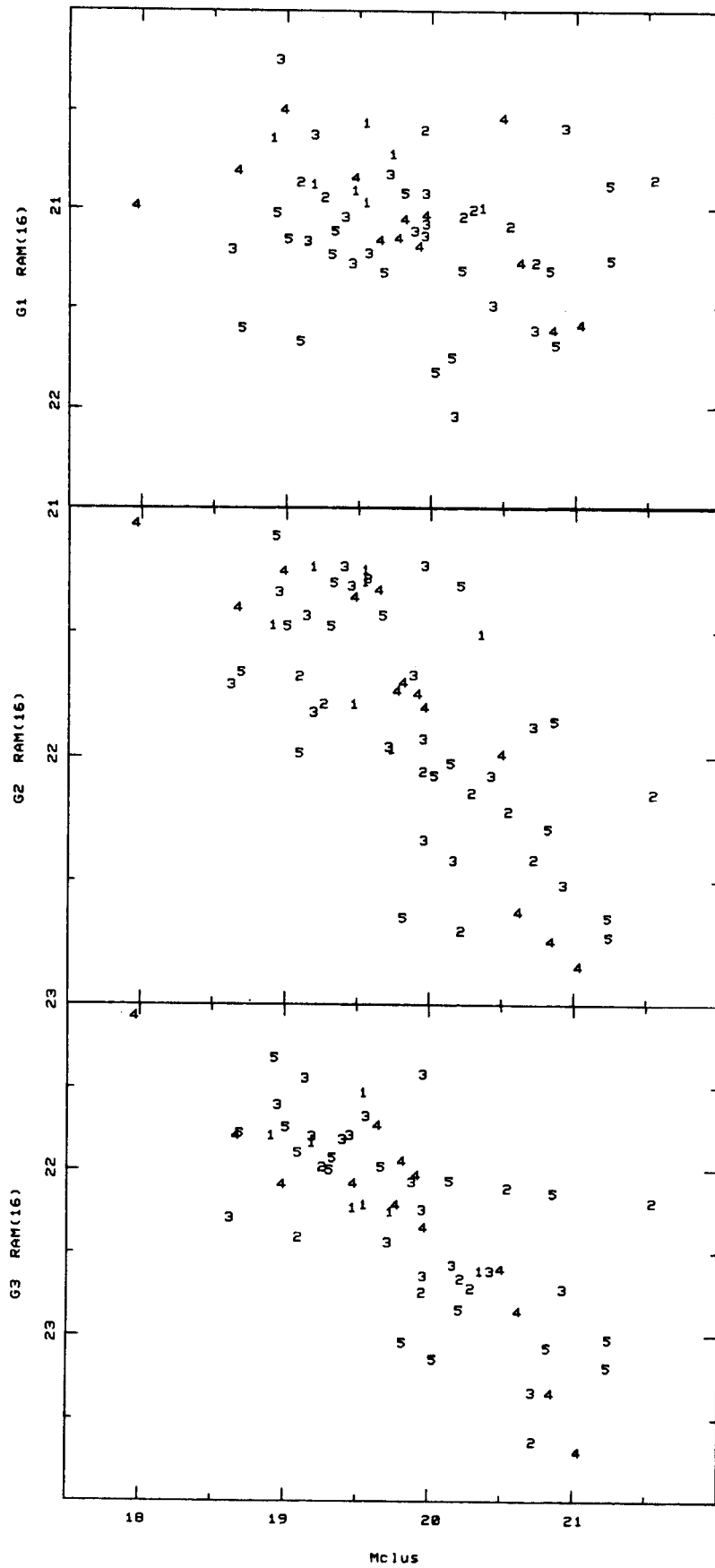
Figure 14
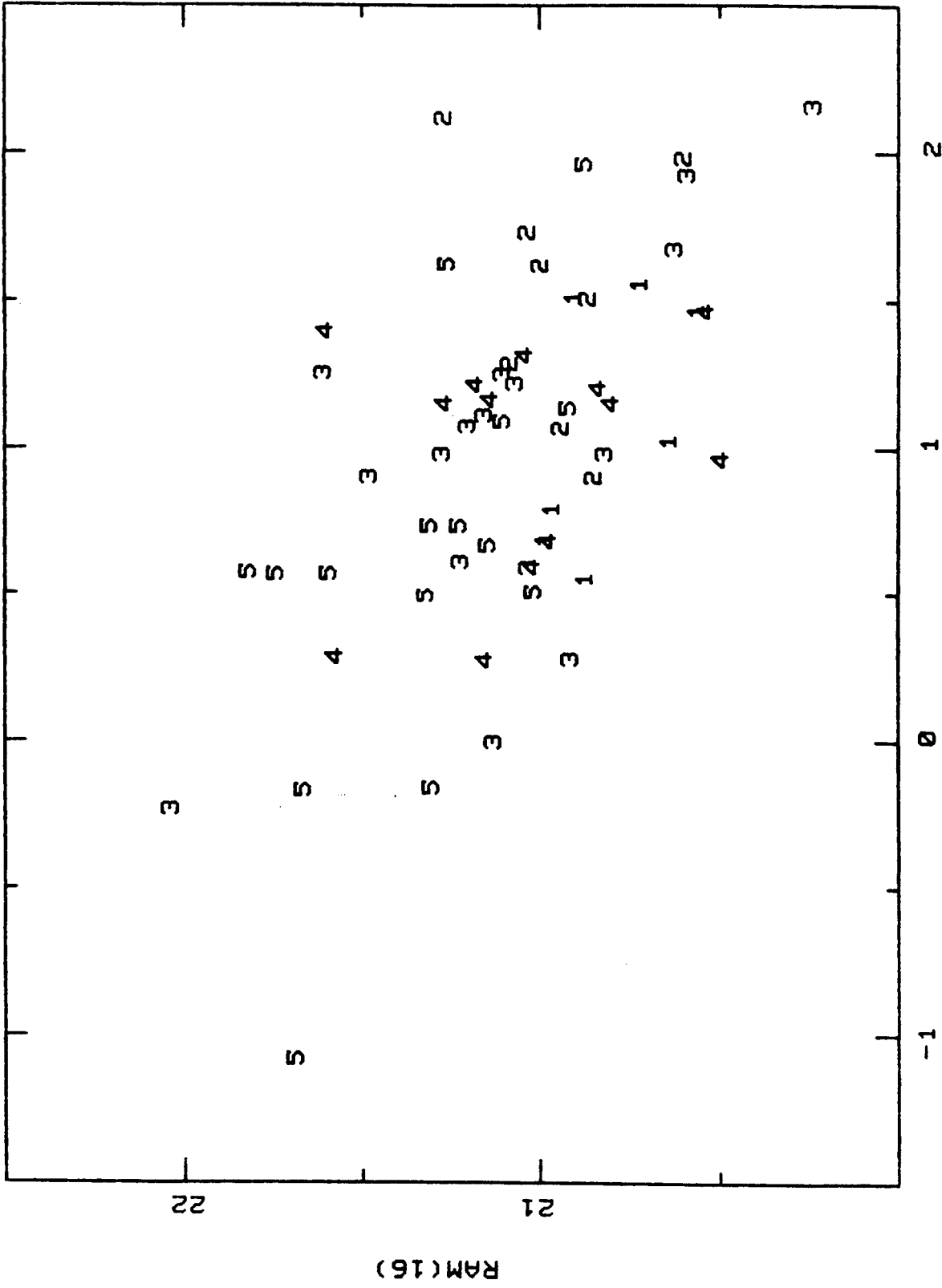
Figure 15

CHAPTER IV

V Zw 311: THE ONCE AND FUTURE cD?

Authors: Donald P. Schneider and James E. Gunn

I. INTRODUCTION

The role of dynamical friction in the evolution of galaxies is of considerable interest both with regard to the question of the origin of galaxies, particularly ellipticals and cD's (Toomre 1977) and in the matter of evolutionary corrections to the classical cosmological tests (Ostriker and Tremaine 1975; Gunn and Tinsley 1976). It is probable that the process also has profound effects on the evolution of clusters themselves, and may be the dominant process which establishes the inner density distribution, luminosity function, and color-magnitude relation in clusters (Hausman and Ostriker 1978).

The present situation regarding "cannibalism" among first-ranked cluster ellipticals is that the phenomenon almost certainly does occur. Hoessel (1980, hereafter JGH) has shown that about 30% of first-ranked galaxies have multiple nuclei, the merger time scales for which are all very short. There is also dynamical evidence from the structure of the galaxies themselves, the radius-luminosity relation having the form predicted by simple cannibalism models to quite high accuracy.

In this paper we investigate probably the most nightmarish of known multiple-nucleus systems, the peculiar central "galaxy" in the poor cluster V Zw 311 (Zwicky 1971), which is also 407 in the catalog of Abell (1958). Zwicky called attention to this remarkable object, which has many compact nuclei imbedded in a luminous matrix; at least nine condensations with luminosities comparable to the outlying cluster galaxies make

up the central object. The object is a moderately luminous
radio source (4C35.6, $L_{radio} = 10^{42}$ erg/sec, Moffet [1975]).
The redshift, based on the spectra of two of the nuclei, is
0.0473 (Peterson 1970). We will use a slightly extended
version of Zwicky's nomenclature for the system. Compare
Figure 2 of this paper with the photographs on pp 102-102a of
his catalog.

We describe the spectroscopic observations in § II,
photometry in § III, dynamical and frictional calculations in
§ IV, and discuss the results in § V.

II. SPECTROSCOPIC OBSERVATIONS

Spectra of eight inner and seven halo galaxies were ob-
tained on three nights in 1976-78. Table 1 contains a Journal
of Observations. All spectra were taken at the Cassegrain
focus of the Hale telescope using the SIT digital spectrograph
with a 1200 line mm^{-1} grating. The resolution was slightly
better than 5 Å in the center of the target (4600 Å), 6.5 Å
at the ends. The spatial resolution was approximately 2".

The slit was rotated to acquire two galaxies and the intra-
cluster light simultaneously. Usually the strongest five
channels (7") were summed to form an inner galaxy spectrum.
Intracluster light spectra were created by adding all frames
on a given night. Figure 1 displays two of the best galaxy
spectra along with a radial velocity standard. Wavelength
calibration was accomplished with an He-Ne lamp; the polynomial
fits had a rms error of 20 km s^{-1}. The inner galaxies had

comparison spectra taken for each slit position. The spectra had instrumental variations removed by subtraction of an erase frame and division by a flat field (incandescent lamp exposure). Sky frames were taken to be subtracted from the intracluster light spectrum.

One must approach velocity measurements with the SIT with care, as the exposure level on the target has a systematic effect on the redshift, i.e., "beam bending" (see Schechter and Gunn 1979). This phenomenon was found to be linear with a correction of 80 km s^{-1} when the device had a mean level of 50% of saturation. In this work no corrections have been made for possible beam bending. When possible, strong arc lines were avoided in the wavelength calibration. The exposure levels for the standards were equal to within 10%; the galaxies had such low signal (20% saturation) that beam bending will be negligible compared to the errors from other sources. There may be a small zero point error in the redshifts, but the relative velocities should be unaffected.

The velocities were measured using the procedure described in Sargent, Schechter, Boksenberg, and Shortridge (1976). Two stars were used as velocity standards; HD 221585 (G5 III) and HD 58683 (K0 III). These stars had 12,000 and 3000 photons per resolution element (the G5 standard was trailed). A typical galaxy spectrum contained 300 photons per resolution element.

Table 2 lists the mean redshifts (cz) for each of the

objects observed. These measurements have been corrected for solar motion (see de Vaucouleurs, de Vaucouleurs, and Corwin 1976). Zwicky numbered only 16 halo galaxies; galaxy 17 in Table 2 is 40" from galaxy 10 at position angle 52°. The velocity for a given galaxy did not depend systematically on which standard was used in the reduction; the mean scatter was < 30 km s^{-1}. Three galaxies and the diffuse light were observed on different nights. Galaxies B and I were very consistent, with redshifts in agreement to 35 km s^{-1} from night to night. Galaxy 9, however, had one measurement 200 km s^{-1} greater than the other, and neither spectrum of the intracluster light yielded a useful redshift. The spectra for each of these 4 objects were summed, and the redshift listed in Table 2 refers to this value.

Attempts to determine the internal velocity dispersions of the individual galaxies met with little success, due to the rather low signal-to-noise and the high background (the envelope). The five highest quality spectra (for galaxies B, C, D, G, and I) did yield some marginal results. Galaxies C, D, and I have an upper limit of 200 km s^{-1} for their dispersions. Galaxies B and G possessed dispersions on the order of 300 km s^{-1}, but these should be treated as upper limits for the following reasons: (1) This dispersion is based heavily on the H and K lines of Ca II (see Schechter and Gunn [1979] for a discussion of the disadvantages of using this part of the spectrum). (2) The uncertainty in the

dispersion measured with this technique is roughly $\sqrt{2}$ times the error in the redshift (Schechter and Gunn 1979), and the detected values are significant at only the 2σ level. An inspection of the spectra of galaxies E and F clearly show the σ_r must be less than 300 km s^{-1}.

III. PHOTOMETRY

a) Instrumentation and Reductions

Direct pictures of the central object in V Zw 311 were taken on three different nights; Table 1 summarizes these observations. All exposures were obtained with the PFUEI (Gunn and Westphal 1982) coupled with a 500 x 500 Texas Instruments low noise CCD. (See Young et al. [1980] for a description of the 5-m system.) On the Palomar 1.5-m the PFUEI was mounted at the Cassegrain focus (f/8.75); the re-imaging yielded an image scale of 0.58" per pixel (vs. 0.44" for the 5-m).

Instrumental variations were removed by subtracting an erase level, then flattening the picture using exposures of the illuminated dome. Pictures of the central object were obtained in the g(4900 Å) and r(6500 Å) passbands described in Thuan and Gunn (1976). Photometric calibration was accomplished using 4-6 standards per night; these standards indicated a photometric accuracy of ~2%. The observations were transformed to the Thuan-Gunn system using the procedure given in Schneider, Gunn, and Hoessel (1982, hereafter SGH). Multi-aperture photomultiplier photometry of the central object

taken with the 1.5-m (given to us by J. Hoessel) agrees to within 1% of the CCD data. The seeing on the 5-m CCD data was 1.2" (FWHM).

b) Profiles

The average of the two exposures taken with the Hale telescope is displayed in Figure 2 via a contour map. The outermost contour is 24th mag per sq arcsec (r); the envelope clearly extends farther but poor sky flattening renders much fainter isophotes inaccurate. The nine inner nuclei are well resolved, as are several galaxies lying within or close to the envelope.

The galaxies on the 5-m exposure were fit to a modified Hubble model with

$$I(x) = \frac{I_o}{1+(x/a)^2} \qquad (1a)$$

corresponding for constant M/L to a space density of

$$\rho(r) = \frac{\rho_o}{[1+(r/a)^2]^{3/2}} \qquad \text{where} \qquad \rho_o = \frac{I_o}{2a}. \qquad (1b)$$

The observed profiles were compared to these models convolved with two component Gaussian seeing profiles. The results are given in Table 3, as well as the magnitude inside the 25th mag per sq arcsec (isophote in the rest frame) and the (g-r) color. This exercise was not especially enlightening, as none of the objects have resolved cores. The values for the inner nuclei are quite sensitive to the uncertain background level. Although the individual I_o's and a's are not well determined, the product

I_o a^2 (and thus the total magnitude) is fairly well established.

It is interesting to compare the central object photometrically to first-ranked galaxies in other clusters, since it is likely, as we shall see, that this system will probably become a cD-like object in a relatively short time. SGH define the brightest cluster galaxy and its magnitude in terms of the maximum light through an aperture of standard radius, in their case 16 kpc for H_o = 60 km s^{-1} Mpc and q_o = 0.5. We adopt that Hubble constant and cosmological model for the remainder of this paper. The points in Figure 3 represent the surface brightness in circular azimuthally smoothed rings which are centered using the above criterion. The resulting profile is very lumpy due to the presence of the quite distinct nuclei A, B, C, D, E, F, and G within the 16 kpc (15.2") radius.

In order to estimate the photometric behavior of the smooth background, the following procedure was developed. Contours at various surface brightness levels were constructed, and the areas enclosed were measured. The "radius" at a given surface brightness is then defined as

$$R = \sqrt{\frac{\overline{Area}}{\pi}} \ .$$

At small radii, the major contribution is from the nuclei themselves, but outside about 10", the profile so constructed is reasonably smooth, and is plotted as the x's in Figure 3. We will describe the luminous background as a modified Hubble law (eq. [1]) with I_o ~ 21.2 and a ~ 10 kpc. The fit is less

than perfect, the main discrepancy being the steeper slope in the data. The limited size of the field and the imperfect flattening make accurate sky subtraction impossible, however, and the slope in actuality is not well determined.

c) Colors

Colors for the bright object were found from the 1.5-m data, and are given in Table 3. The colors of the outer galaxies are probably good to ±0.04; those for the inner galaxies are less reliable. The colors were measured using the techniques in SGH (mean multi-aperture colors). The inner galaxies suffered from (1) a high, uncertain background, and (2) the fact that the apertures were not much larger than the seeing disk. The (g-r) color of the central object as a function of radius is given in Figure 3.

Inspection of Table 3 and Figure 3 leave one with the impression that the nuclei are distinctly redder than the envelope. This was confirmed by constructing a two-dimensional color map. Regions associated with the nuclei has a (g-r) ~0.80; the envelope appeared to have a (g-r) ~0.65 - 0.70. The envelope is roughly the same color as the outer galaxies.

d) Galactic Absorption

This object suffers a considerable amount of galactic absorption (b = -19°9). Adopting the method in SGH (absorption determined by the intervening galactic H I column density)

$A_r = 0.45$ mag and $A_g = 0.66$ mag. While this is quite high, there is some evidence that it is roughly correct (see § V).

IV. DYNAMICS

a) Central Object

In V Zw 311 we have data on three different dynamical systems--the inner nuclei, the envelope, and the cluster. Table 4 gives $\langle cz \rangle$/the radial velocity dispersion for each (the envelope σ_r is in parentheses as it is inferred, see below). The mean redshift for all agree quite well. The dispersion of the nuclei is a bit lower than the cluster galaxies, but this difference is not significant.

Since we have only upper limits on the internal dispersions of the nuclei, we can deduce only upper limits on the value of M/L (we shall define M/L on the B_T system following Faber and Gallagher [1979, FG] but with $H_o = 60$. To compare with our results, increase the FG values by 20%). King (1966) has shown that

$$\rho_o = \frac{9\sigma_r^2}{4\pi G a^2} \quad .$$

Define $I_o a^2 = K$ (which is reasonably well determined). Then it can easily be shown that for a system which has the form defined in equation (1):

$$\frac{M}{L} = \frac{330\, a\sigma_r^2}{K} \qquad \begin{array}{l} a \text{ in pc} \\ \sigma_r \text{ in km s}^{-1} \\ K \text{ in } L_\odot \end{array} \quad . \tag{2}$$

The M/L's for B, C, D, G, and I range from 5-11, similar to that of nuclei of elliptical galaxies (FG), which, after all,

is what these objects presumably were.

To find the M/L of the envelope, we will make the following assumptions: (1) The orbits of the nuclei have been circularized by dynamical friction, and (2) the potential in the center is dominated by the mass in the envelope. (The nuclei then become test particles.) This requires that the M/L of the envelope to be much greater than that of the nuclei as the luminosity of the envelope and nuclei are comparable, but this is consistent with our dispersion data.

If the nuclei are in circular orbits, then

$$v_c^2(r) = \frac{G\,M(r)}{r} \quad .$$

Defining

s = projected distance

i = inclination of orbit

ϕ = orbital phase

$\gamma = (\cos^2 i + \cos^2\phi \, \sin^2 i)^{1/2}$

then $s = r\gamma$

and $v_r^2 = \dfrac{G\,M(s/\gamma)\gamma\,\sin^2 i\,\cos^2\phi}{s/\gamma}$

$$\langle v_r^2 \rangle^{1/2} = \left\{ \frac{G \int_0^\pi \int_0^{2\pi} M(s/\gamma)\gamma\,\cos^2\phi\,\sin^3 i\,d\phi\,di}{s \qquad \int_0^\pi \int_0^{2\pi} \sin i\,d\phi\,di} \right\}^{1/2} \quad . \tag{3}$$

For example, if $M(r) = M_o r/r_o$ (constant circular velocity),

then $\langle v_r^2 \rangle = \dfrac{G\,M_o}{3\,r_o} = \dfrac{v_c^2}{3}$.

Assuming the surface brightness profile of the envelope

follows equation (1), then

$$M(r) = 4\pi\rho_0 a^3 [\ln(\sqrt{1 + x^2} + x) - \frac{x}{\sqrt{1 + x^2}}] \qquad (4)$$

where $x = r/a$.

The mean projected distance of the nuclei from the center of the envelope is known ($\langle s \rangle \sim 1.5a$, $a = 10$ kpc). The projection integral (3) was numerically integrated using equation (4) for the mass distribution. In addition, Monte Carlo simulations were run with eight objects to check on the accuracy and give an estimate of the statistical errors. The results are, for the central regions of the envelope:

$$\rho(0) = 0.63 \pm 0.25 \ M_\odot \ pc^{-3}$$

$$M/L = 90 \pm 35 \qquad \text{(one sigma errors)}$$

$$\sigma_v = 610 \pm 200 \ km \ s^{-1} \ .$$

One might be concerned that the nuclei are not in circular orbits but are spiraling in at a pitch angle β. Fortunately, for all the expected values of β ($< 15°$), the observed dispersion is practically independent of the pitch angle. This happens because the circular velocity as a function of radius for the envelope is nearly constant at the distance where the nuclei are located (two to three core radii).

It appears that the assumption that the motion of the nuclei is dominated by the envelope is at least self-consistent. The mass-to-light ratio is approaching the value found for clusters of galaxies (FG). If the nuclei are at a mean

distance of two core radii from the center, their apparent sizes (radii of ~5 kpc) are not inconsistent with the expected tidal cutoff for these M/L's. The two component model, while self-consistent, is perhaps not overly compelling in view of the fact that the velocity dispersions in the nuclei are not well determined. If the nuclei and the envelope have the same M/L, a value of 30-40 fits the observations. This value would require very large velocity dispersions in the nuclei, considerably in excess of either our upper limits or values for elliptical nuclei in general, and may be thus regarded as extremely unlikely if not rejected outright. In addition, the frictional time scale, which already presents a problem, is a factor of two shorter (see § IVc) for this model.

b) Cluster Dynamics

Table 4 also lists the dispersion for the outer galaxies based on the seven redshifts given in Table 1. To calculate a crude value for the cluster M/L we assumed that the density of the cluster was represented by a singular isothermal sphere:

$$\rho(r) = \rho_o \left(\frac{r_o}{r}\right)^2 \quad M(r) = 4\pi\rho_o r_o^2 r = \frac{2\sigma_v^2 r}{G} \quad .$$

The mass inside of 500 kpc is about 8×10^{13} $M_\odot$.

For the luminosity function we take the Schechter form (1976):

$$n(L) = n_* \left(\frac{L}{L_*}\right)^\alpha \exp(-L/L_*) \frac{dL}{L_*} \quad . \tag{5}$$

For the galaxies in de Vaucouleurs, de Vaucouleurs, and

Corwin (1976), Kirshner, Oemler, and Schechter (1979) find:

$$L_{*_{B_T}} = 2.7 \times 10^{10} \, L_\odot$$

$$M_{*_{B_T}} = -20.60$$

$$\alpha = -1.0 \, .$$

The predicted observed r magnitude for a galaxy of magnitude

M_* is ~15.6. If N_ε = number of galaxies brighter than εL_*,

then

$$L_{cluster} = \frac{N_\varepsilon L_*}{\int_\varepsilon^\infty \frac{e^{-x}}{x} \, dx} \, .$$

There are ~10 galaxies brighter than $0.5 \, L_*$ within a 500 kpc

radius, so

$$L_{cluster} = 18 \, L_* = 5 \times 10^{11} \, L_\odot \, .$$

The cluster M/L ~160, which conforms to the trend of increasing

M/L as one moves to larger structures.

c) Frictional Evolution

The nuclei moving in the massive envelope in the central

object are subject to dynamical friction and will spiral into

the center. It is clearly of interest to know the time scale

for this process. Of the final outcome there can be little

doubt; as we shall show later, the photometric properties of

the system indicate that when all the nuclei have merged the

object will be a typical cD galaxy in a poor cluster of the

sort first found and studied by Morgan and co-workers (Morgan and Lesh 1965; Morgan, Kayser, and White 1975), and not dissimilar to the supergiant systems found in richer clusters.

Chandrasekhar (1942) showed that the acceleration of a test particle of mass m moving in a background of density ρ is

$$\frac{dv}{dt} = \frac{-4\pi G^2 m\rho \ \ln \ \Lambda \ f(x)}{v^2}$$

$$f(x) = \text{erf}(x) - x \ \text{erf}'(x)$$

$$x = \frac{v}{\sqrt{2}\sigma_r}$$

(6)

σ_r = one component velocity dispersion of the background,

v = velocity of the test particle.

The time scale is $\tau = v/\frac{dv}{dt}$, or

$$\tau = 4.2 \times 10^9 \ \frac{v^3}{m\rho \ \ln \ \Lambda \ f(x)} \ \text{years}$$

v in km s^{-1}
m in $M_\odot$
ρ in $M_\odot$ pc^{-3}

Adopting $\ln \ \Lambda = 2$, $m = 7.0 \times 10^{10} \ M_\odot$ (biggest nuclei), $v = \sqrt{3} \ \sigma_{r_{\text{nuclei}}}$, $x = 1.16$, and $\rho = 0.06 \ M_\odot$ pc^{-3} (density at two core radii),

$$\tau = 7.3 \times 10^8 \ \text{years for a large nucleus,}$$

$$\tau = 2.5 \times 10^9 \ \text{years for a small nucleus.}$$

This is a fairly short time (a few crossing times), about 10% of the Hubble time. The primary sources of error would be due to uncertainties in the mass-to-light ratios of the nuclei and envelope. The large nuclei are stopped relatively quickly.

This would seem to be supported by the observations, as the three largest ones all have velocities within 200 km s^{-1} of the mean. The smaller galaxies, however, have velocities on the order of 500-700 km s^{-1}.

To aid in interpreting what we are observing in V Zw 311, a computer simulation of the cannibalism process was developed. Our simulation consisted of small nuclei interacting with a giant extended envelope. The density profile of both the nucleus and envelope is assumed to be of the form given by equation (1), with a tidal cutoff discussed below for the nuclei.

As the nuclei move through the background, the force due to dynamical friction is calculated from equation (6). At each point the nucleus is stripped down to the point where its density equals the local background value. This radius is roughly 30% larger than the "tidal" cutoff at distances greater than two core radii from the center of the envelope. The mass of the nucleus, however, is not sensitive to the exact cutoff when $r_{cutoff} \gg a_{gal}$, which is the case with the observed nuclei. The stripped mass is transferred to the envelope, as is the energy and angular momentum lost by the nucleus.

The envelope was terminated at 15 core radii to give a finite mass . During the simulation the envelope kept the same profile form (eq. [1]), but the core radius and central density were varied to conserve energy. Defining

$$f_e = \frac{\text{Binding energy of the envelope (t)}}{\text{Binding energy of the envelope (0)}}$$

and

$$f_m = \frac{\text{Mass of the envelope (t)}}{\text{Mass of the envelope (0)}} \; ;$$

then

$$a(t) = \frac{f_m^2}{f_e} \, a(0) \qquad \rho_o(t) = \frac{f_e^3}{f_m^5} \, \rho_o(0) \quad .$$

Three representative galaxies were fed to the envelope-- a "large" one (B, D, or G); a "small" one (A, C, E, F, or I); and a regular cluster member (8, 9, or 10). The nuclei had the parameters given in Table 6; the mass-to-light ratios were 7 (nuclei) and 90 (envelope). The envelope cutoff corresponds to 150 kpc. Each nucleus was placed in a circular orbit at five core radii. The results are given in Table 7.

The times in Table 6 are in reasonable agreement with those calculated at the start of this section (the nuclei at the present time are at 2-3 core radii; the decay time is quite linear with distance). The nearby cluster galaxies (8, 9, and 10) will be able to resist the envelope for times comparable to the age of the Universe.

The relatively small effect of the cannibalism upon the dynamics of the envelope is probably not realistic. The most appealing picture of the origin of the system, as we shall see, is that the envelope is the outer stripped parts of the nuclei we see now plus, probably, a few past victims. The high M/L of the envelope indicates that there must have been a large M/L gradient in the original galaxies if this picture is correct, so that the ingestion of each new victim has a much larger

effect on the total mass and energy of the system than it does in our simulations. The models do, however, adequately deal with the situation once the dark outer parts of the nuclei have been stripped.

V. DISCUSSION

The fate of the system is doubtless that in a few billion years all the nuclei seen currently within the envelope will have merged; probably none, but at most one or two, of the other cluster members will be pulled in on that time scale. The object will at that time look like a typical first-ranked cD galaxy. Table 5 compares the current parameters of the V Zw 311 to those of the typical first-ranked galaxy,/ The *using the nomenclature of SGH.* colors agree quite well (correct amount of galactic absorption?), and the luminosity is about 2σ high. The structural parameters are bizarre at present because of the spatial extent of the distribution of the bright nuclei, but will become much more reasonable (and more like those of typical first-ranked-galaxies) as the system evolves and the nuclei merge in the center. The increased central concentration of light in the final configuration will probably decrease the roughly 10 kpc core radius of the present envelope somewhat, and it seems likely that the resulting galaxy will fit quite neatly on the core radius-luminosity relation (JGH). It is of interest and somewhat discouraging that the present configuration does not fit the mold of first-ranked galaxies at all well, and in fact has essentially constant surface brightness averaged over the

standard aperture of SGH. Fortunately, systems of this type are extremely rare, and can in any case be recognized as bizarre at very great distances.

We are left with a few intriguing questions, the most insistent of which is the origin of the system. It is difficult to understand how such an object can exist. The current configuration should last only a billion years or so, and yet during a similar period the central object has managed to ensnare a sizable fraction of the bright galaxies in the cluster. Statistical arguments must be viewed with suitable caution, however, since the object was chosen from some hundreds of clusters at similar distances precisely because of its unusual appearance.

The hypothesis that there was a giant originally is probably the less attractive, since it offers no explanation of the existence of so many nuclei now with such short lifetimes. It should be noted that the situation in V Zw 311 is quite different from that in multiple-nuclei systems; in rich clusters, there is a continuing supply of food, and one can regard the multiple-nucleus condition as a steady state. Here there is no possibility that this is the case. A further difficulty is that the material stripped from the presently observed nuclei plausibly makes up a large fraction of the light now seen in the envelope. The magnitudes in Table 3 are extrapolated to the 25 mag/sq arcsec isophote with the structural parameters in the table. The difference

between the luminosity represented by these "total" magnitudes and those actually present in the nuclei in the stripping model accounts for about 30% of the luminosity in the envelope. While this number is quite uncertain, it does indicate that the observed victims are not a negligible contribution to the structure as seen today, and thus not only has its construction essentially stopped now, it must have started at some relatively recent time in the past. Statistics or no , it stretches credulity to believe that such a substantial shell of galaxies could have arrived at the cannibal's maw in such a short interval.

Rather more attractive is the notion that there was no central giant, but a relatively compact subcluster of the original cluster. At some time in the relatively recent past, inelastic encounters finally brought about a merger of two of the most massive members of that system, and that merger and the pre-merger tidal interactions spread material throughout the subcluster, providing a medium with which the other galaxies began to frictionally interact. This picture at least provides a possible reason for the beginning of the frictional evolution in the relatively recent past. It is also in better accord with the color observations--in this last, "mutual stripping" picture, the envelope is the stripped outer material of the original galaxies and should therefore be bluer, given that the original galaxies had color gradients. In the "pre-existing giant" hypothesis, the envelope should in

large part reflect the colors of the giant and should be
red.

In summary, V Zw 311 seems to provide us with a case
of a cD galaxy in the making and emphasizes the long-sus-
pected composite nature of these objects. The short time
scale inferred for the evolution of the object is disturbing
but is in accord with the rarity of the phenomenon. We are
fortunate to observe it - it will almost certainly very soon
be another of the many cD's in poor clusters, and though it
does not provide definitive answers about the origin of such
objects, it provides many clues.

TABLE 1

JOURNAL OF OBSERVATIONS

Date (U.T.)	Telescope	Instrument	Wavelength/ Filter	Exposure (seconds)	Number
1976 Nov 24	P200	SIT Spectrograph	3650-5250	1000-2000	6
1977 Sep 19	P200	" "	3750-5350	1000	3
1978 Oct 7	P200	" "	3950-5550	1000	4
1979 Mar 3	P200	PFUEI	r	300	2
1979 Aug 30	P60	"	r	100	1
1979 Aug 30	P60	"	g	300	2

TABLE 2

V Zw 311   REDSHIFTS

Object	cz (km s^{-1})
A	13600
B	14480
C	15170
D	14260
E	13440
F	14340
G	14130
I	13660
Envelope	13950 :
4	14250
8	14700
9	13930
10	13150 :
14	13820
15	15020
17	13860

TABLE 3

GALAXY PHOTOMETRY

Object	I	a (")	r	(g-r)
A	16.51	0.12	17.65	+0.79
B	16.76	0.31	15.80	+0.81
C	17.37	0.28	16.70	+0.83
D	16.16	0.21	15.90	+0.79
E	16.00	0.06	18.35	+0.59
F	17.45	0.32	16.55	+0.77
G	15.72	0.19	15.70	+0.77
H	20.14	0.53	18.55	+0.86 :
I	15.36	0.09	16.90	+0.68
J	19.79	0.35	19.00	+0.55
K	19.46	0.35	18.65	+0.48
Envelope	21.2	9.5		+0.70 :
8	17.84	0.38	16.55	+0.68
9	17.14	0.29	16.40	+0.72
10	18.99	0.68	16.60	+0.72
17	18.00	0.28	17.45	+0.66

TABLE 4

DYNAMICS

Object	$\langle cz \rangle$ (km s^{-1})	$\langle \sigma_r^2 \rangle^{\frac{1}{2}}$
Inner nuclei (8)	14130 ± 200	540 ± 150
Envelope	13950 ± 200	(610 ± 150)
Outer galaxies (7)	14110 ± 220	590 ± 170

TABLE 5

PROPERTIES OF THE CENTRAL OBJECT

Parameter	$\langle$First Rank Galaxy$\rangle$	V Zw 311
RAM	21.14 ± 0.33	20.60
(g-r) rest	+0.47 ± 0.06	+0.44
α	0.49 ± 0.11	2.00
a (kpc)	2.0 ± 0.8	> 20
RSB	18.13 ± 0.62	20.55

TABLE 6

CANNIBALISM SIMULATIONS

Galaxy I	a (")	Infall Time From Five Core Radii (yrs)
17.0	0.20	1.5×10^{10}
16.0	0.30	1.7×10^{9}
17.5	0.40	5.8×10^{9}

REFERENCES

Abell, G. O. 1958, *Ap. J. Suppl.*, 3, 211.

Chandrasekhar, S. 1942, *Principles of Stellar Dynamics* (Chicago: University of Chicago Press).

de Vaucouleurs, G., de Vaucouleurs, A., and Corwin, H. G. 1976, *Second Reference Catalog of Bright Galaxies* (Austin and London: University of Texas Press).

Faber, S. M., and Gallagher, J. S. 1979, *Ann. Rev. Astr. Ap.*, 17, 135.

Gunn, J. E., and Tinsley, B. M. 1976, *Ap. J.*, 210, 1.

Gunn, J. E., and Westphal, J. A. 1982, preprint.

Hausman, M. A., and Ostriker, J. P. 1978, *Ap. J.*, 224, 320.

Hoessel, J. G. 1980, *Ap. J.*, 241, 493 (JGH).

Hoessel, J. G., Gunn, J. E., and Thuan, T. X. 1980, *Ap. J.*, 241, 486.

King, I. R. 1966, *A. J.*, 71, 64.

Kirshner, R. P., Oemler, A., and Schechter, P. L. 1979, *A. J.*, 84, 951.

Moffet, A. T. 1975, *Galaxies and the Universe*, ed. A. Sandage, M. Sandage, and J. Kristian (Chicago and London: University of Chicago Press), p. 264.

Morgan, W. W., Kayser, S., and White, R. A. 1975, *Ap. J.*, 199, 545.

Morgan, W. W., and Lesh, J. R. 1965, *Ap. J.*, 142, 1364.

Ostriker, J. P., and Tremaine, S. D. 1975, *Ap. J. (Letters)*, 202, L113.

Peterson, B. A. 1979, A. J. 75, 695.

Sargent, W. L. W., Schechter, P., Boksenberg, A., and
    Shortridge, K. 1977, Ap. J., 212, 326.

Schechter, P. L. 1976, Ap. J., 203, 297.

Schechter, P. L., and Gunn, J. E. 1979, Ap. J., 229, 472.

Schneider, D. P., Gunn, J. E., and Hoessel, J. G. 1982,
    in preparation (SGH).

Thuan, T. X., and Gunn, J. E. 1976, Pub. A.S.P., 88, 543.

Tinsley, B. M., and Gunn, J. E. 1976, Ap. J., 203, 52.

Toomre, A. 1977, The Evolution of Galaxies and Stellar
    Populations, ed. B. Tinsley and R. Larson (New Haven:
    Yale University Observatory), p. 401.

Tremaine, S. D., Ostriker, J. P., and Spitzer, L. 1975,
    Ap. J., 196, 407.

Young, P. J., Gunn, J. E., Kristian, J. E., Oke, J. B.,
    and Westphal, J. A. 1980, Ap. J., 241, 507.

Zwicky, F. 1971, Catalog of Selected Compact and of Post
    Eruptive Galaxies (Zurich: Zwicky).

FIGURE CAPTIONS

Fig. 1. - Representative spectra; a standard (K0 III) and two inner galaxies. The data have a resolution of 5 Å and have been logarithmically rebinned at 170 km s^{-1}. The data are plotted on a linear flux scale; absolute spectrophotometry is not implied.

Fig. 2. - A contour plot of the central object in V Zw 311. The seeing (FWHM) was 1.2 arcsec in this 600 sec exposure with the Hale telescope and the PFUEI/CCD detector. One edge of the figure is 133 arcsec (140 kpc). The contours represent r surface brightnesses from 19.0 to ~24.0 mag per sq arcsec (uncorrected for galactic absorption). North is at the top, east to the left. The stars with distorted profiles were saturated. Galaxies are labeled following Zwicky's notation. Interesting features include the extent of the common envelope and the multitude of small galaxies lurking in the outer environs.

Fig. 3. - Surface photometry of the central object in V Zw 311. The dots represent all of the light, while the crosses are an estimate of the smooth background. The color of the object (g-r) as a function of radius is given in the lower left corner.
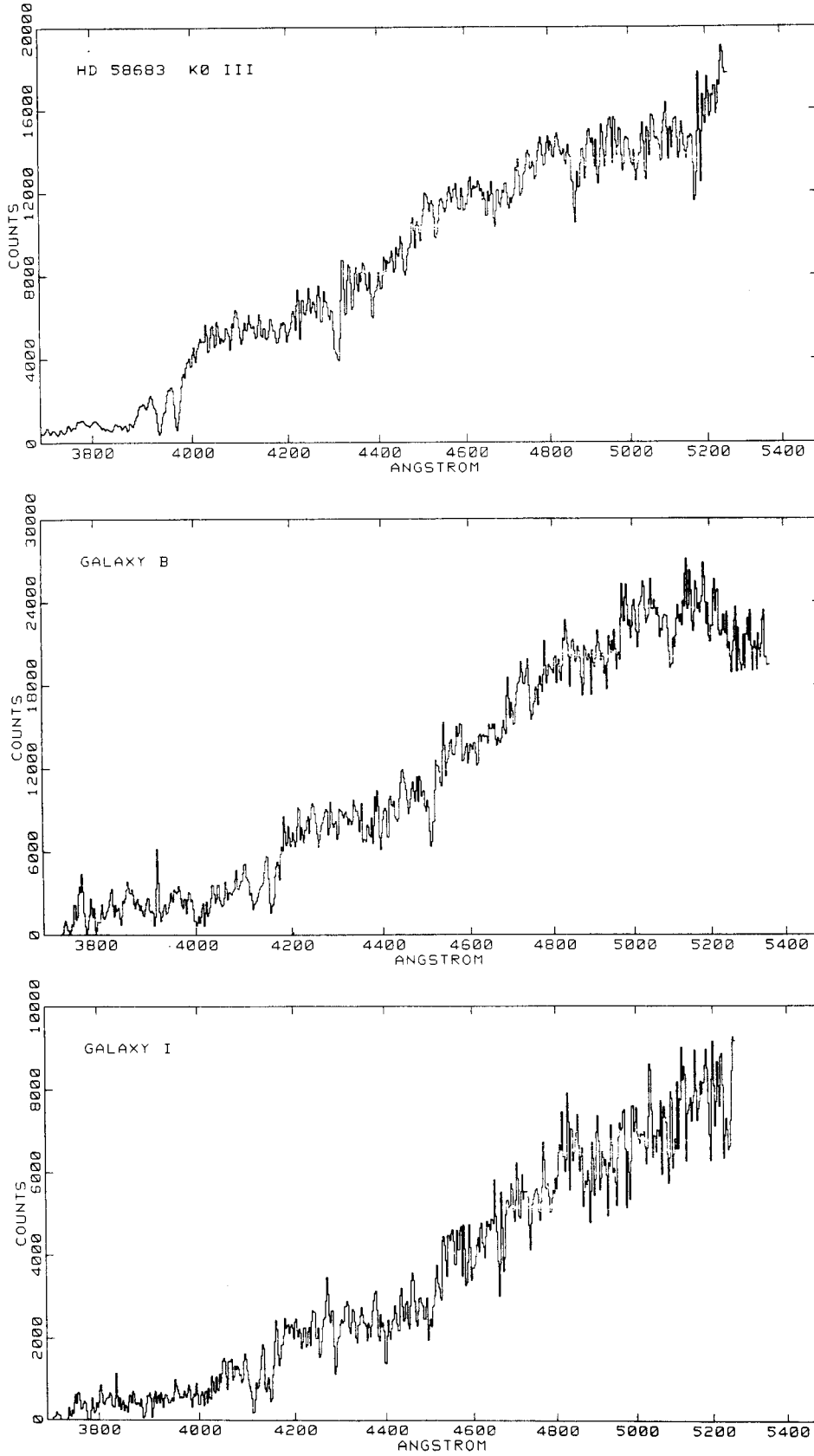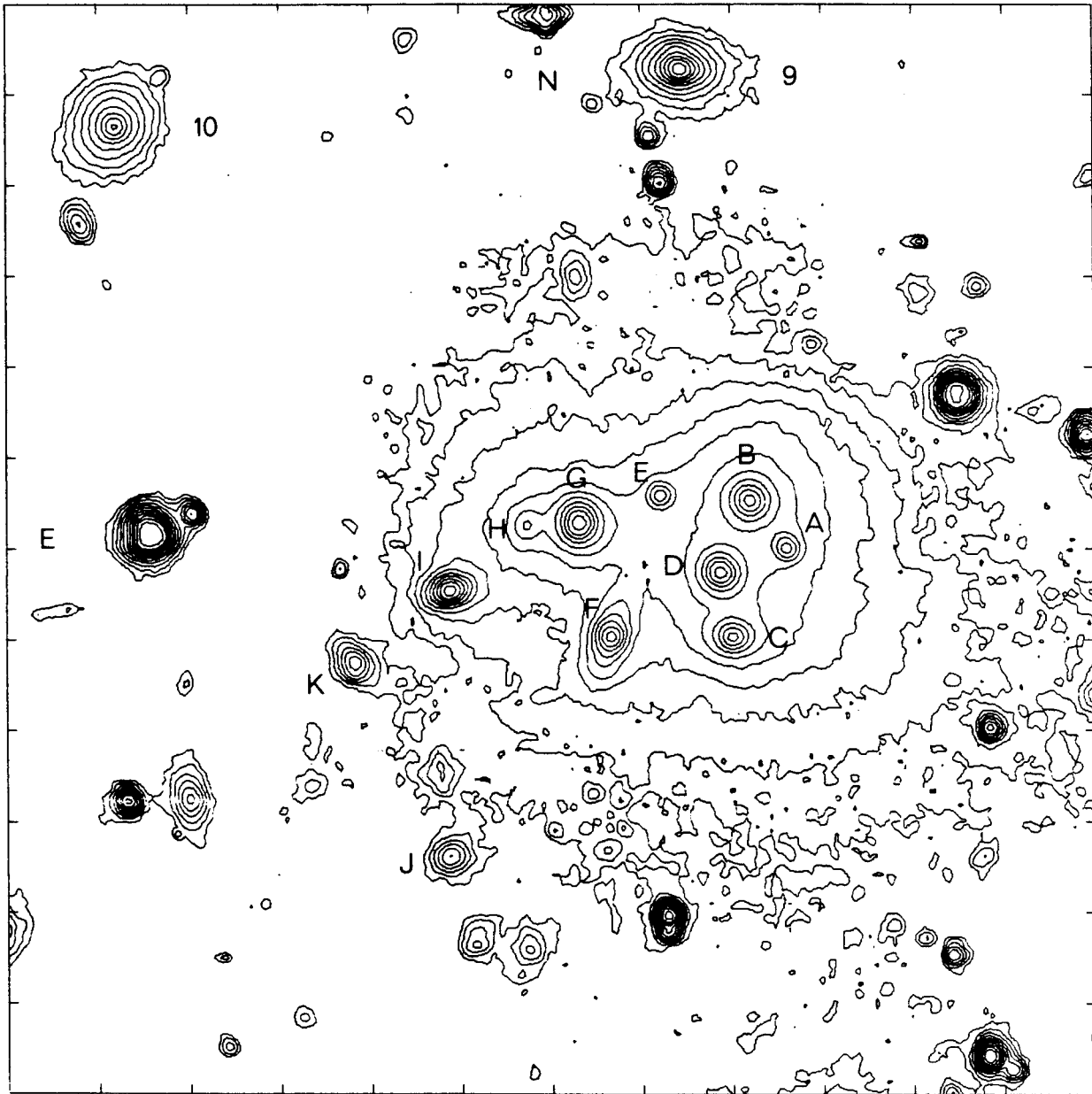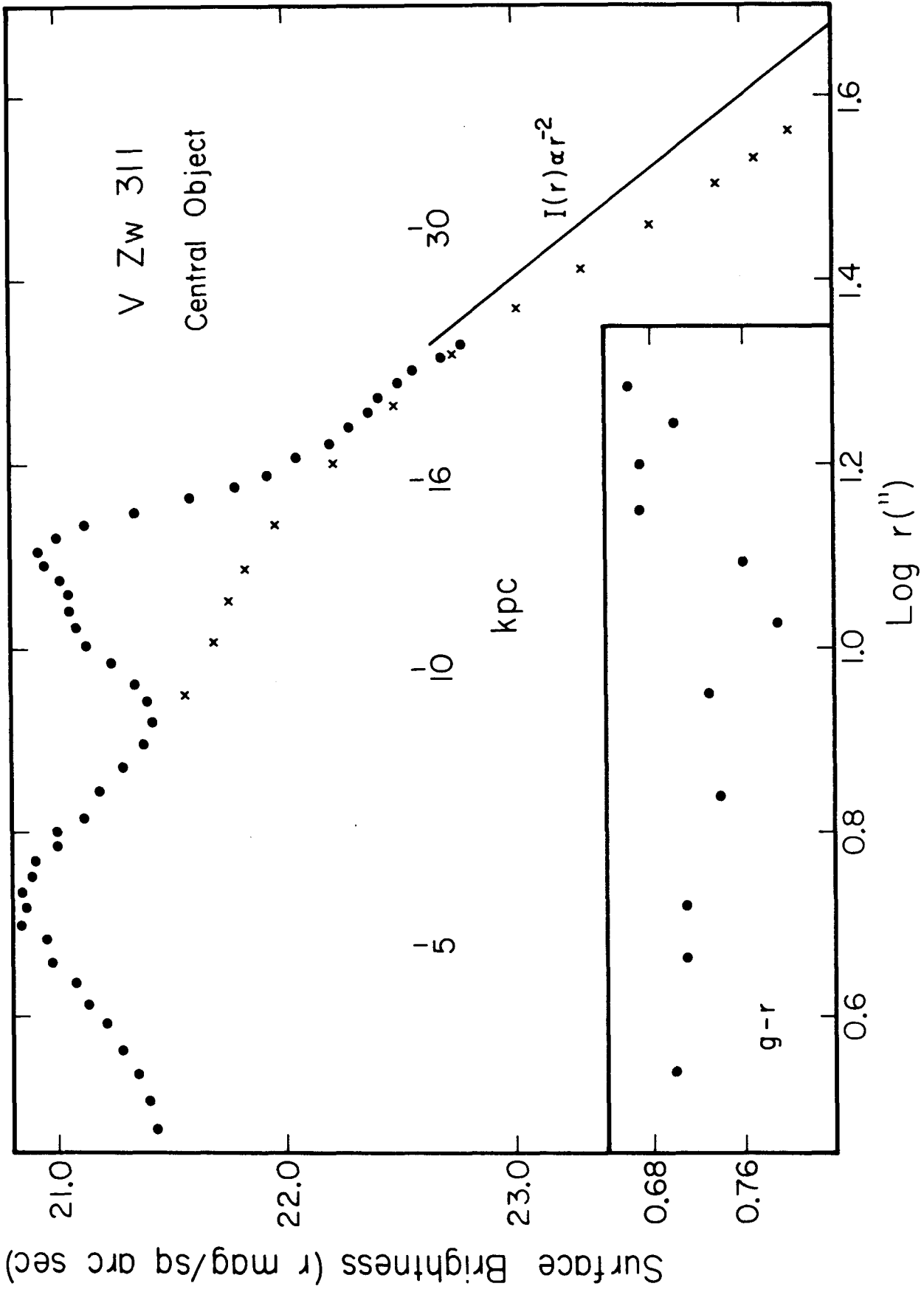
Figure 1

Figure 2

Figure 3